PRYMNESIOPHYCEAE AS PALEOCEANOGRAPHIC TOOLS: AN OPEN-OCEAN ASSESSMENT OF ALKENONE δDEUTERIUM AS A PALEO-SALINITY PROXY

by

Jessica Gould

Submitted in partial fulfilment of the requirements
for the degree of Master of Science

at

Dalhousie University
Halifax, Nova Scotia
November 2017

Table of Contents

LIST OF TABLES

LIST OF FIGURES

ABSTRACT

Sea surface salinity (SSS) is arguably the least constrained variable of the past ocean, which is unfortunate because it is a fundamental variable controlling the density of seawater - thus large-scale circulation - and is also reflective of the hydrological cycle. The hydrogen isotopic (δD_{water}) composition of surface seawater is correlated with SSS. Laboratory algae cultures have shown that δD_{water} is reflected in biomarkers – for instance, alkenones ($\delta D_{alkenone}$), where $\delta D_{alkenone}$ is linearly correlated with δD_{water}. However, a large-scale field study testing the validity of this proxy is lacking. This study presents the first evaluation of δD_{water} and coincident $\delta D_{alkenone}$ of open-ocean surface alkenone samples from both the Atlantic and Pacific Oceans. The data agree remarkably well with regressions for $\delta D_{alkenone}$ vs. δD_{water} observed in laboratory cultures. Scatter in the data is discussed vis-à-vis physiological factors observed in culture to affect the fractionation between δD_{water} and $\delta D_{alkenone}$.

LIST OF ABBREVIATIONS AND SYMBOLS USED

‰ – per mil
$\alpha_{alk\text{-}water}$ – fractionation factor for $\boldsymbol{\delta}D_{alkenone}$ and $\boldsymbol{\delta}D_{water}$ ($\alpha = (\delta D_{alk}+1000)/(\delta D_{water}+1000)$)
$\boldsymbol{\delta}^{13}C$ – carbon isotopic signature ($\boldsymbol{\delta}^{13}C = (({}^{13}C/{}^{12}C_{alk})/({}^{13}C/{}^{12}C_{standard})-1)*1000$ (‰))
$\boldsymbol{\delta}^{18}O$ – oxygen isotopic signature ($\boldsymbol{\delta}^{18}O =(({}^{18}O/{}^{16}O_{sample})/({}^{18}C/{}^{16}C_{standard})-1)*1000$ (‰))
$\boldsymbol{\delta}D_{(water)}$ – hydrogen isotopic signature ($\boldsymbol{\delta}D = ((D/H_{water})/(D/H_{standard})-1)*1000$ (‰))
$\boldsymbol{\delta}D_{(alk)}$ – hydrogen isotopic signature ($\boldsymbol{\delta}D = ((D/H_{alkenone})/(D/H_{standard})-1)*1000$ (‰))
AMT20 – Atlantic Meridional Transect (20)
BODC – British Oceanographic Data Centre
C37:2 – di-unsaturated alkenone
C37:3 – tri- unsaturated alkenone
CI – Confidence Interval
CO_2 – Carbon Dioxide
DCM – dichloromethane
E. huxleyi – Emiliania huxleyi
FID – flame ionization detector
G. oceanica – Gephyrocapsa oceanica
GEOTOP-UQAM – Centre de recherche en géochimie et en géodynamique at Université du Québec à Montréal
GC – gas chromatograph
ITCZ – Intertropical Convergence Zone
KOH – potassium hydroxide
MARUM – Center for Marine and Environmental Sciences
MeOH – methanol
Mg/Ca – magnesium calcium ratio
N_2 – nitrogen gas
$NADP^+$ - nicotinamide adenine dinucleotide phosphate
NADPH - reduced form of $NADP^+$
ODV – Ocean Data View
OPP - oxidative pentose phosphate cycle
pCO_2 – partial pressure carbon dioxide
psu – practical salinity unit
SPOM – suspended particulate organic material
Sr/Ca – Strontium Calcium ratio
SSS – sea surface salinity
SST – sea surface temperature
U^{K}_{37}' – alkenone unsaturation index (U^{K}_{37}' = (C37:2)/(C37:3 + C37:2))
VSMOW – Vienna standard mean ocean water

ACKNOWLEDGEMENTS

I would first like to thank my supervisor, Dr. Markus Kienast for the incredible opportunity to learn from him; for his encouragement and optimism throughout the years and for his fostering of confidence and curiosity. My work with Dr. Kienast has allowed me to experience many facets of ocean research, including two incredible trips out on the Scotian Shelf with the Bedford Institute of Oceanography (AZMP program) aboard the CGS Hudson and an unforgettable experience onboard the RV Sonne from Auckland to Darwin. These first-hand experiences at sea have taught me a great deal, and I will cherish the memories, friendships and science earned on each voyage. Dr. Kienast also afforded me the opportunity to visit MARUM in Bremen, DE, giving me the chance to work at another world-class laboratory, to collaborate with international scientists in my field and to explore Europe. I would like to thank Dr. Enno Schefuß for his collaboration on this project, and for teaching me a number of valuable analytical techniques. I would also like to thank Dr. Schefuß for his guidance and discussions while visiting MARUM. I would like to thank Dr. Michael Dowd for his collaboration and for his guidance over the years, and Dr. Hugh MacIntyre for his valuable expertise. Thank you also to Claire Normandeau & Ralph Kreutz who were tireless sources of knowledge in the lab, without whom I would have been lost. I am very grateful for the entire Kienast lab for their insight, invaluable discussions, and friendship, without whom this entire experience would not have been the same. Thank you also to Mike Fraser and Liz Kerrigan, for their help in collecting this dataset. I would also like to thank the government of Nova Scotia, and the National Science and Engineering Council of Canada for funding this research. Finally, to my parents Bob and Shelley, my brothers Alex and Hayden and my partner Curtis Gamble, thank you all for your endless love, support, and encouragement - this is for you.

CHAPTER 1: INTRODUCTION

1.1 Motivation

Reconstruction of past (paleo) ocean and atmospheric properties fuels our understanding of natural climate variability through time, especially during periods of rapid climatic variability in earth's history (e.g. glacial-interglacial transitions). In particular, paleoceanographic reconstructions provide critical constraints on amplitudes and rates of change in the natural climate system, thereby improving climate predictions. In light of the current push to understand and to constrain rates of anthropogenic impacts on climate, providing climate models with data from historical reconstructions can improve the reliability of model forecasts.

Inherently, reconstructions of past ocean properties must rely on biological and geochemical proxies - records of variables of interest from the past. Biomarkers, in particular, are principle components of this analysis. The exact make-up of these organic molecules is a result of systematic responses to environmental conditions during biosynthesis, such as temperature (Rosell-Melé & McClymont, 2007). Together with other paleoceanographic proxies many key climate variables (i.e. temperature and ice volume) can be reconstructed, which provide insight into past changes in ocean dynamics such as circulation and heat transport, marine productivity and CO_2 sequestration.

The ocean, being the largest transporter of energy (heat) on earth, is a driver of earth's climate variability (Houghton et al., 1995; Macdonald & Wunsch, 1996). Large-scale circulation (thermohaline) in the oceans, which redistributes heat from low latitudes to high latitudes, is controlled mainly by density gradients of different water masses (Ganachaud & Wunsch, 2000). Unfortunately, no direct proxy for water mass density exists. However, because both temperature and salinity are two of the primary drivers of seawater density, the reconstruction of these two metrics can provide a means by which density and thus circulation can be reconstructed. While there exists a number of fairly reliable proxies for reconstructing paleo-sea surface temperatures (SST) (e.g. Mg/Ca, $\delta^{18}O$, alkenone U^{K}_{37}', Sr/Ca, transfer functions etc.), there lacks a well constrained proxy for paleo-sea surface salinity (SSS). This is particularly unfortunate because, as mentioned, salinity plays a fundamental role in determining the density of seawater. At the same time, SSS is

also reflective of the global hydrological cycle; in particular, the distribution and movement of freshwater (e.g. water vapor, rainfall, ice formation/melt) between the oceanic and atmospheric systems. For example, shifts in the latitudinal positioning of the Intertropical Convergence Zone (ITCZ) - a region of active rainfall- are of great interest to paleo-climatologists interested in understanding geographical precipitation variability through space and time (e.g. Waliser & Gautier, 1993; Braconnot et al., 2007; Fleitmann et al., 2007). The ability to accurately reconstruct significant variability in surface ocean salinity, therefore, would provide valuable insight on past oceanic and atmospheric dynamics (Chivall et al., 2014).

This study conducts a large-scale open-ocean evaluation of a potentially powerful independent proxy for the reconstruction of paleo-SSS; the hydrogen isotopic composition (δD or δDeuterium) of alkenones. The 'novel' proxy relies on the assumption that variability in the δD of seawater, which is mechanistically linked (positively correlated) with sea surface salinity (Craig, 1961; Friedman et al., 1964), is 'recorded' in the isotopic signature of carbon-bound, non-exchangeable hydrogen of organic matter; in particular of biomarkers (Schwab & Sachs, 2009). The δD of one such biomarker; alkenones, which are exclusively synthesized by haptophyte algae (prymnesiophytes), has been proposed as an ideal biomarker proxy for paleo-SSS (Englebrecht & Sachs, 2005). Indeed, a number of laboratory culture studies have shown the δD of alkenone molecules ($\delta D_{alkenone}$) to reflect (be linearly correlated with) the δD of the water the algae were grown in, and a number of sediment studies have already used this novel proxy to infer past changes in SSS (van der Meer et al., 2007; 2008; Pahnke et al., 2007; Coolen et al., 2013; Kasper et al., 2014). However, a large-scale field study testing the validity of this proxy in the open-ocean, under natural environmental conditions, is lacking. In this study, I investigate the relationship between the $\delta D_{alkenone}$ and the δD_{water} from surface ocean suspended particulate organic material (SPOM) samples collected from the Atlantic Ocean and Western Tropical Pacific Ocean. I also present a comparison between the relationships observed in the open-ocean SPOM dataset presented here and previously published relationships from both laboratory algae culture and small-scale field studies. Finally, using the open-ocean SPOM dataset, I present an exercise in quantifying uncertainty around the reconstruction of salinity from sedimentary core $\delta D_{alkenone}$ analysis.

1.2 Background

1.2.1 Salinity

There exist a number of formal definitions of salinity, although in simplest terms, ocean salinity refers to the amount of solutes (salts) (g) dissolved in a kg of seawater (kg). The quantification of salinity in seawater is typically made through the simultaneous measurement of conductivity, pressure and *in situ* temperature (Joint Panel, 1980; Millero, 1996). Globally, mean modern day ocean salinity is approximately 35 (Broecker & Peng, 1982), with sea surface salinities ranging between ~31-38, varying with latitude (Figure 1.1). Open-ocean surface salinities are largely dictated by the relative proportion of evaporation and precipitation with roughly 86% of precipitation and 78% of evaporation world-wide occurring over the oceans (Baumgartner & Reichel, 1975, Figure 1.1). Variability in solar insolation determines the amount of evaporation over the surface ocean. Mid-low latitudes (high insolation) experience higher evaporation than precipitation, yielding high SSS compared to equatorial and mid-to-high latitudes that experience more precipitation than evaporation (Antonov et al., 2006) (Figure 1.1). Coastal ocean and high latitude surface ocean salinities are also impacted by freshwater input from riverine outflow and glacial meltwater.

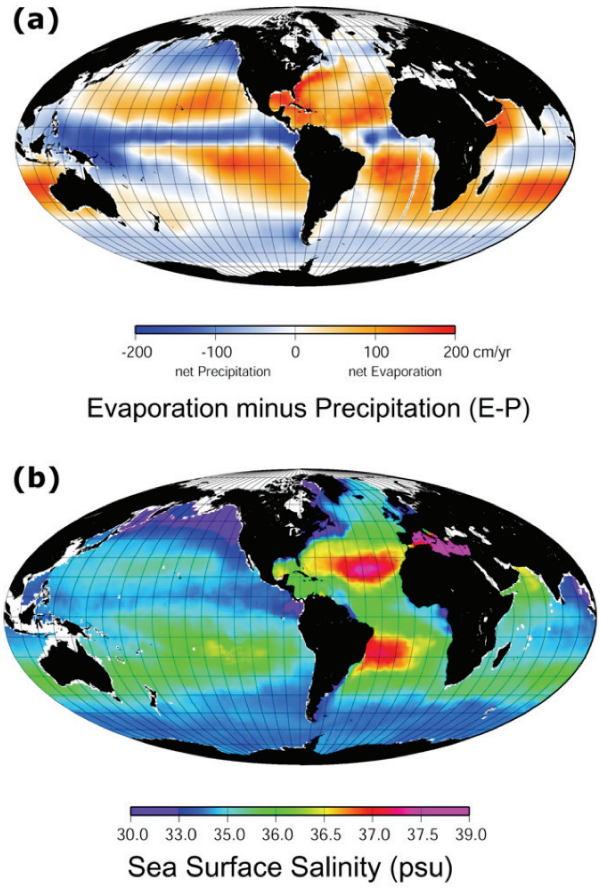

Figure 1.1: Global distribution of (a) evaporation minus precipitation (Schmitt, 1995) and of (b) surface water salinity (Curry, 1996). (© 2012 Nature Education – Courtesy of R. Curry (1996)). Figure obtained from Nature Education: Oppo, D.W. & Curry, W.B. (2012; https://www.nature.com/scitable/knowledge/library/deep-atlantic-circulation-during-the-last-glacial-25858002).

1.2.2 Paleo-Salinity

Traditionally, reconstructions of past SSS have relied on a combination of two or three independent proxies. First, there are biological proxies that analyze relative species abundances and distributions through time (e.g. distributions of diatoms and dinocysts throughout a sediment core) coupled with an age model (Kolbe, 1927; Hustedt, 1953; Ehrlich, 1978; Gasse, 1987 *as cited in* Fritz, 2013; de Vernal et al. 1993; 1994; 1996; 1997, Rochon et al., 1998 *as cited in* de Vernal et al., 2000). This type of proxy relies on an empirical relationship between species assemblages and salinity that is assumed to hold true temporally and spatially, at the same time, assuming shifts in species assemblages are associated only with salinity variability. Both assumptions can lead to a very large associated error. Alternatively, there are

approaches that measure chemical signatures of inorganic and organic material recorded in sediments. Typically, these studies measure oxygen isotope residuals ($\delta^{18}O$) (Rohling & DeRijk, 1999 and references therein) to reconstruct salinity variation through time. Here $\delta^{18}O$, typically measured in calcite from calcareous organisms, is used to reconstruct the $\delta^{18}O$ of seawater, which must be corrected for both global ice volume and for SST obtained from additional proxy records in order to yield a salinity signal. Both biological and chemical approaches have advantages and disadvantages, although both have large associated uncertainties due to error propagation through the use of multiple proxies. This is unfortunate and limits a comprehensive understanding of past ocean circulation and global hydrological cycle dynamics.

Over the last two decades, with improvements in analytical techniques, compound specific isotope analysis has facilitated the development of an alternative paleo-salinity proxy – the hydrogen isotopic composition of biomarkers (δD or δDeuterium; Equation 1) (Burgoyne & Hayes, 1998, Hilkert et al., 1999, Scrimgeour et al., 1999, Tobias & Brenna, 1997 *as cited in* Sachse et al., 2012). Taking advantage of a mechanistic link between the relative proportion of the heavy (Deuterium) versus light (Protium) hydrogen isotopes (δD_{water}) and SSS in the open-ocean, the proxy relies on the assumption that the signature of δD_{water} is 'recorded' in a biomarker molecule. In particular, alkenones – long chain unsaturated ketones – have been targeted as an ideal biomarker because they are very resistant to diagenesis over time, they are found almost ubiquitously in all surface ocean waters, and they are produced exclusively by a small set of marine (and lacustrine) prymnesiophyte algae (Herbert, 2013). Hydrogen isotopic signatures are reported in delta notation (Equation 1), and are given in units of per mil (‰).

$$\delta D_{(alkenone)(water)}(‰) = \left(\frac{D/H_{alk\,(water)} - D/H_{VSMOW}}{D/H_{VSMOW}}\right) * 1000$$

(Equation 1, Sachse et al., 2012)

$D/H_{alk\,(water)}$: the relative proportion of deuterium to hydrogen in an alkenone (water) sample

D/H_{VSMOW}: the relative proportion of deuterium to hydrogen in 'Vienna Standard Mean Ocean Water'

Thus far, $\delta D_{alkenone}$ measurements have been applied to marine sediment cores from the Mediterranean Sea (van der Meer et al. 2007), the Eastern Tropical Pacific (Pahnke et al., 2007), the Black Sea (van der Meer et al., 2008; Coolen et al., 2013), and the Agulhas region (Kasper et al., 2014) to reconstruct past variations in salinity. Taken as an example, in their study Pahnke et al. (2007) draw conclusions about increased freshwater input and corresponding variability in sea surface salinity. They measure a shift in $\delta D_{alkenone}$ from ~ -190 to ~ -210 ‰ through a sedimentary record from the Eastern Tropical Pacific, which also agrees with the down-core record of $\delta^{18}O_{sw}$ (reconstructed from planktonic foraminifera $\delta^{18}O$ measurements).

Uncertainties associated with the δD proxy, initially identified by inconsistencies between this proxy's and the $\delta^{18}O$ record's account of past SSS, may hinder the applicability and certainly the accuracy of the paleoceanographic tool (Sachse et al., 2012). A number of subsequent culture studies have evaluated the influence of parameters such as lipid synthesis, species composition, salinity, irradiance, temperature, growth rate and growth phase on the $\delta D_{alkenone}$ signal, in particular of their effect on the fractionation between δD_{water} and $\delta D_{alkenone}$, and the associated implications of these effects on paleoceanographic reconstructions.

1.2.3 Hydrogen Isotopic Fractionation in Seawater

There exist two stable isotopes of hydrogen; Protium and Deuterium. Deuterium (D) is the heavier of the two and makes up only ~0.0156% of all hydrogen on earth (Harold Urey, 1932). The relative proportion of Deuterium to Protium in surface seawater is primarily driven by kinetic fractionation processes that occur during phase changes, i.e. during both evaporation and condensation/precipitation (van der Meer et al., 2015) and is also a function of global ice volume (D'Andrea et al., 2007). Preferential fractionation of the heavy versus light isotopes of hydrogen during evaporation, for example, results in water vapor that is relatively depleted in deuterium (isotopically light) and ocean surface water that is left relatively enriched in deuterium (isotopically heavy) (Gat, 1996 and references therein). These same fractionation processes cause both 'latitudinal' and 'continental' gradients in isotopic signatures of evaporated ocean water (or rainwater) as progressively more of the

heavy Deuterium isotopes 'rain out'. The residual water vapor becomes lighter as it travels from low to high latitudes and from coastal to continental areas. Globally, the isotopic signatures of freshwater precipitation and river water vary significantly from place to place, so much so that coastal ocean waters with significant riverine input as well as high latitude regions with both ice formation and melt have distinct isotopic signatures. However, because evaporation and precipitation primarily drive both the salinity of open-ocean surface waters and the isotopic signature of open-ocean surface water (δD_{water}), there exists a strong positive linear correlation between these two variables in the open-ocean (Craig & Gordon, 1965).

1.2.4 Alkenones as Biomarkers

Alkenones are long-chain carbon (carbon chain length 37) unsaturated methyl ketones produced exclusively by prymnesiophycean algae (Marlowe et al., 1984). These compounds range in their level of unsaturation, having four, three or two double bonds and are referred to as tetra-, tri- and di-unsaturated alkenones, respectively (de Leeuw et al., 1980). Globally, there are two dominant cosmopolitan open-ocean species of alkenone producers; *Emiliania huxleyi* and *Gephyrocapsa oceanica* (Conte et al., 1994a; Volkman et al., 1995), which both form coccoliths. There are also coastal prymnesiophytes, some of which are non-coccolith forming, such as *Isochrysis galbana* and *Chrysotila lamellosa*. Due to their source specificity, and their resistance to diagenesis over time, alkenones make for ideal biomarkers (Volkman et al., 1980, Prahl et al., 2000). In fact, alkenones found in the marine sedimentary record younger than 250 Kya are assumed to have originated primarily from *E. huxleyi* (Herbert, 2013).

While alkenone molecules can account for approximately 5-10% of the cell's carbon (Prahl et al., 1988; Conte et al., 1994b; Epstein et al., 2001; Versteegh et al., 2001), their exact physiological role and synthesis is not well understood. Nonetheless, due to up-regulation of alkenones in prymnesiophyte species under nutrient stress-induced stationary-growth conditions, these ketones are thought to play a role in energy storage (Epstein et al., 2001). Alternatively, they have been suggested to aid in maintaining membrane fluidity, as the relative degree of unsaturation (C37:3 tri-unsaturated vs. C37:2 di-unsaturated alkenones) is highly

correlated with growth temperature (Marlowe et al. 1984, Brassell et al. 1986b). This has made possible the reconstruction of past SST from measurements of C37:3 to C37:2 (U^{K}_{37}') in sediment cores (Brassell et al., 1986a;1986b; Prahl et al., 1988; Volkman et al.,1995). In addition to the SST proxy (U^{K}_{37}' index), $\delta^{13}C$ signatures in these molecules have been proposed as both a paleo pCO_2 proxy (e.g. Jasper & Hayes, 1990) and as a growth-rate proxy (e.g. Bidigare et al., 1997; Riebesell et al., 2000; Popp et al., 1998; Benthien et al., 2002, and a review by Laws et al., 2002). More recently, the hydrogen isotopic composition ($\delta D_{alkenone}$; Equation 1) of non-exchangeable, covalently-bonded hydrogen in these molecules has been proposed as a means of reconstructing paleo-salinity (e.g. Sauer et al., 2001). While the SST proxy (U^{K}_{37}') is likely the most well constrained of the alkenone proxies, each has associated uncertainties - in particular physiological and ecological effects on the primary signal- that require further investigation.

1.2.5 Hydrogen Isotopic Fractionation in Alkenones

External growth water, or ocean surface water in the case of marine prymnesiophytes, is the ultimate source of hydrogen used for the synthesis of organic matter. Indeed, initial laboratory culture studies have shown a very strong linear correlation between the δD signature of growth medium water and the δD in alkenones (Estep & Hoering, 1980; Sauer et al., 2001; Paul, 2002; Englebrecht & Sachs, 2005; Schouten et al., 2006; Sachse et al., 2012, Figure 1.2).

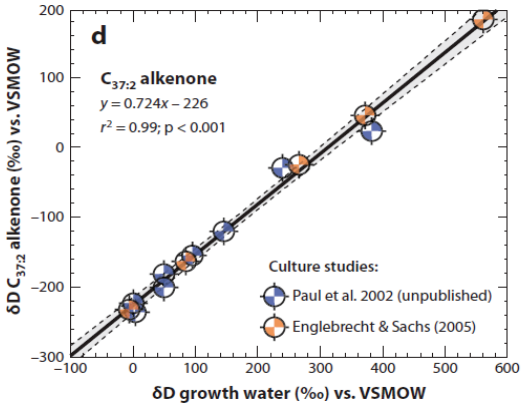

Figure 1.2: δD of di-unsaturated alkenones (C37:2) versus δD of culture water for Paul (2002) and Englebrecht & Sachs (2005) *E. huxleyi* cultures (Figure from Sasche et al., 2012).

While a strong correlation between $\delta D_{alkenone}$ and δD from growth water was found in the early culture studies (Figure 1.2), it is not a simple 1:1 relationship. Significant fractionation between the external water hydrogen and alkenones exists. 'Vital effects' cause the δD of lipids to be consistently deuterium- depleted by ~100-400 ‰ relative to external growth water; a consequence of the kinetic isotope effects of biosynthesis (Sessions et al., 1999; Sachs & Kawka, 2015). The isotopic signature of internal cell water is potentially influenced by fractionation processes occurring during exchange with the external water source and metabolic water production (Sachse et al., 2012, see Figure 1.4 below), although no direct hydrogen isotopic data for alkenone producer intracellular water have been made (Sachse et al., 2012).

To quantify the relative isotopic fractionation between δD of a biomarker compound (e.g., an alkenone) and the external growth water, the fractionation factor ($\alpha_{alk\text{-}water}$) is computed, which in an ideal system would be a constant value.

$$\alpha_{alk-water} = \frac{\delta D_{alk}+1000}{\delta D_{H_2O}+1000} \qquad \text{(Equation 2; Sasche et al., 2012)}$$

In fact, culture studies conducted by both Paul (2002) and Englebrecht & Sachs (2005) report similar fractionation factors with fairly consistent offsets in $\delta D_{alkenone}$ of 232 and 225 $^{0}/_{00}$, respectively, for *Emiliania huxleyi* grown on artificially deuterium enriched growth water at constant salinity (Figure 1.2). These initial batch culture studies (e.g. Paul 2002; Englebrecht & Sachs 2005) that regulate external growth water δD values by enriching with 'heavy' (deuterium-replete) water in excess of values found in the natural environment, and also ignore the effect of covarying salinity in the open-ocean natural environment, likely observe 'artificial' or unnatural responses in lipid synthesis. If the fractionation factor were indeed consistent, measurements of $\delta D_{alkenone}$ could be used reliably to reconstruct δD_{water} and in turn salinity. With an assumed constant $\alpha_{alk\text{-}water}$ value of 0.790 and a precision of $\delta D_{alkenone}$ measurements of ±3-5 $^{0}/_{00}$, the salinity error would be approximately ±1- 1.6 units (Wolhowe et al., 2009). However, recent culture work has found that a number of factors contribute to substantial variation in $\alpha_{alk\text{-}water}$.

For instance, Schouten et al. (2006) observed a significant relationship between $\alpha_{alk\text{-}water}$ and SSS for laboratory batch cultures of *E. huxleyi* and *G. oceanica* (Figure 1.3). It has since been suggested that this relationship could be used to reconstruct past salinity with an independent measure of δD_{water}.

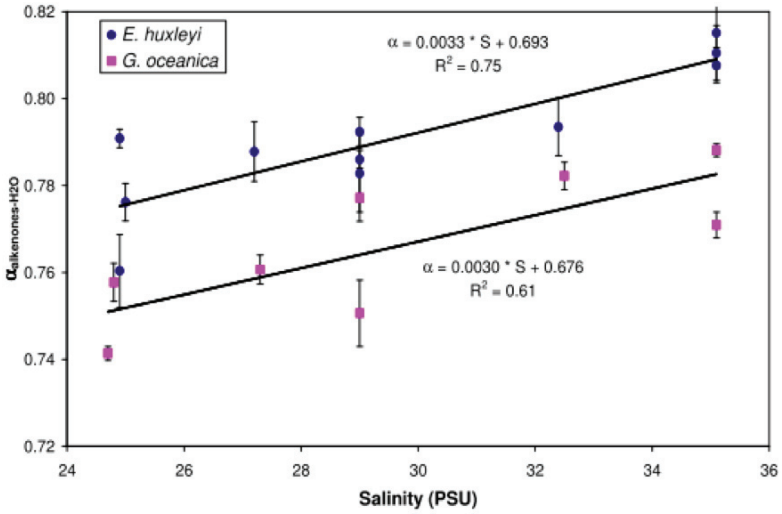

Figure 1.3: The δD fractionation factor between alkenone-and growth water from Schouten et al. (2006), based on laboratory cultures of *E. huxleyi* and *G. oceanica*. Results are shown for cultures reared over a salinity range of 12 psu (24-36). Linear regression shows a significant relationship between fractionation and salinity, albeit with some scatter, that differs between species. (Figure from Schouten et al., 2006).

In recent years, numerous batch- and continuous-culture studies of haptophyte algae have focused on evaluating the sensitivity of $\alpha_{alk\text{-}water}$ to variables such as species composition, salinity, irradiance, temperature, growth rate, growth phase and nutrient availability (Sessions et al., 1999; Zhang & Sachs, 2007; Schouten et al., 2006; M'Boule et al., 2014, Chivall et al., 2014; Wolhowe et al., 2009; 2015; Zhang et al., 2009; Weiss et al., 2017). These recent studies typically use evaporation as a means of increasing salinity and thereby δD_{water}; a process more representative of fractionation processes at play in the open-ocean environment relative to the injection of 'heavy' water in earlier culture work (Paul, 2002; Englebrecht & Sachs, 2005). While the biosynthetic mechanisms responsible for the observed sensitivities of $\alpha_{alk\text{-}water}$ to these various environmental variables are not yet fully understood, these empirical case studies provide semi-quantitative constraints on factors that influence the proposed salinity proxy. Below, a number of key findings from laboratory culture studies and small-scale field study observations

detailing the effects of these environmental and physiological parameters on $\delta D_{alkenone}$ and $\alpha_{alk\text{-}water}$ are reviewed.

1.2.6 Potential factors influencing the fractionation factor ($\alpha_{alk\text{-}water}$)

LIPID SYNTHESIS

The δD of a lipid molecule is inferred to be generally dictated by three factors; the initial isotopic composition of the biosynthetic precursor (or primary photosynthate), fractionation during biosynthesis (source of nicotinamide adenine dinucleotide phosphate (NADPH) for example; Martin et al., 1986) and hydrogenation during chain elongation in biosynthesis (Smith & Epstein, 1970; Luo et al., 1991 *as cited in* Englebrecht & Sachs, 2005). As stated earlier, the δD of lipids are consistently deuterium- depleted by ~100-400 ‰ relative to external growth water, and of this offset approximately 170 ‰ can be attributed to the D-depletion of the initial photosynthate (Yakir & DeNiro, 1990). The hydrogen isotopic composition of the cell's internal cell water pool is also important in determining the δD of a lipid molecule, which is itself influenced by fractionation during transport of external cell water into and out of the cell, as well as through the production of metabolic water (Kreuzer-Martin et al., 2005) (Figure 1.4).

With approximately 25% of H incorporated into alkenone molecules 'donated' from cell water, ~50% from NADPH and 25% from acetyl-coA, $\delta D_{alkenone}$ values can easily vary dependent on algal physiological status. NADPH produced during photosynthetic light reactions at PSI (in the chloroplasts) is understood to be one of the main donors of hydrogen during the synthesis of acetogenic lipids, which is likely a similar pathway to that of alkenones (Sachse et al., 2012). NADPH synthesized during these light reactions is posited to be very D-depleted, up to 600 ‰, (Sachse et al., 2012) compared to NADPH that has been synthesized through sugar metabolism via the oxidative pentose phosphate (OPP) cycle, which is inferred to be relatively less D-depleted (Sachse et al., 2012). The theory that the relative contribution of NADPH sourced from alternative pathways drives the majority of D-depletion in lipid molecules was first proposed by Estep & Hoering (1980). Since this prediction, a number of laboratory culture studies have supported this hypothesis, indicating that photosynthetically-derived NADPH (produced during the light reactions of

photosynthesis) is a large source of D-depleted hydrogen in lipids molecules relative to the external water source (Estep & Hoering, 1980; Zhang et al., 2009; Sachs & Kawka, 2015).

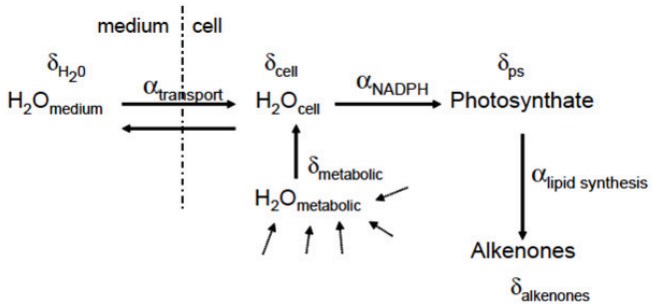

Figure 1.4: Illustration of a conceptual model for hydrogen sources during the synthesis of alkenone molecules. (Figure from Schouten et al., 2006).

The relative contribution of NADPH from alternate pathways during the synthesis of alkenones through time may or may not significantly impact the paleo-salinity proxy, depending on the physiological state of alkenone producers at the time of deposition to the sedimentary record. For example, if most alkenone molecules are transported to the sediments consistently during periods of alkenone up-regulation, which occurs during periods of nutrient depletion and stationary growth, but potentially also during periods of high growth rate (Sachs & Kawka 2015), and if the effects of an increase in the relative production of NADPH from OPP on the $\delta D_{alkenone}$ signature during this growth phase can be constrained, then the overall effect on α (fractionation) would also likely be constrained. An increased understanding of alkenone production in the water column as well as transport to the seafloor is required in order to quantify the significance of these, and other, biosynthetic effects.

SALINITY

Salinity itself is one of the most thoroughly studied parameters with respect to its influence on $\alpha_{alk\text{-}water}$, and has generally been understood to be one of the primary controls on the hydrogen isotopic fractionation in alkenones. A positive relationship between $\alpha_{alk\text{-}water}$ and salinity has been observed in a number of laboratory culture studies. Schouten et al. (2006) first observed that for every unit increase in salinity (ranging between 25-35) in their *E. huxleyi* culture, there was a corresponding increase in $\alpha_{alk\text{-}water}$ of 0.003 or (3‰), indicative of less fractionation

between $\delta D_{alkenone}$ and $\delta D_{growthwater}$ at higher salinities (Figure 1.3). Due to the strong positive correlations observed between $\delta D_{growthwater}$ and growth water salinity and between $\delta D_{alkenone}$ and $\delta D_{growthwater}$ and the observation that $\alpha_{alk\text{-}water}$ is also positively correlated with growth water salinity, a strong correlation is observed between $\delta D_{alkenone}$ and the salinity of the growth medium, with $\delta D_{alkenone}$ increasing ~3 to 5 $^{0}/_{00}$ per unit salinity increase (Schouten et al., 2006; M'Boule et al., 2014). This so-called 'salinity effect' ($\alpha_{alk\text{-}water}$ vs. salinity relationship) is considered to be an 'amplifier' of the relationship between $\delta D_{alkenone}$ and salinity, with more negative $\delta D_{alkenone}$ values (D-depleted alkenones) associated with fresher waters (D-depleted water). Subsequently, M'Boule et al. (2014) were the first to observe a relationship between $\alpha_{alk\text{-}water}$ and salinity for the coastal *Isochrysis galbana* species sampled in exponential growth phase, where $\alpha_{alk\text{-}water}$ increased 0.002 (2 $^{0}/_{00}$) per unit salinity - not substantially different from the values found by Schouten et al. (2006). This suggests that indeed, both open-ocean and coastal species' hydrogen isotopic fractionation may respond in a similar way to salinity variability.

One mechanism hypothesized as responsible for the positive correlation between $\alpha_{alk\text{-}water}$ and salinity is the regulation of osmotic pressure and turgor as the cell experiences salinity variations. A decrease in the exchange with external water at high salinities - facilitated by a reduction in aquaporins and an increase in osmolyte synthesis – would draw down the cell's internal light-hydrogen (D-depleted) water pool, rendering it more D-enriched (Sachse & Sachs, 2008; Schwab & Sachs, 2011; Sachse et al., 2012). A D-enriched internal water pool during periods of high salinity thus becomes the source of hydrogen for lipid synthesis, causing $\delta D_{alkenone}$ to be heavier and $\alpha_{alk\text{-}water}$ to increase. Furthermore, Sachse et al. (2012) suggest that perhaps lower growth rates at high salinities may also contribute to a reduction in fractionation (increase in $\alpha_{alk\text{-}water}$) between lipids and external water. However, in the recent *E. huxleyi* culture study by Sachs et al. (2016), where the effect of salinity on $\alpha_{alk\text{-}water}$ was isolated by controlling for constant growth rate and temperature, it was shown that regardless of the relationship between growth rate and salinity, there still exists a relationship between salinity and $\alpha_{alk\text{-}water}$, where $\alpha_{alk\text{-}water}$ increased ~1.5 $^{0}/_{00}$ per unit salinity increase. Although amplifying in effect, salinity itself adds another level of uncertainty to the $\delta D_{alkenone}$ paleo-proxy, which requires further investigation.

GROWTH RATE

Kreuzer-Martin et al. (2005) found that the internal water pool of alkenone producers can consist of up to 70% metabolic water (relatively D-depleted) during periods of high growth rate, making it conceivable that the δD of internal cell water and the $\delta D_{alkenone}$ may vary as a function of growth rate. During periods of low growth rate, these algae increase the production of lipids relative to other cellular components (Eltgroth et al., 2005), focusing energy on acetogenic – i.e. alkenone - lipid synthesis relative to isoprenoid (structural) lipid synthesis, both of which have different $\delta D_{alkenone}$ isotopic signatures. A number of studies have directly addressed the effect of growth rate on $\alpha_{alk\text{-}water}$. Both Schouten et al. (2006) and Sachs & Kawka (2015) found that fractionation between alkenones and growth water in *E. huxleyi* culture experiments increases with increasing growth rate, such that fractionation increased between 25 - 38 $^{0}/_{00}$ per unit increase in growth rate (d^{-1})). It is conceivable that an increase in metabolic water production during high growth rate contributes to the corresponding D-depleted alkenones observed by both Schouten et al. (2006) and Sachs & Kawka (2015).

Measurements of growth rates of alkenone producers can be difficult and require *in situ* incubations of algal samples taken from surface ocean samples (e.g. Landry & Hassett, 1982). While direct measures of growth rate in laboratory algal culture studies have helped to elucidate the effects of growth rate on $\alpha_{alk\text{-}water}$, a full understanding of these processes in the open-ocean setting is lacking. As suggested by Wolhowe et al. (2015), an alternative approach to estimating *in situ* growth rates is to measure the fractionation factor (ε_p) of carbon isotopes in alkenone molecules ($\delta^{13}C_{alkenone}$). $\delta^{13}C_{alkenone}$ have been suggested as both a potential paleo-$pCO_{2(aq)}$ proxy as well as an algal growth rate proxy (e.g. Jasper & Hayes, 1990; Bidigare et al., 1997; Riebesell et al., 2000; Popp et al., 1998; Benthien et al., 2002; and a review by Laws et al., 2002). Wolhowe et al. (2015) estimated growth rates of alkenone producers in water samples taken from the Gulf of California/Eastern North Tropical Pacific from ε_p values, concentrations of dissolved inorganic carbon (DIC) which were used to calculate concentrations of $CO_{2(aq)}$ and assumed cell volume to surface area ratios (Wolhowe et al., 2015). They estimated high algal growth rates in samples with coincident low $\alpha_{alk\text{-}water}$ (high hydrogen fractionation) values. In analogy

to that work, the present study will also evaluate $\delta^{13}C_{alkenone}$ measurements from SPOM alkenones sampled in the Atlantic and Pacific basins.

COMPOUND-SPECIFIC AND SPECIES-SPECIFIC δD SIGNATURES

Apparent compound-specific ($\alpha_{C37:3\text{-}C37:2}$) and species-specific variability in the fractionation between $\delta D_{alkenone}$ and $\delta D_{growthwater}$ ($\alpha_{alk\text{-}water}$) have been observed in culture studies. D'Andrea et al. (2007) found that *E. huxleyi* cells grown in culture have different tri-unsaturated (C37:3) and di-unsaturated (C37:2) $\delta D_{alkenone}$ signatures, such that the C37:3 compound was consistently D-deplete relative to C37:2, with a fractionation factor between the two molecules of $\alpha_{C37:3\text{-}C37:2}$ =0.944. These findings are in agreement with subsequent culture studies by both Wolhowe et al. (2009) and Schwabs & Sachs (2009), who found similar fractionation between the two compounds of $\alpha_{C37:3\text{-}C37:2}$ =0.97. The values are consistent with fractionation processes that are associated with hydrogenation and dehydrogenation processes (Chikaraishi et al., 2004; D'Andrea et al., 2007; Schwab & Sachs, 2009). Interestingly, Schwabs & Sachs (2009) found similar hydrogen isotopic fractionation between C37:2 and C37:3 in a coastal haptophyte species (*Chrysotila lamellosa*) in the Chesapeake Bay, suggesting that this compound-specific fractionation may not be species-specific, and that a general mechanism - i.e. elongation and desaturation processes during synthesis – may occur in all marine algae. The accuracy of utilizing individual versus combined compound-specific isotopic measurements for use in paleo work is thus debatable. However, obtaining individual C37:3 and C37:2 $\delta D_{alkenone}$ measurements is both analytically challenging and very inefficient. Furthermore, recently Chivall et al. (2014) found no dependence of relative alkenone distribution (i.e. C37:3 and C37:2) on $\alpha_{alk\text{-}water}$, such that measuring bulk $\delta D_{alkenone}$ values could be more appropriate than measuring individual C37:3 and C37:2 δD values. Similarly, van der Meer et al. (2013) indicated that utilizing a combined $\delta D_{alkenone}$ value would be more representative of both the internal water pool and salinity signal, and thus should be utilized when interpreting $\delta D_{alkenone}$ for paleo-salinity purposes. For these reasons, and for ease of measurement, the combined $\delta D_{alkenone}$ signal will be interpreted in this thesis.

However, species-specific combined $\delta D_{alkenone}$ signatures have been found. Generally, lab batch-culture studies find that of the two prevalent open-ocean species, *G. oceanica* consistently fractionates ~30‰ more relative to *E. huxleyi* (Schouten et al., 2006). Further, some studies argue that coastal ocean species fractionate deuterium differently from open-ocean species (Englebrecht & Sachs 2005; Schwab & Sachs, 2011, M'Boule et al., 2014). Small-scale field and lab culture results based on species-specific fractionation contribute uncertainty to the overall applicability of the $\delta D_{alkenone}$ paleo-salinity proxy, and it is clear that additional studies are required to resolve species-specific effects. However, this is outside the scope of this thesis.

IRRADIANCE

Arguably, one of the least constrained environmental influences on $\delta D_{alkenone}$ and $\alpha_{alk\text{-}water}$ is irradiance. In recent years Wolhowe et al. (2015) evaluated irradiance and fractionation ($\alpha_{alk\text{-}water}$) in the field, and van der Meer et al. (2015) have run experiments to test the effect of irradiance on fractionation ($\alpha_{alk\text{-}water}$) on cultured *E. huxleyi* cells. Both have found a positive linear correlation between $\alpha_{alk\text{-}water}$ and irradiance. The field study conducted by Wolhowe et al. (2015) in the Gulf of California and the Eastern Tropical North Pacific observed that $\alpha_{alk\text{-}water}$ decreased with increasing depth; a relationship they attribute to a decrease in light availability or to an increase in proximity to the nutricline (thus an increase in growth rate). Van der Meer et al. (2015) found a positive relationship between $\alpha_{alk\text{-}water}$ and irradiance for the range of 15-200 µmol photon m^{-2} s^{-1}, with a maximum $\alpha_{alk\text{-}water}$ ~ 0.82 at an irradiance of 200 µmol photon m^{-2} s^{-1}. Beyond 200 µmol photon m^{-2} s^{-1} they observe $\alpha_{alk\text{-}water}$ to decrease similarly to what would be expected at the light-saturated end of a growth-irradiance curve during photoinhibition. A modified Eilers Peeters equation (Eilers & Peeters, 1988) fits the relationship (r^2=0.94), leading van der Meer et al. (2015) to suggest that irradiance might play an important role in influencing $\alpha_{alk\text{-}water}$ for these batch-cultured *E. huxleyi*. However, they conclude that irradiances higher than 500 µmol photon m^{-2} s^{-1}, often experienced during bloom-like conditions, would not significantly impact $\alpha_{alk\text{-}water}$. Furthermore, recent work by Weiss et al. (2017), who ran a batch-culture experiment with *E. huxleyi* at high light intensities, showed that the $\alpha_{alk\text{-}water}$ - salinity relationship holds true at high light

intensities (600 μmol photon m^{-2} s^{-1}), such that high light would not appreciably affect $\alpha_{alk\text{-}water}$ values in *E. huxleyi*. This finding, however does not speak to the effect of low light availability, for example at depth, on $\alpha_{alk\text{-}water}$. Furthermore, while algae at the ocean surface during a bloom would certainly be exposed to higher irradiances than those at depth, consideration of algal cells beneath the surface during the bloom shaded by the extensive cell concentrations at the surface would certainly be exposed to much lower light availability and this should be considered when discussing the effect of irradiance in the open-ocean environment.

Constraining the depth at which haptophyte species produce the alkenone molecules that are eventually recorded in the marine sedimentary record is crucial to quantify the uncertainty associated with irradiance's influence on $\alpha_{alk\text{-}water}$ and ultimately on the $\delta D_{alkenone}$ record. If in fact *E. huxleyi* cells from bloom assemblages are the primary origin of alkenones recorded in open-ocean sediments, it is possible that the effect of irradiance on the $\delta D_{alkenone}$ paleo-proxy would be minimal due to the observation that these organisms bloom at irradiances of greater than 530 μmol photon m^{-2} s^{-1} (Nanninga & Tyrrell, 1996, Harris et al., 2005; van der Meer et al., 2015), at which, van der Meer et al. (2015) suggest, there is no appreciable effect of irradiance on $\alpha_{alk\text{-}water}$. However, if the bulk of alkenone producers experience low-light regimes in the water column prior to final accumulation in the sediment, and low light availability is indeed found to impact $\alpha_{alk\text{-}water}$, this would have a direct impact on the $\delta D_{alkenone}$ signals recorded in the sediment.

TEMPERATURE

Growth-temperature effects on $\alpha_{alk\text{-}water}$ are also unresolved. Schouten et al. (2006) found no effect of temperature on $\alpha_{alk\text{-}water}$ for cultures of *E. huxleyi and G. oceanica*, whereas both the Zhang et al. (2009), working with green algae, and Wolhowe et al. (2009) working with *E.* huxleyi, found an increase in $\alpha_{lipid\text{-}water}$ with increasing temperature (2-4 $^{0}/_{00}$ °C^{-1}). A suite of temperature-induced changes to cellular physiology and growth - for example changes in the activity of NADP+ reducing enzymes or cellular metabolism - could potentially impact the isotopic signature of alkenones. However, these impacts are not yet fully understood. Recently, Wolhowe et al. (2015) found that in field samples from the Gulf of

California and Eastern Tropical North Pacific an apparent correlation between temperature and $\alpha_{alk\text{-}water}$ exists that opposes the negative correlations observed in lab culture studies. Temperature was positively correlated with $\alpha_{alk\text{-}water}$, suggesting that the effect of temperature in natural populations needs to be further constrained. It is important to recognize that temperature in the field will also co-vary with multiple environmental variables, especially with salinity; thus, it does not necessarily reflect an independent influence on fractionation in the field as it would in a controlled, single-variable manipulation of a laboratory culture.

NUTRIENT LIMITATION AND GROWTH PHASE

Nutrient limitation, or stress-induced growth-phase changes have been found to impact $\alpha_{alk\text{-}water}$ and $\delta D_{alkenone}$ significantly. Wolhowe et al. (2009) and Sachs & Kawka (2015) found a three-fold increase in alkenone concentrations in cells that were nutrient-starved. A significant correlation between $\alpha_{alk\text{-}water}$ and nutrient-stress induced growth-phase changes - such that $\alpha_{alk\text{-}water}$ decreases (i.e. hydrogen fractionation between alkenones and growth water increases) as the cells shift from exponential to nutrient-stressed stationary growth - further complicates the $\delta D_{alkenone}$ paleo-salinity proxy (Wolhowe et al., 2009; 2015). *E. huxleyi* culture experiments have shown that stationary-phase alkenones have consistently lighter $\delta D_{alkenone}$ (D-depleted) relative to exponential or log phase-synthesized alkenones (Wolhowe et al., 2009; 2015), with $\alpha_{alk\text{-}water} = 0.819 \pm 0.003$ during exponential and $\alpha_{alk\text{-}water} = 0.792 \pm 0.003$ during stationary phase growth (Wolhowe et al., 2009). Interestingly, Englebrecht & Sachs (2005) measured $\delta D_{alkenone}$ from core-top samples on the Scotian Margin and δD_{water} of overlying surface waters; with a resulting $\alpha_{alk\text{-}water} = 0.79$, which is equal to that found for stationary phase *E. huxleyi* culture cells (Wolhowe et al., 2009). This finding suggests that perhaps alkenones reaching the seafloor are from stationary growth-phase producers.

A mechanism proposed to explain the trends here has been attributed to an increasingly D-depleted internal water pool as cell division is reduced in stationary phase growth, with little exchange between external (D-enriched) water, while NADPH production continues and acetogenic lipid production increases resulting in more negative (lighter) $\delta D_{alkenone}$ during stationary phases (Sachse et al., 2012). The

proposed effects of nutrient-stress induced growth phase changes on $\alpha_{alk\text{-}water}$ are greater than the effect δD_{water} variation would have on the $\delta D_{alkenone}$ signal in open-ocean settings (Wolhowe et al., 2009), implying a growth-phase signal rather than a δD_{water} or salinity signal may be recorded in alkenone molecules. Ideally, improved sampling of internal cell water would facilitate a better understanding of these processes.

If in fact the response of $\alpha_{alk\text{-}water}$ is a continuous function of growth phase changes from exponential or log growth to stationary or nutrient-limited stress, as it was suggested by Wolhowe et al. (2009), it is possible that $\delta D_{alkenone}$ could be indicative of a certain phase of growth akin to what would be expected at the onset (exponential-phase) and termination (stationary-phase) of *E. huxleyi* blooms in the field (Wolhowe et al., 2015). Perhaps, $\delta D_{alkenone}$ could then be utilized to determine growth phase and/or stress of alkenone producers at the time of alkenone synthesis and thus reduce uncertainties associated with U^{K}_{37}' values as well as pCO_2 paleo-reconstructions. Nonetheless, processes such as high growth rates and low light availability have been reported to cause increases in isotopic fractionation between alkenones and growth water (Schouten et al., 2006; Sachs & Kawka, 2015; van der Meer et al., 2015; Wolhowe et al., 2015). For example, Sachs and Kawka (2015) report an increase in fractionation of ~ 25-38 ‰ $(div^{*}day^{-1})^{-1}$ in *E. huxleyi* cultures associated with increases in growth rates from 0.2 to 1 div/day. In this case, the interpretation of low $\alpha_{alk\text{-}water}$ values in the sediment record could be indicative of either of these two opposing scenarios (i.e. high growth rate vs. stationary phase growth).

Overall, while it has become increasingly clear that many non-salinity related factors influence alkenone hydrogen isotope fractionation and thus possibly compromise the use of $\delta D_{alkenone}$ as a salinity proxy (see Table 1.1 for summary), it must be noted that many of these inferred controls are based on laboratory culture studies that isolate, and possibly exaggerate, the effects of individual parameters on $\delta D_{alkenone}$. Furthermore, most of these culture studies do not necessarily reflect ranges of δD_{water}, salinity, nutrient concentrations or light levels, as well as community compositions, effects of grazing, and vertical distribution throughout the water column commonly associated with most alkenone producers in the open-ocean

environment. Nor are they conducted on the same timescales at which these factors would affect natural communities.

To shed light on the significance of these influences from a natural environmental perspective, I present the first large-scale field study testing the validity of this proxy in the open-ocean, under natural environmental conditions. I investigate the relationship between the $\delta D_{alkenone}$ and δD_{sw} of surface ocean suspended particulate organic material (SPOM) collected from both a ~100-degree latitudinal transect in the Atlantic Ocean and a ~ 50-degree latitudinal transect in the Western Pacific and compare these results to the findings of the culture studies and field experiments summarized above (Table 1.1).

Table 1.1 Summary of reported influences on $\alpha_{lipid\text{-}water}$ values from Ladd et al. (2017). It should be noted that this table includes information from studies that also evaluate algal species and lipid biomarkers other than the open-ocean species and alkenone biomarkers evaluated in this study.

Table 1. Summary of expected changes in $\alpha_{lipid\text{-}water}$ in response to different environmental variables, based on laboratory cultures and field studies in marine settings.

Variable	Sign of correlation with $\alpha_{lipid\text{-}water}$	Magnitude	References
Temperature	Negative	2–4 ‰ $°C^{-1}$	Zhang et al. (2009b); Wolhowe et al. (2009)
Growth rate	Negative	~ 30 ‰ division^{-1} day^{-1}	Schouten et al. (2006); Zhang et al. (2009b); Sachs and Kawka (2015); Wolhowe et al. (2015)
Nutrient availability	Negative	~ 40 ‰ difference between nutrient limited and nutrient replete cultures	Zhang et al. (2009b); Wolhowe et al. (2015)
Light availability	Positive	Below ~ 250 µmol photons m^{-2} s^{-1}, ~ 0.2 ‰ µmol^{-1} photons m^{-2} s^{-1}	van der Meer et al. (2015); Wolhowe et al. (2015); Sachs et al. (2017)
Salinity	Positive	0.5–3 ‰ practical salinity unit (PSU)$^{-1}$	Schouten et al. (2006); Sachse and Sachs (2008); Sachs and Schwab (2011); Chivall et al. (2014); M'boule et al. (2014); Nelson and Sachs (2014); Heinzelmann et al. (2015b); Maloney et al. (2016); Sachs et al. (2016)
Species assemblage	Variable	Differences up to 160 ‰ observed for $nC_{16:0}$ fatty acid among species growing under identical conditions	Schouten et al. (2006); Zhang and Sachs (2007)

1.3 Thesis Objectives

1. To measure $\delta D_{alkenone}$ and to derive the fractionation factor ($\alpha_{alk\text{-}water}$) from a set of filtered particulate samples taken from open-ocean surface waters.
2. To evaluate variability in the fractionation between $\delta D_{alkenone}$ and δD_{water}, and in particular in the relationship between the fractionation factor ($\alpha_{alk\text{-}water}$) and surface ocean salinity.

3. To compare the relationships between (a) $\delta D_{alkenone}$ and δD_{water},(b) $\alpha_{alk\text{-}water}$ and SSS and (c) $\delta D_{alkenone}$ and SSS in these open-ocean particulate samples to relationships previously established from laboratory cultures and small-scale field studies.
4. To compute a measure of uncertainty for the reconstruction of salinity from alkenone hydrogen isotopic values measured in sediment cores based on the open-ocean SPOM calibration presented here.

1.4 Thesis Outline

In Chapter 2, I present the research methodology, including the field-work and laboratory protocol, as well as details of ancillary data collection. This section also includes a discussion of uncertainties and limitations associated with the study. In Chapter 3, I present the raw data obtained from field-work and laboratory analyses, as well as the linear regression analyses between key parameters - $\delta D_{alkenone}$, δD_{water}, the fractionation factor ($\alpha_{alk\text{-}water}$) and salinity - in addition to a comparison with previously established (cultured algae) $\delta D_{alkenone}$ vs. δD_{water}, $\alpha_{alk\text{-}water}$ vs. salinity, and $\delta D_{alkenone}$ vs. salinity relationships. This is followed, in Chapter 4, by an investigation of the observed scatter in the SPOM data. Through the evaluation of $\alpha_{alk\text{-}water}$ and $\delta D_{alkenone}$ residual values, a number of SPOM samples (6 of 69) are characterized as having 'anomalous' isotopic signatures relative to the remainder of the samples. As an exercise, I remove these data from analysis and re-evaluate the $\delta D_{alkenone}$ vs. δD_{water}, $\alpha_{alk\text{-}water}$ vs. salinity, and $\delta D_{alkenone}$ vs. salinity relationships for a reduced SPOM dataset and compare them with published culture study relationships. I conclude this discussion with a quantification of uncertainty associated with SSS reconstructions from $\delta D_{alkenone}$ records via an inversion of the regression describing the $\delta D_{alkenone}$ vs. SSS relationship for the reduced SPOM dataset. Finally, I provide an outlook on possible future analyses and unresolved research questions in Chapter 5.

CHAPTER 2: METHODS

In this chapter, the datasets analyzed in this study are introduced, along with a description of the field collection of samples, laboratory methodology, the statistical approaches for analysis and associated uncertainties and limitations.

2.1 Field Sampling

2.1.1 Atlantic Ocean

A set of 46 samples of filtered sea-surface (0-5m) suspended particulate organic matter (SPOM) was collected between October and November 2010, along an Atlantic Meridional Transect (AMT20) spanning approximately 100° of latitude, from Southampton, UK, to Punta Arenas, Chile (Figure 2.1(a)). In situ surface (~5m depth) temperatures (°C) and salinities were obtained from the ship's hull-mounted SBE45 MicroTSG thermosalinograph. Data were recorded at one-minute intervals while underway. Reported accuracy of the thermosalinograph temperature and salinity measurements are 0.002°C and 0.005, respectively (metadata report for BODC series reference number 1762212). An average of 550 ± 135 litres of sea surface water from the ship's underway seawater pump was filtered through 142mm glass-fibre filters (0.45 µm pore size) for each sample. The samples were filtered over a period of 10 hours on average. Filters were subsequently wrapped in pre-combusted aluminum foil, contained within plastic zip-locked bags and stored in a freezer (-20 °C) onboard the research vessel in preparation for analysis. Additionally, surface ocean water samples were taken in 60-ml glass amber bottles (boston round) from the same ship's underway intake system at the beginning of each sampling period for water isotopic composition analysis.

2.1.2 Western Pacific

A set of 10 samples of filtered sea-surface (0-5m) SPOM collected in May of 2010 along a transect spanning ~31° latitude in the Western Equatorial Pacific (onboard the R/V Sonne Cruise SO228) and a set of 13 SPOM samples collected in May of 2017 along a transect spanning 21° latitude from Auckland, NZ to the Torres Strait (onboard the R/V Sonne Cruise SO256) are also analyzed in this study (Figure

2.1 (b)). Samples collected during the SO228 and SO256 cruises are referred to as the Northern West Pacific and Southern West Pacific samples, respectively. An average of ~300 ± 100 litres of sea surface water were filtered through 142mm glass fibre filters (0.45 µm pore size) for each sample. The samples were filtered over a period of 3 hours on average. Filters were subsequently wrapped in pre-combusted aluminum foil, contained within plastic zip-locked bags and stored in a freezer (-20 °C) onboard the research vessel in preparation for analysis. Additionally, surface ocean water samples were taken in 60-ml glass amber bottles at the beginning of each sampling period for water isotopic composition analysis.

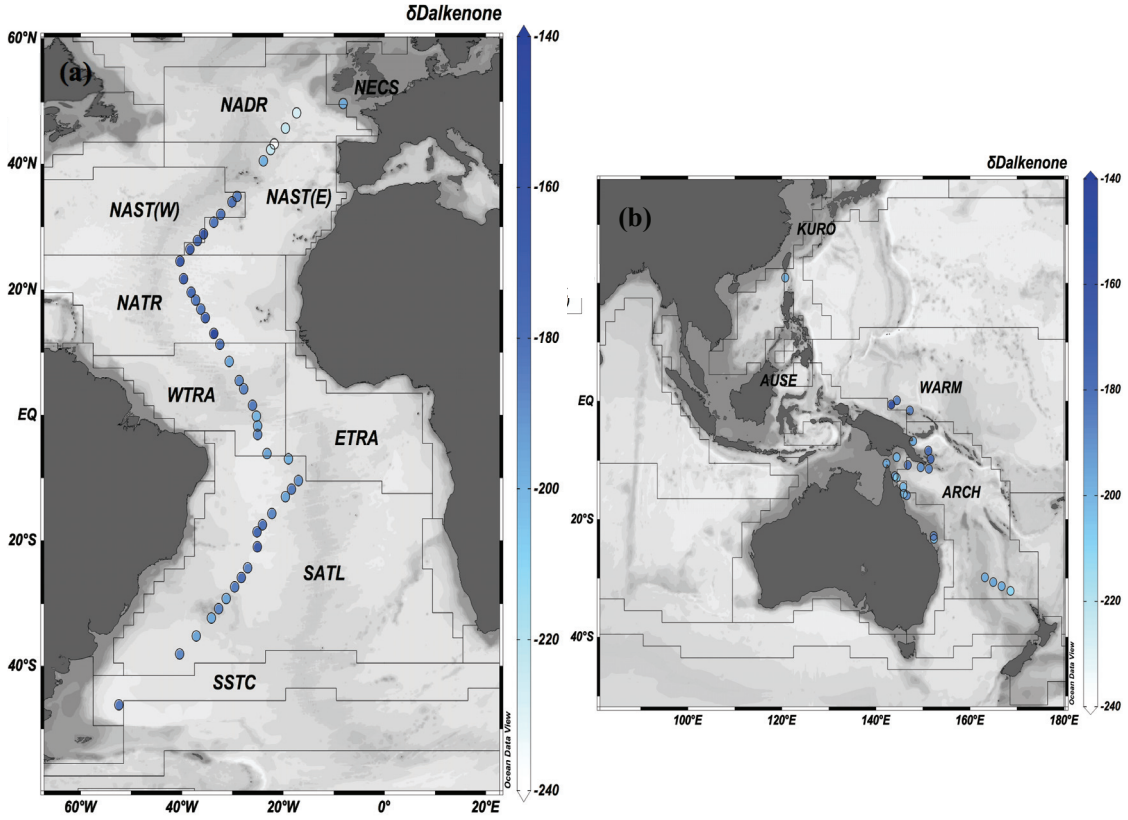

Figure 2.1: (a) AMT20 sample locations. **(b)** Pacific Ocean sample locations. Colour bar indicates $\delta D_{alkenone}$ values (‰). Also shown are the Longhurst (2007) biogeochemical provinces. (Figure constructed in ODV [Schlitzer, R.] using an imported Longhurst Biogeographical Provinces shapefile [VLIZ, 2009]).

All data (69 SPOM samples), from both the Atlantic and Pacific basins are evaluated together as a singular dataset in the following analyses, as there is no obvious a priori reason to separate the two: both contain samples from open-ocean

surface waters and from regions that have been observed to include the two most prevalent and globally ubiquitous species of alkenone producers (*E. huxleyi* and *G. oceanica*) (Conte et al., 1994a; Volkman et al., 1995). Furthermore, in their study Conte et al. (2006) conducted both regional (basin-scale) and global-scale calibrations of the alkenone unsaturation (U^{K}_{37}'; see Chapter 1.2.4 above) vs. SST proxy in a dataset of ~ 1400 global SPOM alkenone samples and concluded that a universal calibration of the U^{K}_{37}' temperature proxy was suitable. Through this analysis, Conte et al. (2006) determined that any species-specific factors that may affect the U^{K}_{37}' vs. SST relationship in the world's oceans must be minimal. Indeed, when the U^{K}_{37}' data from both the Atlantic and Pacific SPOM data presented here (see Chapter 4.2 - Figure 4.1) are regressed against SST, the agreement with previously published data from the Atlantic, Indian and Pacific oceans indicates a globally-consistent signal. Because there is no comparable large-scale evaluation of the global surface-ocean $\delta D_{alkenone}$ vs. δD_{water} relationship, I cannot confidently draw the same conclusions about a universal calibration in the hydrogen isotope proxy. Nonetheless, for this first-order analysis of open-ocean SPOM alkenone isotopic data, I assume that the conclusions of Conte et al. (2006) apply and that any genetic variation on a basin-level scale minimally, if at all, impacts open-ocean alkenone synthesis. Therefore, I evaluate both the Atlantic and Pacific data sets together.

2.2 Laboratory Methodology

2.2.1 Surface Water Isotope Analysis

δD_{water} was measured on surface ocean water collected from the ship's hull-mounted underway seawater pump system only once at the beginning of the filtration period for each individual AMT and Pacific SPOM sample. Atlantic Ocean water isotope analysis was performed by GEOTOP-UQAM on a Micromass Isoprime™ dual inlet Isotope Ratio Mass Spectrometer (IRMS) coupled to an Aquaprep™ system with an analytical uncertainty of 1‰ for δD_{water}, and Pacific Ocean water analysis was performed at Dalhousie University on a Picarro water analyzer (L2130-i) with an analytical uncertainty of 0.3‰.

2.2.2 Alkenone Extraction and Quantification

At Dalhousie University, each 142 mm SPOM filter was cut with sterile scissors and placed in 60ml combusted glass vials. An internal standard (100 µl of hexatriacontane; Sigma #52919 was added to each vial prior to lipid extraction as a reference for determining alkenone concentrations. A series of three-10-minute sonications first with methanol (MeOH), then with a 1:1 solution of MeOH: dichloromethane (DCM), and finally with only DCM, was used to extract organic matter from each filter. The supernatant was decanted after each sonication period, and was subsequently concentrated until almost dry using a standard nitrogen (N_2) evaporation bath. The resulting total lipid extracts (TLE) were subsequently removed from each vial using a sterile glass pipette, and concentrated into 4ml vials**.** A 5% split of the total lipid extract was then performed with DCM for additional subsequent analysis if required. The TLEs were saponified using a solution of 0.1M Potassium Hydroxide (KOH) in MeOH, facilitated with a heating plate set at 85 °C for a period of 2 hours. Separation of the lipids from the MeOH solution was achieved using a mixture of E-pure water and hexane, transferring with a sterile glass pipette. After drying the lipid fraction overnight in the fume hood, column separation using combusted 10%-deactivated silica gel was conducted to produce apolar, polar, and ketone fractions. Apolar and polar fractions were set aside for alternate analysis, and the ketone fractions were transferred to small Gas-Chromatograph (GC) vials with glass inserts for GC analysis.

Individual samples of 1µl were then injected by autosampler into the GC (Agilent Technologies 6890N Network GC system coupled with a 7683B Series Injector). A standard GC coupled Flame Ionization Detector (FID) method was used for alkenone detection and quantification, based on retention time in comparison to an *Emiliania huxleyi* culture extract (see Figure 2.2 for example chromatogram). The analytical precision of the GC was determined from 10 repeat injections of a selected alkenone extract resulting in a standard deviation of ±0.003 U^{K}_{37}' units (the ratio of di- to tri-unsaturated alkenones detected in a sample where U^{K}_{37}' = C37:2/ [C37:2 + C37:3]), well within a published analytical error of ±0.01 U^{K}_{37}' units (Müller et al., 1998).

Quantification of alkenone concentrations in each sample vial, necessary for the hydrogen isotopic composition analysis, were computed using the peak area measured from the GC-FID chromatograms converted to concentration via a pre-established calibration curve developed from subsequent dilutions of an alkenone standard. Concentrations were then divided by sample injection volume (100 µl) to arrive at a quantification of alkenone material per sample vial. These quantities (ng) were then corrected for the volume of surface water filtered (l) to estimate alkenone concentration (ng/l). With the exception of AMT sample #1, which had a very high alkenone content (84 ng/l), alkenone contents ranged between 0.6 ng/l and 23.8 ng/l with an average of 8 ng ±6 ng/l for all samples (Table A1 in Appendix).

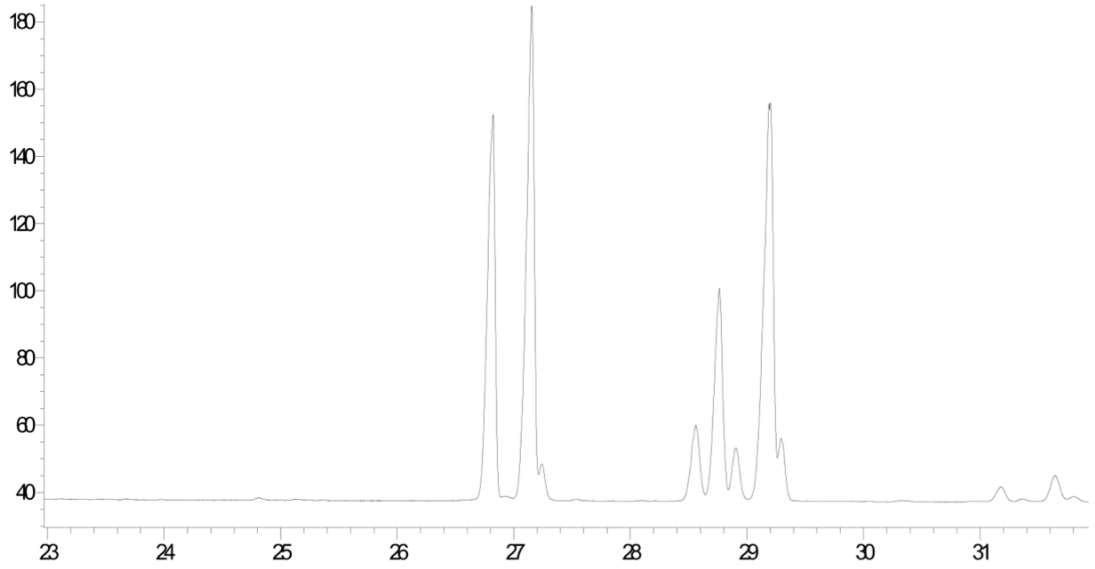

Figure 2.2: Chromatogram for an *E. huxleyi* reference culture injected on the GC-FID at Dalhousie University. The y-axis shows peak amplitude, and the x-axis shows the elution time (min). The two peaks at 26.8 and 27.2 minutes are the tri- and di-unsaturated alkenone peaks, respectively.

2.2.3 Alkenone δD Analysis

Compound-specific isotope analysis was performed on a Thermo Scientific MAT 253™ Continuous Flow IRMS coupled via a GC IsoLink operated at 1420 °C to a Thermo Fisher Scientific TRACE™ GC equipped with a HP-5ms column (30m, 0.25 mm, 1 um; GC – Gas Chromatograph). These analyses were performed at

MARUM in Bremen, Germany, in August-October 2016. Alkenone δD was estimated from both the C37:3 and C37:2 alkenones combined rather than separately to prevent bias (van der Meer et al., 2013; Chivall et al., 2014). 5µl of each sample was injected at a concentration of approximately 100ng・compound^{-1}・µl^{-1} in duplicate or triplicate, when quantities allowed. A cut off for acceptable precision of ±5 ‰ for repeat analysis was followed, where all repeat injections outside of this uncertainty have been omitted from this study. The average standard deviation from repeat injection of all samples measured was ± 2 ‰. N-alkane standards with known isotope composition were injected every 6 measurements to track and to maintain analytical accuracy. The long-term mean standard deviation of external alkane standards was ±3 ‰ (n=4737). The H_3^+ factor was determined daily using H_2 reference gas to correct for its influence on the δD signal. The H_3^+ factor consistently varied less than 0.01. Finally, analytical precision was quantified by repeat analyses of a single *E. huxleyi* sample from a culture grown at Dalhousie University. The sample was collected by filtering culture through glass-fibre filters. Three filters were subsequently treated for alkenone extraction and quantification. Each sample was then injected in the mass-spec 6 times. The average $\delta D_{alkenone}$ value was -225 ‰ for the culture with an overall standard deviation of ± 2 ‰.

To address whether sample vial alkenone quantity (ng) had an effect on the measurement error (standard deviation) in MS isotopic analysis, standard deviations of repeat isotopic measurements were regressed against the mass of alkenone (ng) in each sample vial (determined from initial GC quantification, see above). No significant relationship between the two parameters exists (p-value = 0.26) suggesting that alkenone quantity does not bias the estimate of alkenone isotopic composition.

2.2.4 Alkenone $\delta^{13}C$ Analysis

Analysis of $\delta^{13}C_{alkenone}$ for both the Atlantic and Pacific samples was conducted at MARUM, Bremen, in August-October 2016. The analysis was done in the same manner as $\delta D_{alkenone}$ determination, by injection of 100ng・compound^{-1}・µl^{-1} on a GC-coupled Isotope Ratio Mass Spectrometer and calibrated against CO_2

reference gas with known isotopic composition. A total of 41 $\delta^{13}C_{alkenone}$ values were measured. Values ranged between -24‰ and -33‰ with an average error of ± 0.2‰.

2.3 Ancillary Data

The Atlantic Meridional Transect (AMT) is a program that has been running for ~ 20 years, conducting annual transects to obtain a suite of open-ocean chemical, biological and physical data. A number of ancillary datasets exist that are complimentary to the research questions at hand. Data that were obtained from the British Oceanographic Data Center (BODC) online repository include the underway thermosalinograph measurements of SSS, SST, as well as nutrients (nitrate and phosphate; µmol l^{-1}) and marker-pigment concentrations (19' – hexanoyloxyfucoxanthin (19'-hex); ng l^{-1}) collected by CTD deployments along the AMT20 (Airs et al., 2014). These ancillary data facilitate the investigation of environmental and physiological factors that have been shown to affect $\delta D_{alkenone}$ in culture studies (as reviewed above).

Average SSS and SST values were calculated for each Atlantic SPOM sample as the mean of all measured values from the ship's hull-mounted thermosalinograph. Data collected at 1-minute intervals during the entire duration of each individual filter sample were averaged for comparison with the alkenone data. Similarly, underway SSS and SST values were obtained for the Southern West Pacific transect from the ship's hull-mounted thermosalinograph but at 5-minute intervals for the entire period of filtration per sample. SST values for the Northern West Pacific transect, on the other hand, were obtained from the ship's underway thermosalinograph only at the start and end time of sampling for each filter collected. Average SST values for this transect were therefore calculated as the average between the beginning and ending values. SSS values for the Northern Pacific transect samples were measured at Dalhousie University using the same water samples collected for δD_{water} analysis at only the beginning of each filter sample. The accuracy in these salinity measurements was ±0.003 and the precision was ±0.0003. No nutrient nor marker pigment data were available for either of the Pacific datasets.

2.4 Uncertainty & Limitations

2.4.1 Analytical & Sampling Uncertainty

The fact that $\delta D_{alkenone}$ signatures are measured on underway filtered alkenone particles (a time and space-integrated signal), and are compared with only a snapshot sample of δD_{water} at the start of each filtration period, likely introduces error in the regression between the two parameters as well as in the computation of $\alpha_{alk\text{-}water}$. These errors are likely less pronounced for the relationship between $\delta D_{alkenone}$ and average SSS values, where average SSS are computed for most of the samples (not for the Northern West Pacific samples) as the mean value of all underway SSS readings measured during a filtration, a value likely to be more representative of the surface waters the alkenone particulates were indeed sampled from (see Chapter 2.3).

An analysis of the range in SSS measured during filtration can be used to estimate the potential ranges in δD_{water} over the same period in order to assess the potential variability in δD_{water} experienced over a given filtration period. A regression of δD_{water} on SSS from a database of global surface-ocean is used in this exercise. Values were measured between 0-10m depth on open-ocean samples collected between 60°N and 50°S, giving the relationship $\delta D_{water} = 3.10(\text{Salinity}) - 106.12$; Schmidt et al., 1999). I estimate the expected variability in δD_{water} associated with the ranges in SSS measured for each sample by assuming that this relationship holds for the surface waters sampled in this study.

The range of SSS and SST experienced during any single filtration was calculated for both the AMT underway surface waters and Southern West Pacific surface waters only, because no continuous underway thermosalinograph data are available for the Northern West Pacific cruise. Looking at this dataset, and excluding one sample taken at 46°S along the AMT (#60) with a SSS range of 1.5, *in situ* SSS values during a single filtration period varied on average by 0.24 (maximum – minimum) with a maximum variation of 0.81 and minimum of 0.04. Likewise, excluding AMT #60 with a 4.7 °C SST range, SST values varied on

average by 0.6 °C SST with a maximum of 1.95°C and a minimum of 0.08°C, during any single filtration period.

With an average range in salinity of 0.24 per filtered sample, the accompanying average variation in δD_{water} is quantified to be ~0.7 ‰, based on the global δD_{water} –SSS regression above. This translates to an average error in our estimate of $\alpha_{alk\text{-}water}$ by only ~0.0007; an order of magnitude smaller than the analytical error associated with the computation of $\alpha_{alk\text{-}water}$ (±0.002). In addition, the residual values of $\alpha_{alk\text{-}water}$ (the differences between measurements and values estimated from linear regression of $\alpha_{alk\text{-}water}$ on SSS) were regressed on the range in SSS measured during sample filtration for all of the AMT and Southern Pacific data (including AMT #60). There was no statistically significant relationship (p-value = 0.06). For the purposes of this study, it is therefore assumed that these uncertainties are of a smaller magnitude than both the analytical uncertainty (±0.002) and errors associated with environmental/physiological factors that have been shown to significantly affect $\alpha_{alk\text{-}water}$ values (Table 1.1). They are thus ignored.

Additionally, the SPOM dataset presented here consists of alkenone samples collected at only one depth (~5m) from the ships' hull-mounted underway seawater pumps on all three cruises. These samples do not necessarily reflect alkenones synthesized only at 5m depth; therefore, I must consider the possibility that the alkenones sampled could have been synthesized at depths much greater than this. Water-column distribution studies have shown that alkenone producers (e.g., *E. huxleyi*) inhabit depths between 0 and ~200m in the open-ocean water column, in some cases deeper than the surface mixed-layer depth (e.g. Okada & Honjo, 1973; Winter et al., 1994; Kinkel et al., 2000). For instance, a number of sediment trap and core-top sediment studies have found evidence to suggest a significant component of the alkenone flux to the sediments is from subsurface synthesis in the thermocline and from below the surface mixed layer (Prahl et al., 1993; 2001;2005; Ternois et al., 1997; Ohkouchi et al., 1999; Bentaleb, 1999; Goñi et al., 2001; Harada et al., 2006; Richey & Tierney, 2016). Finally, because the sampling in this study is restricted to one depth, there is the possibility that the signal is not representative of the

alkenones that will eventually reach the sediments. Future studies that analyze alkenone samples at multiple depths in the water column, as well as in sediment traps and core-top sediments will help to elucidate the reality and significance of these uncertainties.

2.4.2 Limitations of Analyses

As the literature indicates, a suite of parameters found to affect $\alpha_{alk\text{-}water}$ signatures significantly (e.g. algal growth rates and phases, nutrient and light availability as well as species composition; see Table 1.1) are likely to impact the $\delta D_{alkenone}$ signatures in the samples evaluated in this study. Unfortunately, many of these parameters were not sampled, and therefore cannot be tested directly for their influence on the fractionation of hydrogen isotopes in the alkenones. Nonetheless, it is likely that the variability in $\alpha_{alk\text{-}water}$ measured in our study is a result of any number of possible combinations of species structure and/or variability in algal growth rates and phases in response to nutrient and light availability in the SPOM samples. For example, species-specific fractionation effects are known to vary $\delta D_{alkenone}$ values (Schouten et al., 2006). Field studies indicate that species-effects may overwhelm even the effect of salinity on fractionation, as hypothesized to occur in both the Chesapeake Bay (Schwab & Sachs, 2011) and Amazon plume regions (Häggi et al., 2015). As the majority of our samples are from open-ocean surface waters, I hypothesize that the effect of species-specific fractionation will be limited. The dominant species sampled are likely to be *E. huxleyi* and *G. oceanica*. Isotopic offsets between these two open-ocean species have been reported, such that *G. oceanica* $\delta D_{alkenone}$ values are consistently ~30‰ lighter than *E. huxleyi* grown under the same conditions (Schouten et al., 2006). Certainly, a mix of these two species has the potential to introduce scatter in the $\delta D_{alkenone} - \delta D_{water}$ relationship observed in this study.

In addition, and as with all samples from this dataset, allochthonous or 'detrital' alkenones are alternative possibilities for anomalous observations of $\alpha_{alk\text{-}water}$. It is important to be aware of other factors that are likely to affect the hydrogen isotopic signatures. Unfortunately, they cannot be directly investigated within the scope of this study. To my knowledge, this study is the first presentation of a strictly

open-ocean and large-scale analysis of $\delta D_{alkenone} - \delta D_{water}$ in SPOM alkenone samples. The objectives of the thesis thus remain; to present the isotopic values, to evaluate scatter in the data with such external parameters as are available, and to provide an estimate of uncertainty in the reconstruction of SSS using $\delta D_{alkenone}$ values.

2.5 Statistical Analysis

Linear regression was performed using the least-squares method and was primarily used to define relationships between $\delta D_{alkenone}$ and δD_{water}, $\alpha_{alk\text{-}water}$ and SSS, and $\delta D_{alkenone}$ and SSS. Statistical output from linear regression analyses, including evaluation of residual variance and normality are including in the Appendix. In addition, linear regression and in some cases multiple linear regression analyses were used to explore scatter in the $\delta D_{alkenone}$ and δD_{water}, $\alpha_{alk\text{-}water}$ and SSS, and $\delta D_{alkenone}$ and SSS relationships. Residual values were investigated for all three regressions, whereby residuals were defined as the difference between the observed response values ($\delta D_{alkenone}$ or $\alpha_{alk\text{-}water}$) and the predicted response values. In particular, $\alpha_{alk\text{-}water}$ values and residual values (for both $\delta D_{alkenone}$ and $\alpha_{alk\text{-}water}$) were regressed against alkenone concentrations (ng/l), SST (°C), and $\delta^{13}C_{alkenone}$ to investigate scatter in the relationships between $\delta D_{alkenone}$ and δD_{water}, $\alpha_{alk\text{-}water}$ and SSS, and $\delta D_{alkenone}$ and SSS. Statistical significance was set at the significance level $\alpha = 0.05$ throughout all regression analyses. An exercise in inverting and computing a confidence interval for the linear regression between $\delta D_{alkenone}$ and SSS was conducted with the R package *investr* (Greenwell & Schubert Kabban, 2014).

CHAPTER 3: RESULTS

3.1 Hydrographic Data

All surface ocean data including sampling coordinates, alkenone concentrations, U^{K}_{37}', $\delta D_{alkenone}$, corresponding surface-water δD_{water} as well as SSS, SST, nutrients ([NO_2+NO_3] and [PO_4]), and pigment data, where available, are provided in Appendix Table A1. AMT average SSS range between 34.69 and 37.65, a total range of 3. The freshest surface ocean waters are found in high latitudes (~48° N and ~47° S) and just north of the equator in a band between 0 and 10°N, likely a result of pronounced rainfall associated with the Inter Tropical Convergence Zone (ITCZ). Average West Pacific Ocean surface ocean salinities range between 32.86 and 36.00, with a total range of ~3. In total, the entire dataset (including AMT20, Northern and Southern West Pacific samples) covers a salinity range of ~ 5. Average SST values ranged between 12.7 °C and 29.1 °C (a range of ~16 °C) and between 22.5 °C and 30.4 °C (a range of ~ 8 °C) for the AMT20 and West Pacific Ocean transects, respectively. The temperature range over the entire dataset was ~18 °C.

3.2 Isotope Data

3.2.1 δD_{water} and Salinity

Surface ocean δD_{water} and salinity data from both the Atlantic and Pacific basins align well with a subset of global surface open-ocean data from Schmidt et al. (1999) (Figure 3.1), whereby δD_{water} increases with increasing salinity.

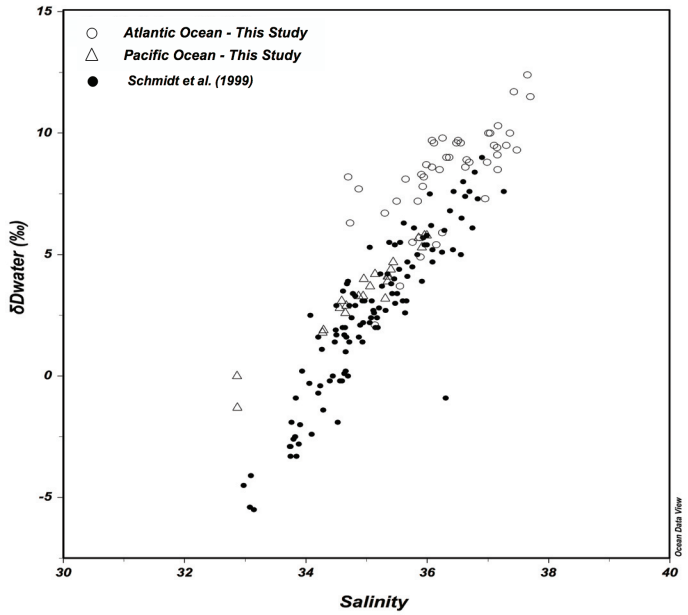

Figure 3.1 Scatter plot of surface ocean hydrogen isotopic signatures (δD_{water} ‰) versus surface ocean salinity from this study (Atlantic Ocean- open circles, Pacific Ocean- triangles) compared to a subset of surface ocean data from Schmidt et al. (1999; this subset includes data sampled between 0 and 10m depth and between 60°N – 50°S in the Atlantic, Pacific and Indian Oceans only, excluding deeper samples, and data from the Mediterranean and the Arctic Ocean).

3.2.2 $\delta D_{alkenone}$ and δD_{water}

$\delta D_{alkenone}$ values range between -239‰ and -147‰ (range of 92‰). The lightest $\delta D_{alkenone}$ values are found between ~48 and 42 °N in the Atlantic basin with the heaviest $\delta D_{alkenone}$ values at 13 °N in the Atlantic basin ($\delta D_{alkenone}$ = -147‰) and at 0.6 °S in the Pacific basin ($\delta D_{alkenone}$ = -163‰). Associated δD_{water} values range between -1‰ and 12‰, with a range of 13‰. The lightest δD_{water} values were found in the Pacific basin nearest to the equator, and in the northern North Atlantic basin; the heaviest values were recorded at the mid latitudes in both the Atlantic and Pacific basins. Linear regression of δD_{water} on $\delta D_{alkenone}$ for the entire dataset is statistically significant (p-value = 0.001), with a positive trend: ($\delta D_{alkenone}$ = $1.85\pm0.55(\delta D_{water}) - 202\pm4$; $R^2 = 0.14$, n = 69; Figure 3.2 (a); see Appendix Table A2 and Figure A1). It should be noted that while $\delta D_{alkenone}$ appears to be negatively correlated with δD_{water} for the West Pacific Ocean, the relationship is not statistically significant (p-value = 0.13; see Appendix Table A3, and Figures A2 & A3).

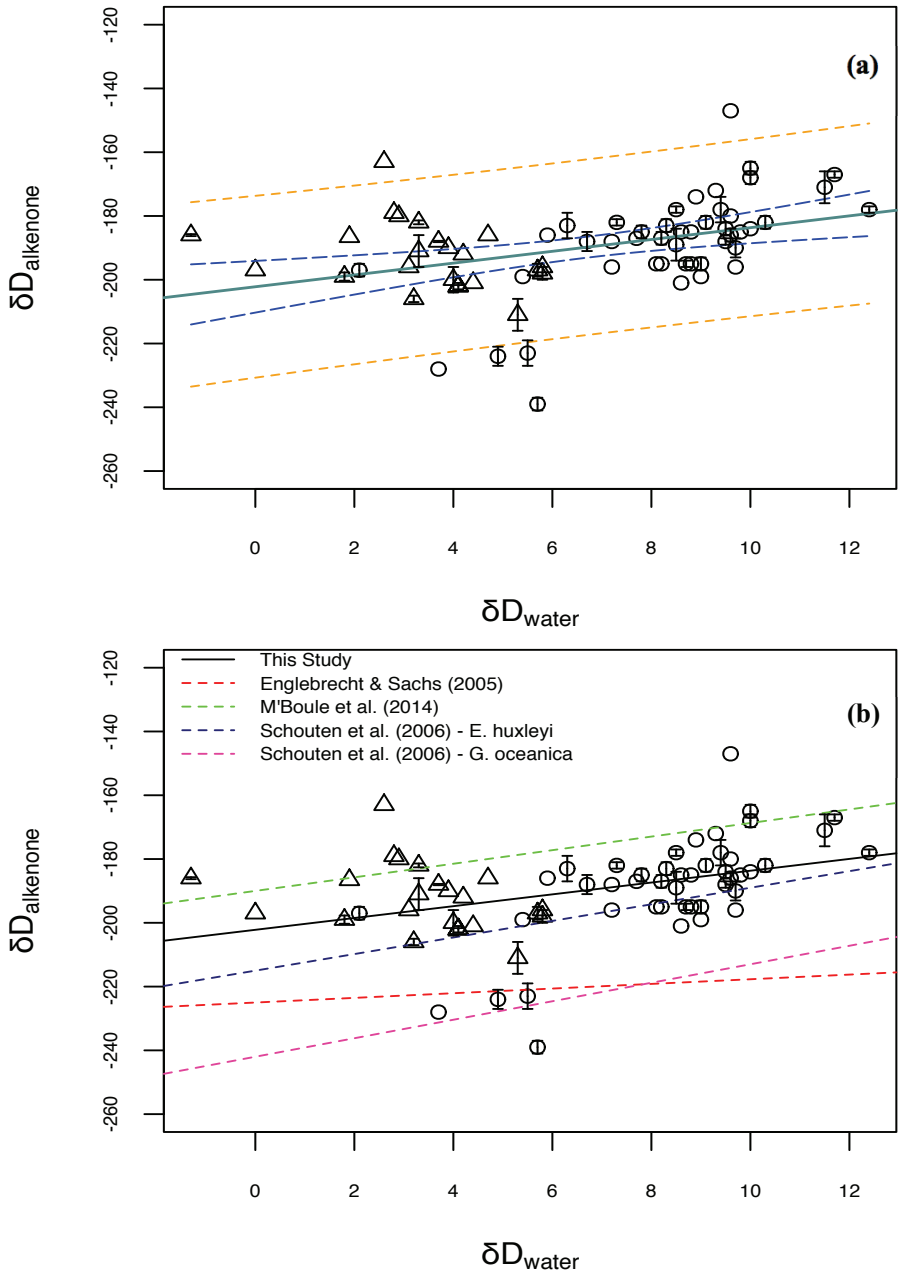

Figure 3.2: (a) Linear regression (teal line) between $\delta D_{alkenone}$ and δD_{water} for 69 SPOM samples (46 Atlantic Ocean samples: circles and 23 Pacific Ocean samples: triangles) $\delta D_{alkenone} = 1.85^* \delta D_{water} - 202$ ($R^2 = 0.14$, p-value = 0.001, n = 69). Also shown are the 95% confidence (blue-dashed lines) and prediction intervals (yellow-dashed lines). **(b)** Linear regression (black solid line) between $\delta D_{alkenone}$ and δD_{water} for 69 SPOM samples. Shown also are the culture study regressions from Englebrecht & Sachs 2005 (red), Schouten et al. 2006 (*E. huxleyi:* dark blue, *G. oceanica*: pink), and M'Boule et al. 2014 (green). Error bars in both figures indicate standard deviation of replicate isotope analysis. Samples without repeat injection are shown with no error bars.

Figure 3.2 (b) shows the relationship between $\delta D_{alkenone}$ and δD_{water} found in this study along with previously-published relationships from laboratory culture studies **(**refer to Chapter 4, Table 4.2). The slope of the $\delta D_{alkenone}$ vs. δD_{water} relationship from the open-ocean samples is similar to, and falls within two standard errors of, the slopes determined from laboratory cultures (Table 4.2). While scatter exists over the entire relationship, six SPOM data fall outside the 95% prediction interval of both the linear regression describing this dataset and published relationships from culture. These are discussed in further detail in Chapter 4.

3.2.3 Fractionation Factor (Alpha: $\alpha_{alk\text{-}water}$)

Considerable variability in the fractionation factor ($\alpha_{alk\text{-}water}$ – Equation 1) in the dataset is observed, with values ranging between 0.76 and 0.84, and a total spread of 0.08 units. The $\alpha_{alk\text{-}water}$ values determined here have an average associated error of ±0.002, which accounts for the analytical errors in both measurement of $\delta D_{alkenone}$ and of δD_{water} (see Appendix Equation A1 for error propagation method). Regression of $\alpha_{alk\text{-}water}$ on SSS for the entire dataset was not significant (p-value = 0.23; Figure 3.3 (a); see Appendix Table A4 and Figure A4).

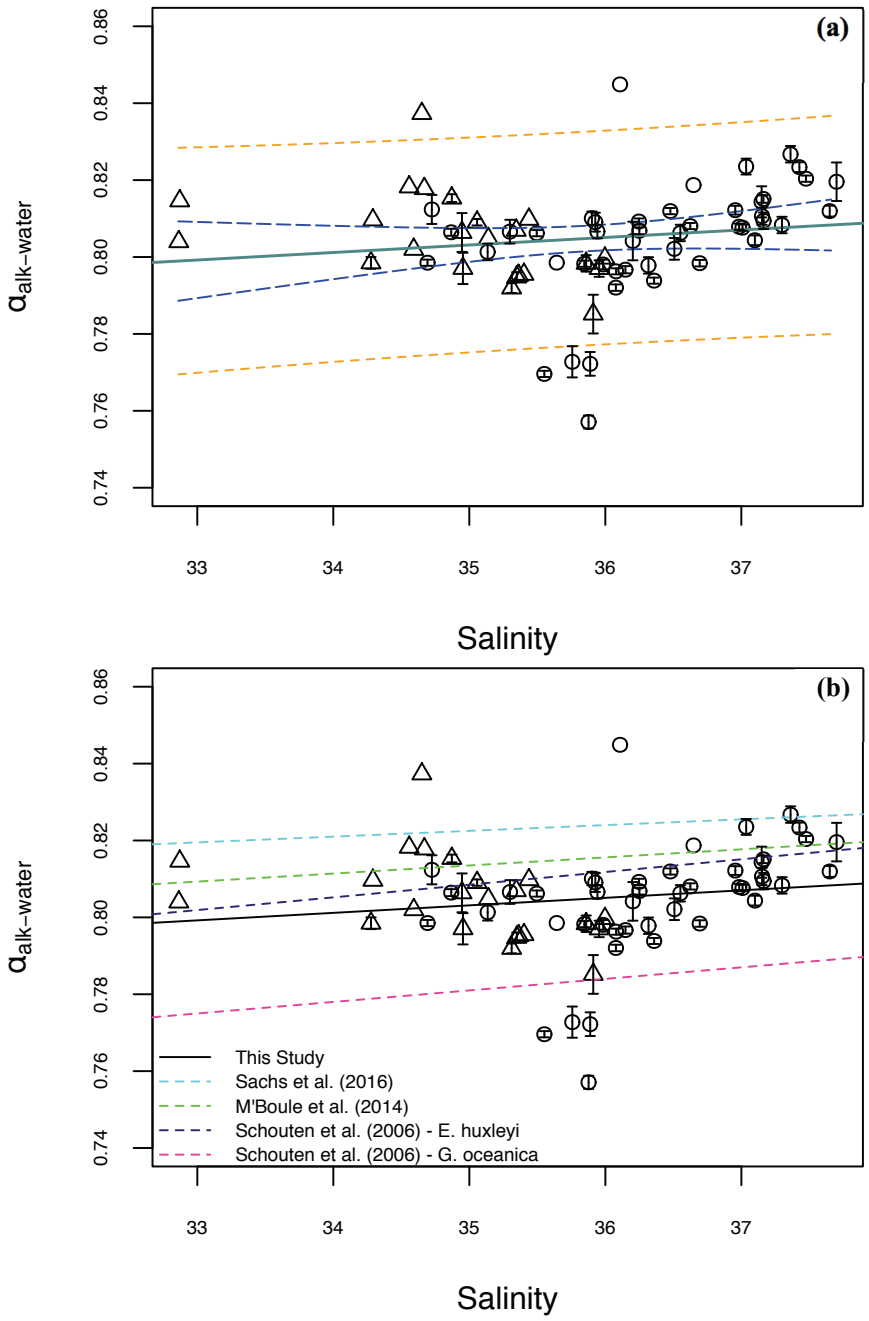

Figure 3.3: (a) Linear regression (teal line) between $\alpha_{alk\text{-}water}$ and SSS for 69 SPOM samples (46 Atlantic Ocean samples: circles and 23 Pacific Ocean samples: triangles) $\alpha_{alk\text{-}water} = 0.002 * \text{Salinity} + 0.735$ ($R^2 = 0.02$, $p = 0.232$, $n = 69$). Also shown are the 95% confidence (blue-dashed lines) and prediction intervals (yellow-dashed lines). **(b)** Linear regression (black solid line) between $\alpha_{alk\text{-}water}$ and salinity for 69 SPOM samples. Shown also are the culture study regressions from Schouten et al. 2006 (*E. huxleyi:* dark blue, *G. oceanica*: pink), and M'Boule et al. 2014 (green) and Sachs et al. 2016 (light blue). Error bars in both figures indicate calculated error in derived $\alpha_{alk\text{-}water}$. Samples without repeat injection are shown with no error bars.

Figure 3.3 (b) shows the relationship between $\alpha_{alk\text{-}water}$ and SSS observed in this dataset along with previously-published relationships from laboratory cultures (refer to Chapter 4, Table 4.3). While the $\alpha_{alk\text{-}water}$ vs. SSS relationship for the SPOM data is not significant (p-value = 0.23), the central tendency falls within one standard error of all of the slopes reported from the laboratory studies. A group of outliers with markedly lower $\alpha_{alk\text{-}water}$ values (between 0.76 and 0.77) relative to the majority of the dataset sampled from the northern region of the AMT20 transect (AMT20 #2-5) as well as two high $\alpha_{alk\text{-}water}$ values (0.84: AMT20 #22 and Northern West Pacific #31) are discussed in detail in Chapter 4.

3.2.4 $\delta D_{alkenone}$ and SSS

$\delta D_{alkenone}$ is significantly correlated with *in situ* average SSS values (p-value = 0.018): $\delta D_{alkenone} = 4.04 \pm 1.7(SSS) - 335 \pm 60$ ($R^2 = 0.08$, n = 69; Figure 3.4 (a); see Appendix Table A5 and Figure A5 for regression output).

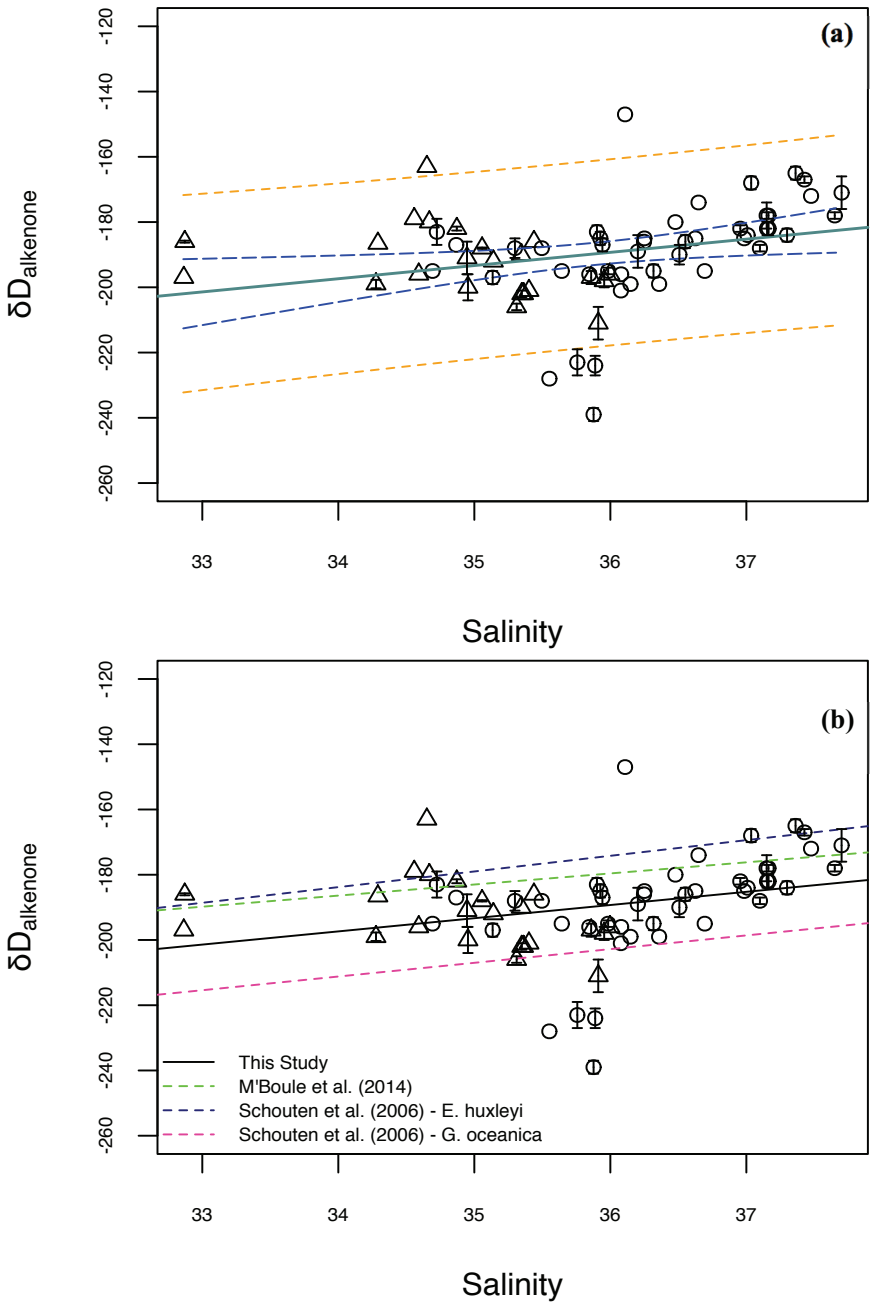

Figure 3.4: (a) Linear regression (teal line) between $\delta D_{alkenone}$ and SSS for 69 SPOM samples (46 Atlantic Ocean samples: circles and 23 Pacific Ocean samples: triangles) $\delta D_{alkenone} = 4.04 * Salinity - 335$ ($R^2 = 0.08$, $p = 0.018$, $n = 69$). Also shown are the 95% confidence (blue-dashed lines) and prediction intervals (yellow-dashed lines). **(b)** Linear regression (black solid line) between $\delta D_{alkenone}$ and salinity for 69 SPOM samples. Shown also are the culture study regressions from Schouten et al. 2006 (*E. huxleyi:* dark blue, *G. oceanica*: pink), and M'Boule et al. 2014 (green). Error bars in both figures indicate standard deviation of replicate isotope analysis. Samples without repeat injection are shown with no error bars.

Figure 3.4 (b) shows the relationship between $\alpha_{alk\text{-}water}$ and SSS from this study alongside previously-published relationships from laboratory cultures (refer to Chapter 4, Table 4.4). Most of the open-ocean $\delta D_{alkenone}$ values (~80%) fall between relationships established for *E. huxleyi* and *G. oceanica* in culture (Schouten et al. 2006). The slope of the $\delta D_{alkenone}$ vs. SSS relationship (Figure 3.4 (b)), falls within one standard error of those reported for both *E. huxleyi* and *G. oceanica* by Schouten et al. (2006) and for *E. huxleyi* by M'Boule et al. (2014) (see Chapter 4, table 4.4). Comparing the open-ocean $\delta D_{alkenone}$ data from this study to the individual data points from Schouten et al. (2006) (Figure 3.5) highlights the good agreement between the open-ocean and the culture observations overall, and the comparable scatter. Figure 3.5 also illustrates the small range of salinities of the open-ocean samples compared to the larger range investigated in the culture study.

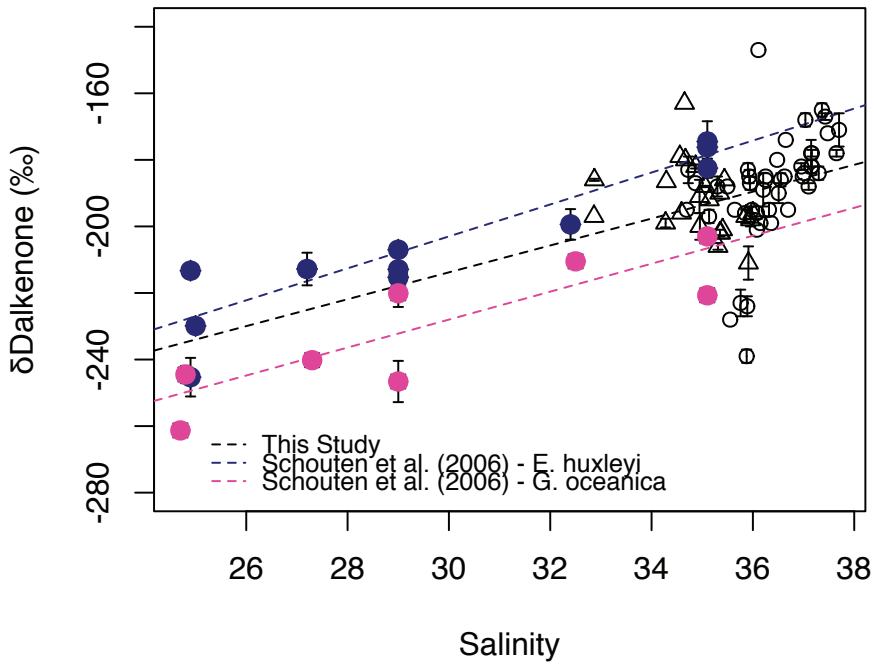

Figure 3.5: Linear regression (dashed black line) between $\delta D_{alkenone}$ and SSS for 69 SPOM samples, same as in Figure 3.4 (46 Atlantic Ocean samples: circles and 23 Pacific Ocean samples: triangles). Shown also are the culture study regressions and data points from Schouten et al. 2006 (*E. huxleyi:* dark blue, *G. oceanica*: pink).

3.2.5 $\delta^{13}C_{alkenone}$

$\delta^{13}C_{alkenone}$ values were measured on 32 of the 49 AMT20 samples and on 9 of the 10 Northern West Pacific samples. $\delta^{13}C_{alkenone}$ values ranged between –34 and –24 ‰, a range of 10‰ (Figure 3.6). By far the lightest values were measured at 13 °N in the Atlantic ($\delta^{13}C_{alkenone}$ = -34 ‰, sample AMT20 #22) and at 0.6 °S in the Pacific ($\delta^{13}C_{alkenone}$ = -34 ‰, sample #31 from the Northern Pacific transect).

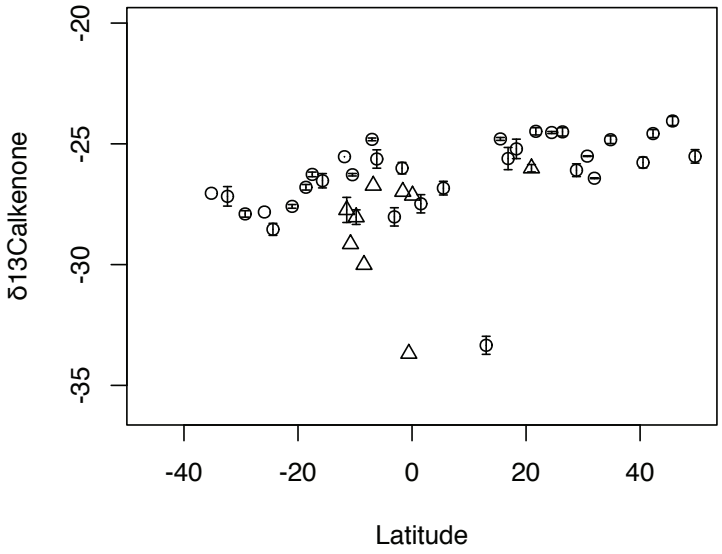

Figure 3.6: Latitudinal distribution of $\delta^{13}C_{alkenone}$ values for 41 of the total 69 SPOM samples analysed in this study. Error bars indicate standard error from repeat isotope analysis. Samples without repeat injection are shown with no error bars.

CHAPTER 4: DISCUSSION

This open-ocean SPOM dataset spans a total of 100 degrees of latitude in the Atlantic in addition to another 50 degrees in the Pacific; includes samples from at least 10 biogeochemical provinces (sensu Longhurst 1995, 2007) collected during different seasons (Boreal Fall and Austral Spring in the Atlantic and Austral Fall in the Pacific); and covers a large range of open-ocean surface water salinities, temperatures, irradiances and nutrient regimes. Even so, it is striking that there is good agreement between the relationships observed ($\delta D_{alkenone}$ vs. δD_{water}, $\alpha_{alk\text{-}water}$ vs. salinity and $\delta D_{alkenone}$ vs salinity) in these field samples and those observed in laboratory culture studies (Figures 3.1 – 3.3). The agreement is particularly noteworthy given that most laboratory studies control for single environmental parameters (e.g. species-composition and nutrient availability) that are widely variable in a natural setting, and in many cases, exceed the observed range of these parameters in the open-ocean. The SPOM dataset presented here is unique in that it is likely a more representative subsample of alkenone signatures that will ultimately be exported to the sediment record, and yet the results suggest that the relationships observed in the open-ocean environment resemble those observed in culture.

4.1 Linear Regression Analysis

4.1.1 $\delta D_{alkenone}$ vs. δD_{water}

While the $\delta D_{alkenone}$ values measured in this study significantly reflect coincident surface water δD signatures and align with many of the regressions developed from algal culture studies (Schouten et al., 2006; M'Boule et al., 2014; Figure 3.1), the spread in residual values (~85‰) suggests that additional factors beyond that of the growth water signal significantly influence the hydrogen isotopic signature in some of the samples. Offsets from culture regressions are largest, and exceed analytical uncertainties by an order of magnitude, in samples AMT20 #22 (13° N) and sample #31 (0.6 °S) from the Northern Pacific transect, and in four northern Atlantic Ocean samples (ATM #2-5 between 43 and 48° N).

4.1.2 $\alpha_{alk\text{-}water}$ vs. SSS

Culture studies observe positive relationships between $\alpha_{alk\text{-}water}$ and SSS with increases in $\alpha_{alk\text{-}water}$ between 0.0015 – 0.003 per unit increase in salinity. However, regression of $\alpha_{alk\text{-}water}$ on SSS in the open-ocean data presented here is not significant when all SPOM data are evaluated (Figure 3.2). Most of the SPOM data points (~80%) fall on or close to the regression reported by M'Boule et al. (2014) for *E. huxleyi* and between the regressions reported by Schouten et al. (2006) for *E. huxleyi* and *G. oceanica*. The relationship reported by Sachs et al. (2016) $\alpha_{alk\text{-}water}$ vs. salinity relationship, which is derived from a continuous culture of *E. huxleyi* and carefully isolates the effect of salinity on $\alpha_{alk\text{-}water}$, is offset most significantly from the open-ocean data presented here, and indeed from previous laboratory batch cultures studies. I infer that the data presented here are likely offset from the Sachs' regression due to variable environmental conditions likely impacting hydrogen isotopic composition in the open-ocean environment in ways that are controlled for in the continuous culture.

4.1.3 $\delta D_{alkenone}$ vs. SSS

The open-ocean data from this study almost entirely fall between the three published culture regressions (Figure 3.3), indicating that the open-ocean samples indeed reflect what has been observed in the laboratory setting. This also suggests a mixture of both *E. huxleyi* and *G. oceanica* species could have been sampled, however this observation is speculative without proper species identification.

Since this salinity proxy relies on a systematic relationship between the $\delta D_{alkenone}$ signature and $\delta D_{water,}$ which is presumably amplified by the relationship between the fractionation factor ($\alpha_{alk\text{-}water}$) and SSS, it is important to evaluate the scatter observed in $\alpha_{alk\text{-}water}$ in this open-ocean dataset. Following the findings reported from numerous published culture studies, this scatter could be a result of the effects of any possible combination of environmental variables such as salinity itself, temperature, nutrient availability, light availability, growth rates and phases, and even species composition, on the fractionation of alkenone hydrogen isotopes

(Table 1.1). Samples deviating from the regression relationships most substantially (AMT20 #22, WEP #31 and AMT20 #2-5) are investigated in more detail below.

4.2 Evaluation of Scatter

While the open-ocean dataset presented here aligns well with the $\delta D_{alkenone}$ vs. δD_{water} , the $\alpha_{alk\text{-}water}$ vs. salinity and the $\delta D_{alkenone}$ vs. salinity relationships observed in culture, a fair amount of scatter exists in the data that warrants investigation. The following analyses make use of a number of ancillary parameters to elucidate possible explanations for observed variability in alkenone hydrogen isotopic fractionation ($\alpha_{alk\text{-}water}$).

4.2.1 U^{K}_{37}' Analysis

As an initial test to characterize anomalous alkenone samples, the U^{K}_{37}' (an index describing the relative amount of di-unsaturated to tri-unsaturated alkenones; Figure 4.1) were examined to identify any odd alkenone signatures. The U^{K}_{37}' is a well described proxy used for the reconstruction of paleo-SST because of the strong positive relationship that exists between the temperature of growth water of the alkenone producers and U^{K}_{37}'. Regions of very high surface ocean temperatures, and thus very low production of tri-unsaturated alkenones make the quantification of U^{K}_{37}' impossible, therefore there are no U^{K}_{37}' values for many of the samples in the tropical/equatorial regions of both basins. When regressed against *in situ* average SST, the open-ocean SPOM U^{K}_{37}' values from this study align well with all available global SPOM U^{K}_{37}' values synthesized by Conte et al. (2006). Both Western Pacific samples and Atlantic Ocean samples also align well with the global ocean third-order polynomial calibration curve developed by Conte et al. (2006) and the Atlantic basin Richard's curve calibration developed by Gould et al. (2017) describing the relationship between SST and U^{K}_{37}' in SPOM, further corroborating the justification for a combined analysis of all isotopic data in this study.

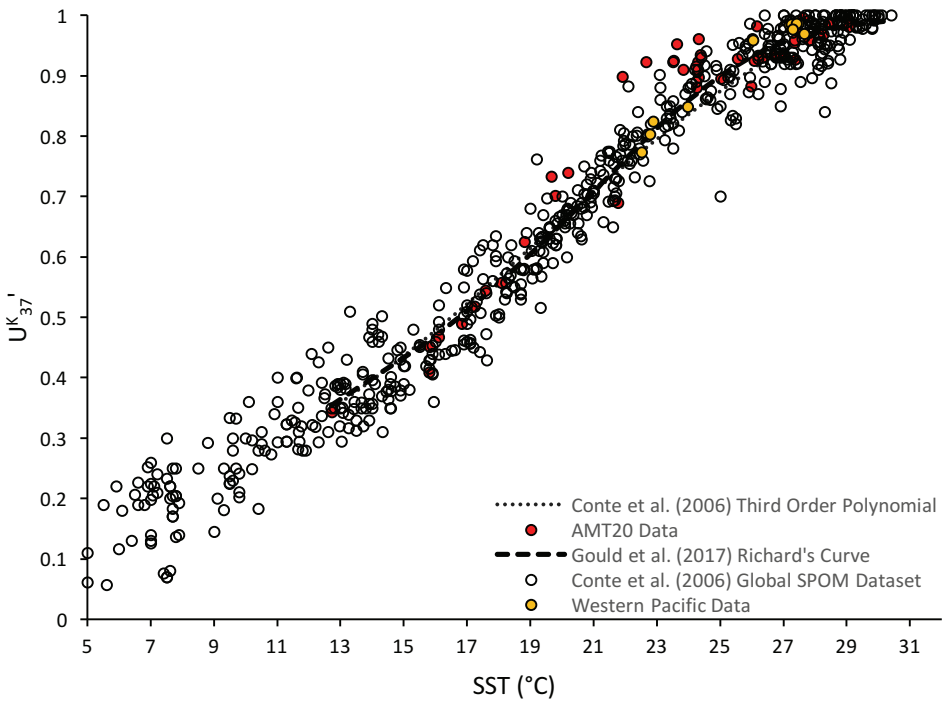

Figure 4.1: U^{K}_{37}' values measured from 55 of the SPOM alkenone samples analysed in this study (Atlantic Basin: red, Pacific Basin: yellow) regressed against in situ average SST (°C) values. The previously published third order polynomial (Conte et al., 2006) as well as Richard's curve (Gould et al., 2017) calibrations are shown for comparison.

A handful of Atlantic Ocean (AMT20) data from this study do appear to fall above both the Conte et al. (2006) and Gould et al. (2017) regression lines between ~22 and 24 °C. These samples were collected in the southern part of the AMT20 transect between 10 and 30 °S and are potentially affected by the dynamic conditions at the convergence between the Malvinas and Brazil currents as previously discussed by Benthien & Müller, 2000. However, these data do not fall away substantially from the overall scatter in the global ocean dataset and the offsets in U^{K}_{37}' here do not correspond to the scatter observed in the alkenone isotopic data. Therefore, these U^{K}_{37}' data do not appreciably inform the offsets in $\alpha_{alk\text{-}water}$ found in this study.

4.2.2. Residual Analysis

To evaluate the scatter in the reported regressions, residual values were computed for all three linear regressions ($\delta D_{alkenone}$ vs. δD_{water}, $\alpha_{alk\text{-}water}$ vs. SSS and $\delta D_{alkenone}$ vs. SSS), defined as the difference between the observed response variable (measured $\delta D_{alkenone}$ and derived $\alpha_{alk\text{-}water}$) and the predicted response variable (estimate from the relevant linear regression relationship). $\delta D_{alkenone}$ residual values were computed for both the $\delta D_{alkenone}$ vs. δD_{water} and the $\delta D_{alkenone}$ vs. SSS relationships, and $\alpha_{alk\text{-}water}$ residual values were computed from the $\alpha_{alk\text{-}water}$ vs. SSS relationship. I note, however, that the explanatory parameters from these regressions (i.e. δD_{water}, SSS) are not independent of one another, and that the $\alpha_{alk\text{-}water}$ value is a derived variable, therefore, is not independent from $\delta D_{alkenone}$ or δD_{water}. Because much of the literature is focused on describing relationships between $\alpha_{alk\text{-}water}$ values and environmental/physiological factors, I investigate correlations between the derived $\alpha_{alk\text{-}water}$ values for this dataset and the ancillary data available. Regression analyses were conducted to describe the relationships between residual values and sampling average latitude, average longitude, average SST, log-transformed alkenone concentration (ng/l), and $\delta^{13}C_{alkenone}$ values. Alkenone concentrations were log-transformed in order to establish a normal distribution of the data. Of the parameters tested, only three parameters; log-alkenone concentrations, SST and $\delta^{13}C_{alkenone}$ values, were significantly correlated with $\alpha_{alk\text{-}water}$ values and residual values (Table 4.1). These relationships are discussed in further detail below.

Table 4.1 Regression results for $\alpha_{alk\text{-}water}$ values, and $\alpha_{alk\text{-}water}$ and $\delta D_{alkenone}$ residual values versus log alkenone concentration (ng/l), sea surface temperatures (SST (°C)) and $\delta^{13}C_{alkenone}$ (‰) values for entire SPOM dataset presented here.

	(Log) Alkenone Concentration (ng/l)		SST		$\delta^{13}c_{alkenone}$	
	Regression	*P-value*	*Regression*	*P-value*	*Regression*	*P-value*
Alpha	y = -0.01±0.004(x) +0.81±0.004	0.009	y = 0.002±0.0004(x) + 0.77±0.01	0.0001	y = -0.004±0.001(x) + 0.71±0.023	0.0001
Residual Alpha (Alpha vs. SSS)	y = -0.01±0.004 (x) + 0.01±0.004	0.002	y = 0.002±0.0004(x) - 0.04±0.01	$3.2x10^{-5}$	y = -0.004±0.001(x) - 0.1±0.022	$1.4x10^{-5}$
Residual δDalk (δD_{alk} vs. δD_{water})	y = -13± 4.3(x) + 10±3.8	0.004	y = 1.6±0.36(x) - 41±9.0	$2.1x10^{-5}$	y = -4.02±0.84(x) -104±22.5	$2.4x10^{-5}$
Residual δDalk (δD_{alk} vs. SSS)	y = -15± 4.4(x) + 12±3.9	0.001	y = 1.7±0.37(x) - 41±9.4	$3.1x10^{-5}$	y = -4.12±0.83(x) -107 ±22.3	$1.4x10^{-5}$

4.2.3. Alkenone Concentration

Much of the literature evaluating U^{K}_{37}' values and/or $\delta D_{alkenone}$ values in the context of paleo-proxy development include a discussion of alkenone concentration, which is thought to be indicative of the growth status and/or concentration of alkenone producers. In this study, I cannot differentiate whether high concentrations of alkenones in the surface waters filtered are a result of a high presence (number) of alkenone producers (i.e. indicative of high growth rates) or of the upregulation of alkenone molecules in coccolithophores transitioning from exponential to stationary growth (e.g. Wolhowe et al., 2009). According to the literature (Table 1.1), both of these scenarios would result in a shift to lower $\alpha_{alk\text{-}water}$ values.

Regression of $\alpha_{alk\text{-}water}$ values on log-transformed alkenone concentrations results in a significant positive correlation (p-value = 0.009; Figure 4.2; Appendix Table A6(a)). However, this relationship is likely driven by (a) the two lowest alkenone concentration values measured in the SPOM dataset (AMT20 #22 and Northern West Pacific #31), which also have the highest $\alpha_{alk\text{-}water}$ values and by (b) the group of samples from the northern part of the AMT20 (#2-5) with the lowest $\alpha_{alk\text{-}water}$ values. Regression of $\alpha_{alk\text{-}water}$ and $\delta D_{alkenone}$ residual values on log-transformed alkenone concentrations (ng/l), also results in statistically significant negative relationships (Table 4.1, and Appendix Tables A6(b-d) for regression output). If the six anomalous samples are removed from the analysis, the regressions of $\alpha_{alk\text{-}water}$ and residual values on log-transformed alkenone concentrations are no longer statistically significant (see Appendix Tables A7(a-d)). This exercise illustrates that for the majority of the dataset (62 of the 69 samples), hydrogen isotopic fractionation of alkenones is not significantly correlated with sample surface water alkenone concentration. Without *in situ* evaluation of growth phase or growth rate in these open-ocean SPOM samples it is not possible to tease apart whether the low (AMT20 #22, WEP #31) and high (AMT20 #2-5) alkenone concentration samples with large and small $\alpha_{alk\text{-}water}$ values, respectively, are a consequence of either a change in growth rate or growth phase (exponential vs. stationary).

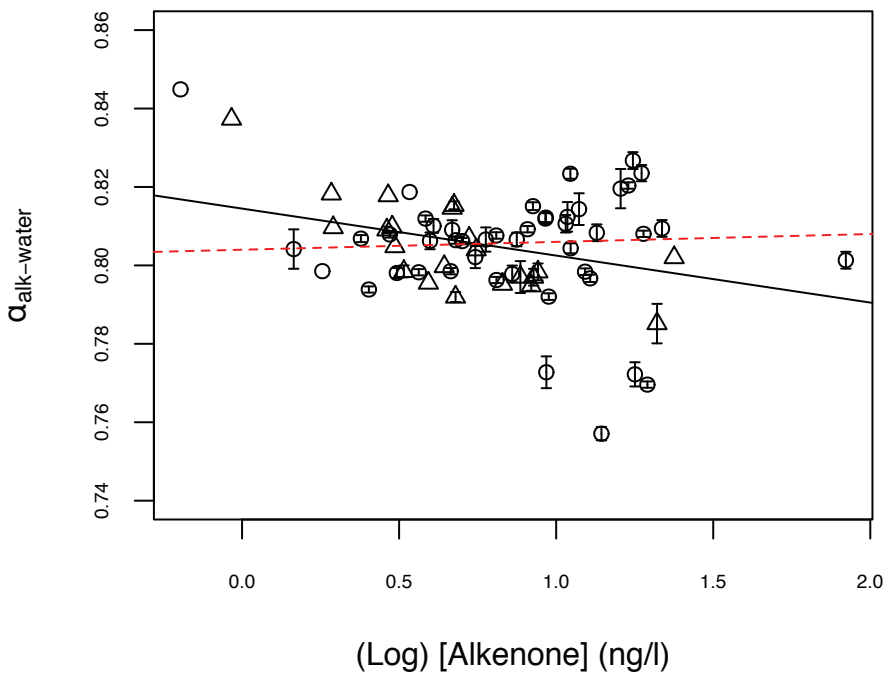

Figure 4.2: Linear regression between $\alpha_{alk\text{-}water}$ and log-transformed alkenone concentration (ng/l) for 68 SPOM samples (Atlantic Ocean samples: circles and Pacific Ocean samples: triangles) $\alpha_{alk\text{-}water}$ = -0.01* [log-alkenone] + 0.814 (R^2 = 0.01, p = 0.009) Error bars indicate calculated error in derived $\alpha_{alk\text{-}water}$. Samples without repeat injection are shown with no error bars. Also shown is the regression for the $\alpha_{alk\text{-}water}$ vs. log-transformed alkenone concentration for a reduced dataset (n=63, red dashed line) which excludes 6 outlier samples (AMT #2-5; 22, WEP#31: see sections 4.2.8 and 4.3 below, and Appendix Table A7(a) for regression output).

4.2.4. Sea Surface Temperature

A number of laboratory cultures observe significant negative correlations between temperature and the fractionation factor, such that $\alpha_{alk\text{-}water}$ values decrease by between 2 and 4‰°C^{-1} (Zhang et al., 2009; Wolhowe et al., 2009). To address this relationship in the open-ocean dataset presented here, linear regression was computed for $\alpha_{alk\text{-}water}$ values on sea surface temperature. SST values are significantly positively correlated with $\alpha_{alk\text{-}water}$ values in this SPOM dataset (p-value = 0.0001, Figure 4.3; see Appendix Table A8 and Figure A6 for regression output). This relationship is opposite to the negative relationship between $\alpha_{alk\text{-}water}$ values and temperature observed in the literature (Zhang et al., 2009; Wolhowe et al., 2009), but agrees with the positive linear relationship observed in Wolhowe et al. (2015). A partial F-test conducted to test the predictive power of including SST in a multiple

linear regression (MLR) for the $\alpha_{alk\text{-}water}$ vs. SSS relationship confirms that the inclusion of SST significantly strengthens the ability to predict $\alpha_{alk\text{-}water}$ values once SSS are taken into consideration in this open-ocean dataset (p-value = 2.8×10^{-5}, see Appendix Tables A9(a) and A9(b) for MLR and Partial F-test (ANOVA) output). Furthermore, residual $\alpha_{alk\text{-}water}$ values computed from the $\alpha_{alk\text{-}water}$ vs. SSS regression, are also linearly correlated to SST (p-value = 3.2×10^{-5}, see Appendix Table A10(a)). Likewise, residual $\delta D_{alkenone}$ values (from both the regression between $\delta D_{alkenone}$ vs. δD_{water} and vs. SSS) are positively correlated to SST values (p-value = 2.1×10^{-5} and p-value = 3.1×10^{-5}, respectively, see Appendix Tables A10(b) and A10(c)).

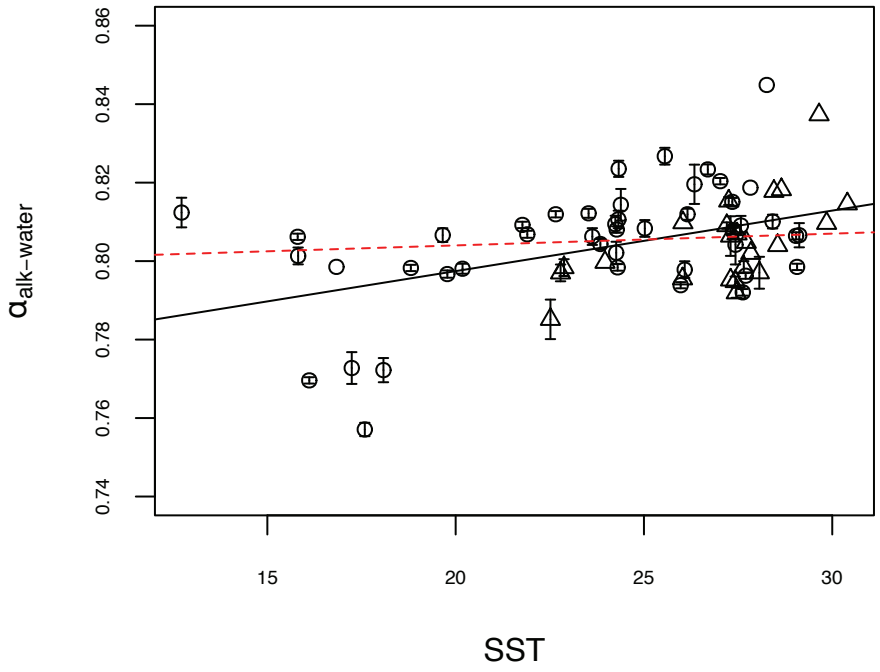

Figure 4.3: Linear regression between $\alpha_{alk\text{-}water}$ and SST (°C) for 69 SPOM samples (Atlantic Ocean samples: circles and Pacific Ocean samples: triangles) $\alpha_{alk\text{-}water}$ = .002* SST + 0.77 (R^2 = 0.20, p = 0.0001). Error bars indicate calculated error in derived $\alpha_{alk\text{-}water}$. Samples without repeat injection are shown with no error bars. Also shown is the regression for the $\alpha_{alk\text{-}water}$ vs. SST relationship for a reduced dataset (n=63, red dashed line), which excludes 6 outlier samples (AMT #2-5; 22, WEP#31: see sections 4.2.8 and 4.3 below, and see Appendix Table A11(a) for regression output).

This analysis suggests that some of the scatter in all the three regressions (i.e. $\delta D_{alkenone}$ vs. δD_{water}, $\alpha_{alk\text{-}water}$ vs. SSS and $\delta D_{alkenone}$ vs. SSS) might in part be explained by variability in associated SST, however, because salinity and temperature are positively correlated (not independent of one another) in the open-ocean environment, individual effects on the hydrogen isotopic fractionation in these

open-ocean samples cannot be teased apart. Furthermore, the positive relationship between $\alpha_{alk\text{-}water}$ values and SST (Figure 4.3) is driven by the same six data points (as mentioned above: AMT20 #2-5, #22, and WEP #31). When these six data points are removed from the analysis, the relationship between $\alpha_{alk\text{-}water}$ and SST is no longer statistically significant (p-value = 0.26, see Appendix Table 11(a)), nor is the multiple linear regression including SST (Partial F-Test results: p-value = 0.12, see Appendix Table A11(b)). This is also true for the regressions of residual values ($\alpha_{alk\text{-}water}$ and $\delta D_{alkenone}$) on SST, which are no longer statistically significant when these six data points are removed (see Appendix Tables A12(a-c)). Overall, this suggests that for the majority of the data (63 of 69 samples) no significant relationship exists between the open-ocean SPOM alkenone hydrogen isotopic fractionation and SST.

4.2.5. $\delta^{13}C_{alkenone}$ Analysis

The carbon isotopic signatures ($\delta^{13}C$) of biomarker molecules have been shown to depend on pCO_2, size and shape of algal producers, and on growth rates, such that $\delta^{13}C$ has been proposed as both a proxy for paleo- pCO2 concentrations (e.g. Jasper & Hayes, 1990; Rau et al., 1991; Fontugne & Calvert, 1992; Jasper et al., 1994; Müller et al., 1994; Bentaleb et al., 1996; Andersen et al., 1999; Pagani et al., 1999 *as cited in* Benthien et al., 2002) and more recently as a proxy for algal growth rates (e.g. Bidigare et al., 1997; Riebesell et al., 2000; Popp et al., 1998; Benthien et al., 2002, and a review by Laws et al., 2002). Because there are no $pCO_{2(aq)}$, $\delta^{13}C_{DIC}$ or $\delta^{13}C_{CO2}$ measurements associated with this open-ocean dataset, I cannot quantify the carbon isotopic fractionation parameter - ε_p, which was observed to be positively linearly correlated with $\alpha_{alk\text{-}water}$ values measured in Gulf of Mexico and ETNP SPOM samples (Wolhowe et al., 2015). Wolhowe et al. (2015) also showed that ε_p – estimated growth rates were negatively correlated with $\alpha_{alk\text{-}water}$ values.

Assuming that $\delta^{13}C_{alkenone}$ values measured in this study reflect not only $pCO_{2(aq)}$ but also some aspect of algal growth, I examine the relationship between $\delta^{13}C_{alkenone}$ values and $\alpha_{alk\text{-}water}$ for the dataset presented in this study. Linear regression of $\alpha_{alk\text{-}water}$ values on $\delta^{13}C_{alkenone}$ values results in a significant negative relationship (p-value = 0.0001, Table 4.1, Figure 4.4; Appendix Table A13 and Figure A7). A partial F-test evaluating the significance of a multiple linear

regression of $\alpha_{alk\text{-}water}$ on SSS including $\delta^{13}C_{alkenone}$ (where available) indicates that $\delta^{13}C_{alkenone}$ values are indeed significant in informing $\alpha_{alk\text{-}water}$ variability once salinity values have been taken into consideration (p –value = $8.8x10^{-6}$ at the 95% confidence level, n = 41, see Appendix Tables A14(a) and A14(b) for statistical output). This follows the findings from Wolhowe et al. (2015) who show heavy $\delta^{13}C_{alkenone}$ values corresponding to smaller ε_p values, lower derived $\alpha_{alk\text{-}water}$ values and higher estimated growth rates. Additionally, when residual values ($\alpha_{alk\text{-}water}$ and $\delta D_{alkenone}$) are regressed against $\delta^{13}C_{alkenone}$ values (where available), all three regressions result in significant negative correlations (see Table 4.1 above and Appendix Tables A15(a-c)).

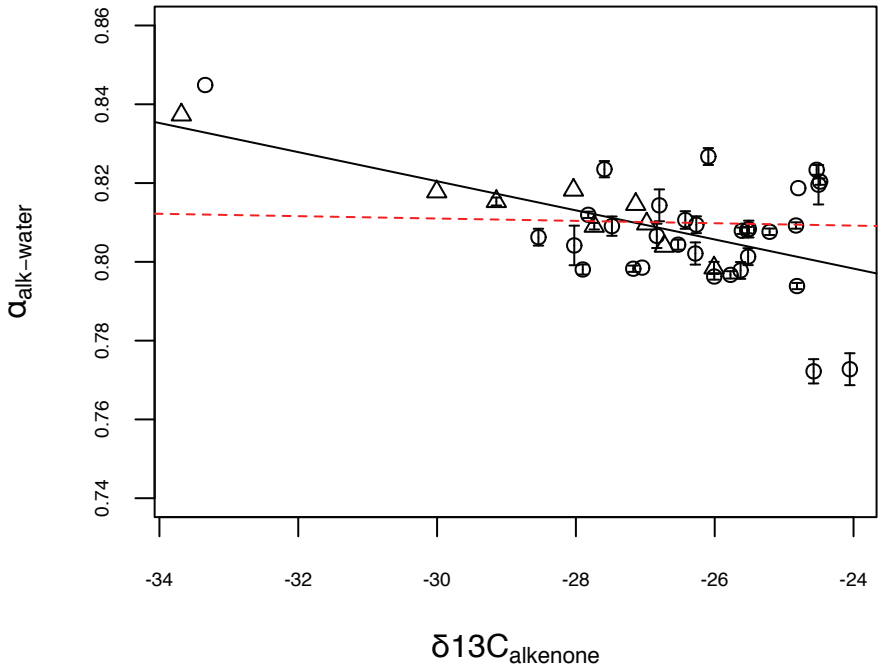

Figure 4.4: Linear regression between $\alpha_{alk\text{-}water}$ and $\delta^{13}C_{alkenone}$ for 41 SPOM samples (Atlantic Ocean samples: circles and Pacific Ocean samples: triangles) $\alpha_{alk\text{-}water}$ = -.004* $\delta^{13}C_{alkenone}$ + 0.71 (R^2 = 0.31, p = 0.0001, n = 41). Error bars indicate calculated error in derived $\alpha_{alk\text{-}water}$. Samples without repeat injection are shown with no error bars. Also shown is the regression for the $\alpha_{alk\text{-}water}$ vs. $\delta^{13}C_{alkenone}$ relationship for a reduced dataset (n=63, red dashed line), which excludes 6 outlier samples (AMT #2-5; 22, WEP#31: : see sections 4.2.8 and 4.3 below, and see Appendix Table A16 for regression output).

These correlations to $\delta^{13}C_{alkenone}$ values appear to be driven primarily by four data points, two with very negative (light) carbon isotopic signatures (Northern Pacific #31, AMT20 #22), and two with some of the heaviest carbon isotopic

signatures (AMT20 # 3 and 5). Indeed, after the removal of these four data points from the linear regression between $\alpha_{alk\text{-}water}$ and $\delta^{13}C_{alkenone}$ the relationship is no longer statistically significant (p-value = 0.82; see Appendix Table A16 for regression output), nor is the multiple linear regression including $\delta^{13}C_{alkenone}$ values (p-value = 0.33; see Appendix Table A17 for Partial F-Test). This is also true for the regressions of residual values ($\alpha_{alk\text{-}water}$ and $\delta D_{alkenone}$) on $\delta^{13}C_{alkenone}$, which are no longer statistically significant when these four data points are removed (see Appendix Tables A18(a-c)). If $\delta^{13}C_{alkenone}$ and $\delta D_{alkenone}$ signatures are in some cases influenced concurrently by a particular physiological or environmental parameter (e.g., growth rate or resource availability) the coincident measurement of 'extreme' or anomalous $\alpha_{alk\text{-}water}$ values and $\delta^{13}C_{alkenone}$ values should be treated with caution. Taking this one step further, the coincident measurements of $\delta^{13}C_{alkenone}$ and $\delta D_{alkenone}$ in sedimentary alkenone samples could prove a useful tool when characterizing anomalous alkenone biosynthesis through time.

Due to the consistent observation that the same group of 6 SPOM alkenone samples falls outside of the average or 'expected' isotopic (both hydrogen and carbon) values as detailed above, a discussion of these offsets and an exercise in the removal of these outliers is conducted below.

4.2.6. Samples AMT20 #22 & Northern West Pacific #31

The two data points with the largest positive residuals are samples #22 from the AMT20 and #31 from the Northern West Pacific transect. Sample #31 from the Northern West Pacific, which was filtered from 0.6 °S, 142.98 °E to 0.5 °S, 143.57 °E, has the second heaviest $\delta D_{alkenone}$ value ($\delta D_{alkenone}$ = -163‰) observed in the entire dataset, and the second highest $\alpha_{alk\text{-}water}$ value ($\alpha_{alk\text{-}water}$ = 0.837). The $\delta D_{alkenone}$ and $\alpha_{alk\text{-}water}$ values here are offset from average transect values by +27‰ and +0.032, respectively. Similarly, sample AMT20 #22, which was filtered from 13.47°N, -33.95°E to 12.55°N, -33.33°E, has both the heaviest of all $\delta D_{alkenone}$ values observed along the Atlantic transect ($\delta D_{alkenone}$ = -147 ‰), and the highest $\alpha_{alk\text{-}water}$ value ($\alpha_{alk\text{-}water}$ = 0.845). The $\delta D_{alkenone}$ and $\alpha_{alk\text{-}water}$ values here are offset from average transect values by +43‰ and +0.04, respectively.

Coincidently, the $\delta^{13}C_{alkenone}$ of samples #31 from the Northern West Pacific ($\delta^{13}C_{alkenone}$ = -34 ‰) and AMT20 #22 ($\delta^{13}C$ = -33 ‰) are also by far the lightest observed in the dataset, suggesting that both isotope systems are affected by the same or a co-varying physiological factor at these sites. The concurrence of low $\delta^{13}C_{alkenone}$ and maximum $\alpha_{alk\text{-}water}$ values at these sites is consistent with slow growth rates in parallel with the observations made in Wolhowe et al. (2015). I note, however, that while algal growth rates are likely to vary along the entirety of the transect, an anomalous shift in growth rate would need to have occurred here to explain these 'extreme' offsets in $\alpha_{alk\text{-}water}$. For example, according to the Schouten et al. (2006) *E. huxleyi* culture relationship reported between $\alpha_{alk\text{-}water}$ and algal growth rates, a shift in growth rate of 1.4 day^{-1}, relative to the filter samples taken before and after these samples, would be required to explain the observed shift in $\alpha_{alk\text{-}water}$ by 0.04 units at station AMT20 #22. While growth rates in the algae sampled in this large scale open-ocean dataset are likely to vary widely, without direct measures or estimates of algal growth rates and resource availability at these sites, I cannot determine the exact driving factor for the offsets observed.

4.2.7. Northern Atlantic Samples (AMT20 - #2-5)

In contrast, some of lightest $\delta D_{alkenone}$ values recorded in the dataset are located north of the Azore Islands (Samples # 2 – 5) in the northeast Atlantic region, ranging between -239‰ and -223‰. This group of samples has, by far, the lowest $\alpha_{alk\text{-}water}$ values observed in the entire SPOM dataset presented in this study ($\alpha_{alk\text{-}water}$ ranging between 0.76 to 0.77). The very large apparent fractionation in $\delta D_{alkenone}$ values here is likely a result of a combination of physiological and environmental factors. Laboratory and small –scale field study literature report decreases in $\alpha_{alk\text{-}water}$ to be caused by any one of the following factors; 1) low salinity, 2) high growth rates, 3) stressed cells in stationary growth phase, 4) exposure to low irradiance, or 5) a species composition change. Because these samples are geographically grouped, I posit that the hydrography of this region and/or a unique algal community composition or growth rate could explain these low $\alpha_{alk\text{-}water}$ values.

Samples 2 and 3 are located in the NADR (north Atlantic drift province) and samples 4 and 5 are located in the NASTE (north Atlantic Subtropical Gyre –East)

(Longhurst, 2007). This group of 4 samples is from a region of the northern Atlantic that separates the northeasterly North Atlantic Current from the southeasterly Azores current – an extension of the Gulf Stream. This is also a region that is characterized by energetic mesoscale eddies associated with the active Gulf Stream system (Longhurst, 2007). Wind speed in the region is highest during the autumn and winter months, during which these filters were sampled. This highly dynamic region north of the Azores also experiences a prominent deepening of the mixed layer, to depths of up to 500m in the winter (Longhurst, 2007). Sampling of alkenones here took place between October 15th and 17th 2010, a period in time where northern Atlantic fall algae blooms have been observed (Okada & McIntyre, 1979) and just days after hurricane Otto, which passed as an extratropical storm above the Azores in this region between October 12th-14th 2010.

The dynamics of the region might in part explain why $\alpha_{alk\text{-}water}$ values measured here are so low compared to the remainder of the dataset. Indeed, extensive vertical mixing from wind-driven as well as eddy-driven forces have the potential to mix up alkenones produced at depth; where growth waters could have higher nutrient concentrations, and receive lower levels of irradiance. Alternatively, deep water rich in nutrients mixed up to the surface might have initiated a late summer (Fall) bloom of coccolithophores in the surface waters here, known to occur elsewhere in the northern regions of the NADR. If either of these scenarios were the case, I would expect growth rates in alkenone producers sampled here to have been relatively high, which could also explain the low $\alpha_{alk\text{-}water}$ values. Consistent with this inference are the relatively heavy $\delta^{13}C_{alkenone}$ signatures measured in this group of samples.

Surface ocean nutrient (e.g. Phosphate and Nitrate + Nitrite) concentrations and prymnesiophyte marker pigment concentrations (19'-hex) available for the Atlantic Ocean (AMT20) (see Appendix Table A1; Harris, C. & Woodward, E.M.S; Airs et al., 2014) both increase approaching 50º South and 50º North along the AMT20. With the caveat that these nutrient and pigment data are sampled from water collected from a CTD rosette deployed at depth from sample locations not directly associated with alkenone filtration for this study, relatively high nutrient and marker pigment concentrations in the northern Atlantic may be indicative of higher productivity there. Although, a direct relationship between higher marker

pigment and nutrient concentrations with increased algal growth rate/phase cannot be established here. It is interesting to note that the coincidence of low $\alpha_{alk\text{-}water}$ AMT20 #2-5 samples with relatively high pigment and nutrient concentrations is consistent with a dynamic balance model for algal resource allocation and balanced growth (Gieder et al., 1997). According to this model, pigment up-regulation can occur when cells are growing under light-limited, high nutrient or high temperature conditions (Gieder et al., 1997). If the alkenone producers from samples AMT20 #2-5 were growing rapidly due to high-nutrient availability either from deep production in close proximity to the nutricline or from an injection of subsurface water high in nutrients to the surface, then I would also expect higher pigment concentrations, consistent with the surface concentration of pigments in the region, as well as the observed low alpha values. On the other hand, if I assume deep alkenone production from producers that would be growing under light-limited stress but in close proximity to the nutricline, I would also expect to see an upregulation of pigment concentrations and low alpha values. The offset in timing of the algal acclimation response to environmental variability in this region (high vs. low resource availability – i.e. irradiance and nutrients) relative to the timing of SPOM sampling is critical, as the cells are acclimating and actively up- or down-regulating lipid stores (i.e. alkenones) and pigments in response to growth water variability.

Finally, comparison with surface ocean Gulf of California and ETNP SPOM data from Wolhowe et al. (2015) show good correspondence with the open-ocean dataset presented here. Indeed, low $\alpha_{alk\text{-}water}$ values taken from station 4-12 in the ETNP (Figure 4.5) resemble low $\alpha_{alk\text{-}water}$ values measured from the northern part of the AMT20 sampled here. Wolhowe et al. (2015) infer the anomalous ETNP $\alpha_{alk\text{-}water}$ values at station 4-12 to be associated with high algal growth rates as inferred from $\delta^{13}C_{alkenone}$ analysis, consistent with the relatively heavy $\delta^{13}C_{alkenone}$ measured in samples AMT20 #2-5. Wolhowe et al. (2015) also observe a negative relationship between $\alpha_{alk\text{-}water}$ values and sampling depth, where low $\alpha_{alk\text{-}water}$ values, derived from samples taken at depth (upwards of 50m) are inferred to be caused either by a decrease in light availability (found in culture literature to be positively correlated with $\alpha_{alk\text{-}water}$) or by an increase in growth rate associated with increasing proximity to the nutricline. Without ancillary growth rate, irradiance data, or knowledge of the depth of alkenone production in the SPOM alkenones sampled in this study, I

suggest that the anomalous $\alpha_{alk\text{-}water}$ values in the northern Atlantic samples are likely a result of any combination of low salinity (at depth), higher growth rates (either at depth in closer proximity to the nutricline or at the surface due to upwelling of nutrients) or lower light availability (if synthesized at depth).

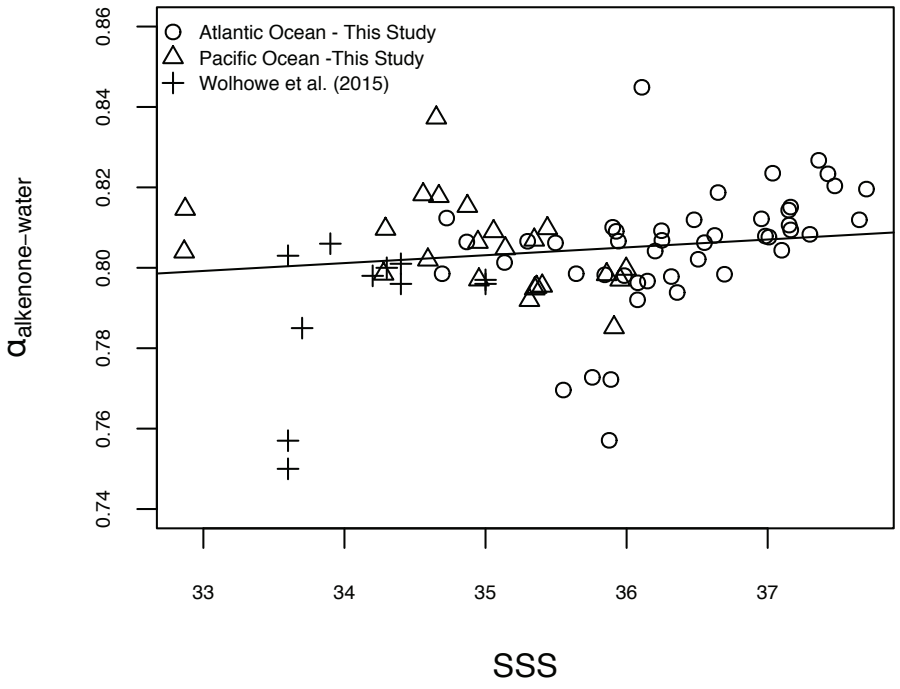

Figure 4.5: Scatter plot showing $\alpha_{alk\text{-}water}$ and SSS for 69 SPOM samples (46 Atlantic Ocean samples: circles and 23 Pacific Ocean samples: triangles). Also shown are 11 Gulf of California/Eastern Tropical North Pacific surface ocean SPOM data from Wolhowe et al. (2015).

Nonetheless, I cannot rule out that the occurrence of these low $\alpha_{alk\text{-}water}$ values in these northern Atlantic samples may also be a result of 'detrital' or stationary-phase alkenones, where perhaps 'bloom-like' or fast-growing conditions occurred in the recent past before sampling during the AMT20. $\alpha_{alk\text{-}water}$ values for stationary phase alkenone producers are known to vary up to 40‰ from exponentially growing producers, which would certainly also be enough to explain the offsets observed here. Unfortunately, a lack of growth rate and phase as well as species composition data inhibit further elucidation of a direct cause of this group of anomalous $\alpha_{alk\text{-}water}$ values.

4.2.8. Summary

The above analyses elucidate a group of samples from the northern Atlantic Ocean basin (AMT20 #2-5) with anomalously light $\delta D_{alkenone}$, low $\alpha_{alk\text{-}water}$ and in some cases heavy $\delta^{13}C_{alkenone}$ measurements, and two samples with anomalously heavy δD_{water} signals, high $\alpha_{alk\text{-}water}$ and light $\delta^{13}C_{alkenone}$ measurements (AMT #22 and Northern West Pacific #31), which are inferred to be indicative of algal cells experiencing 'anomalous' physiological or environmental conditions. Below, as an exercise in reducing the overall scatter in the SPOM dataset presented in this study, these 6 'anomalous' SPOM samples are omitted from the regression analysis between $\delta D_{alkenone}$ and δD_{water}, $\alpha_{alk\text{-}water}$ and SSS and $\delta D_{alkenone}$ and SSS and a 'reduced' SPOM dataset is then compared with laboratory culture results.

4.3 Reduced dataset vs. published cultures

The re-analyses of the $\delta D_{alkenone}$-δD_{water}, $\delta D_{alkenone}$-SSS and $\alpha_{alk\text{-}water}$ –SSS regressions for a reduced dataset, which excludes the 6 SPOM samples inferred as anomalous in the above analyses, is presented here.

4.3.1 $\delta D_{alkenone}$ vs. δD_{water}

Linear regression analysis between $\delta D_{alkenone}$ and δD_{water} for the reduced SPOM data collected in this study results in a significant positive relationship ($\delta D_{alkenone} = 1.48 \pm 0.36(\delta D_{water}) - 199 \pm 3$, p-value = 0.0001, n = 63; Figure 4.6; Appendix Table A19 and Figure A8). Indeed, the removal of these six 'outlier' data points reduces residual scatter by a factor of two. The slope of this relationship is within two standard deviations of the M'Boule et al. (2014) relationship and three standard deviations of the remaining previously published culture studies, excluding Englebrecht & Sachs (2005). Considering the culture studies observed algal responses over ranges in temperature much smaller and salinities much larger than those measured in the SPOM dataset presented here, the overall agreement between the slopes of these regression equations is quite promising.

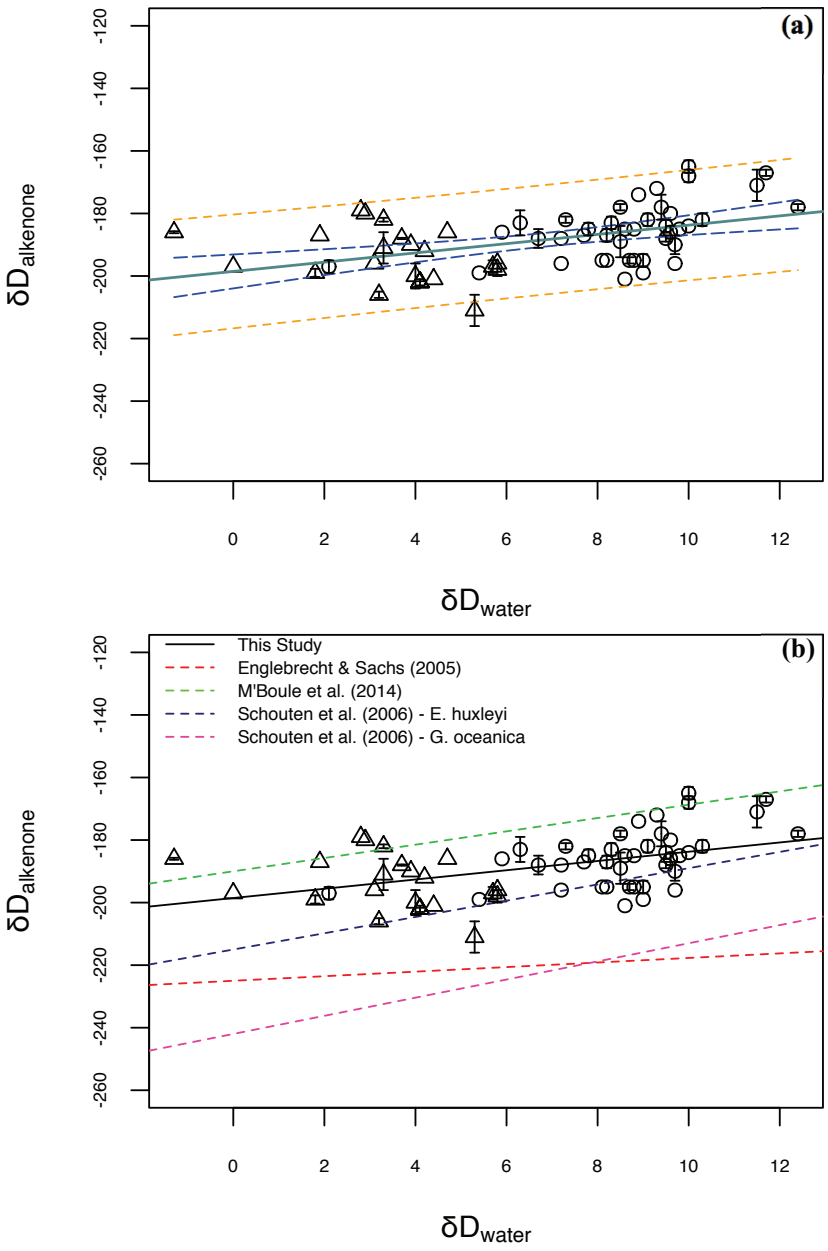

Figure 4.6: (a) Linear regression (teal line) between $\delta D_{alkenone}$ and δD_{water} for the reduced SPOM dataset (Atlantic Ocean samples: circles and Pacific Ocean samples: triangles) $\delta D_{alkenone} = 1.48^* \delta D_{water} - 199$ ($R^2 = 0.22$, p-value = 0.0001, n = 63). Also shown are the 95% confidence (blue-dashed lines) and prediction intervals (yellow-dashed lines). **(b)** Linear regression (black solid line) between $\delta D_{alkenone}$ and δD_{water} for SPOM samples. Shown also are the culture study regressions from Englebrecht & Sachs 2005 (red), Schouten et al. 2006 (*E. huxleyi:* dark blue, *G. oceanica*: pink), and M'Boule et al. 2014 (green). Error bars in both figures indicate standard deviation of replicate isotope analysis. Samples without repeat injection are shown with no error bars.

Table 4.2 Linear regressions for $\delta D_{alkenone}$ vs. δD_{water} from laboratory cultures and this study. Regression coefficient standard errors are reported for the relationships from this study only.

Source	Species	Temperature range (°C)	Salinity range	δD_{water} range (‰)	δD_{water}-$\delta D_{alkenone}$ relationship	n	p-value
Englebrecht & Sachs 2005	*E. huxleyi*	18 (constant)	31.5 -32	-6 to 561	$\delta D_{alk} = 0.73 (\delta D_{water}) - 225$	5	
Schouten et al 2006	*E. huxleyi*	10-21	25 - 35	-5 to 16	$\delta D_{alk} = 2.6 (\delta D_{water}) - 215$	11	
	G.oceanica	15-21	25 - 35	-4 to 11	$\delta D_{alk} = 2.9 (\delta D_{water}) - 242$	6	
M'Boule et al 2014	*E.huxleyi*	15 (constant)	26 - 37	-11 to 7	$\delta D_{alk} = 2.13 (\delta D_{water}) - 190$	20	
This study– full dataset	SPOM	13-30 °C	33 - 38	-1 to 12	$\delta D_{alk} = 1.85 \pm 0.55 (\delta D_{water}) - 202 \pm 4$	69	0.001
This study-reduced dataset	SPOM	13-30 °C	33 - 38	-1 to 12	$\delta D_{alk} = 1.48 \pm 0.36 (\delta D_{water}) - 199 \pm 3$	63	0.0001

4.3.2 $\alpha_{alk\text{-}water}$ vs. SSS

In contrast to the full dataset presented in Chapter 3, the linear regression analysis between $\alpha_{alk\text{-}water}$ and SSS for the reduced SPOM data results in a significant positive relationship ($\alpha_{alk\text{-}water} = 0.002 \pm 0.001(\text{Salinity}) + 0.724 \pm 0.04$, p-value = 0.026, n = 63; Figure 4.7; Appendix Table A20 and Figure A9). The slope of this relationship does not change between the full and reduced SPOM datasets, although the standard error in the slope is reduced from 0.002 to 0.001 in the reduced dataset. The slope of the reduced dataset $\alpha_{alk\text{-}water}$ vs. SSS relationship is within one standard deviation of all slopes reported from culture studies (Table 4.3), and in fact lies directly between the steeper slopes reported from the batch culture literature (Schouten et al., 2006 and M'Boule et al., 2014), and the shallower slope reported from the more recent continuous culture study by Sachs et al. (2016). This observation suggests that there is a relationship between $\alpha_{alk\text{-}water}$ and salinity in the open-ocean environment similar to those reported in laboratory batch culture studies, however a substantial amount of scatter still exists. I infer this scatter to mean that in many of the open-ocean SPOM alkenones sampled, salinity is not the only influential factor in determining or driving increased or decreased fractionation, which is intuitive considering salinity values only vary by 3 units in each of the Atlantic and Pacific basins evaluated in this study. Published relationships observed between other factors such as growth rate, growth phase, irradiance and species effects perhaps overprint the salinity signal on alkenone hydrogen isotopic fractionation in some of these open-ocean samples. Future

analysis addressing these effects in the open-ocean environment will be key to further development of the proxy.

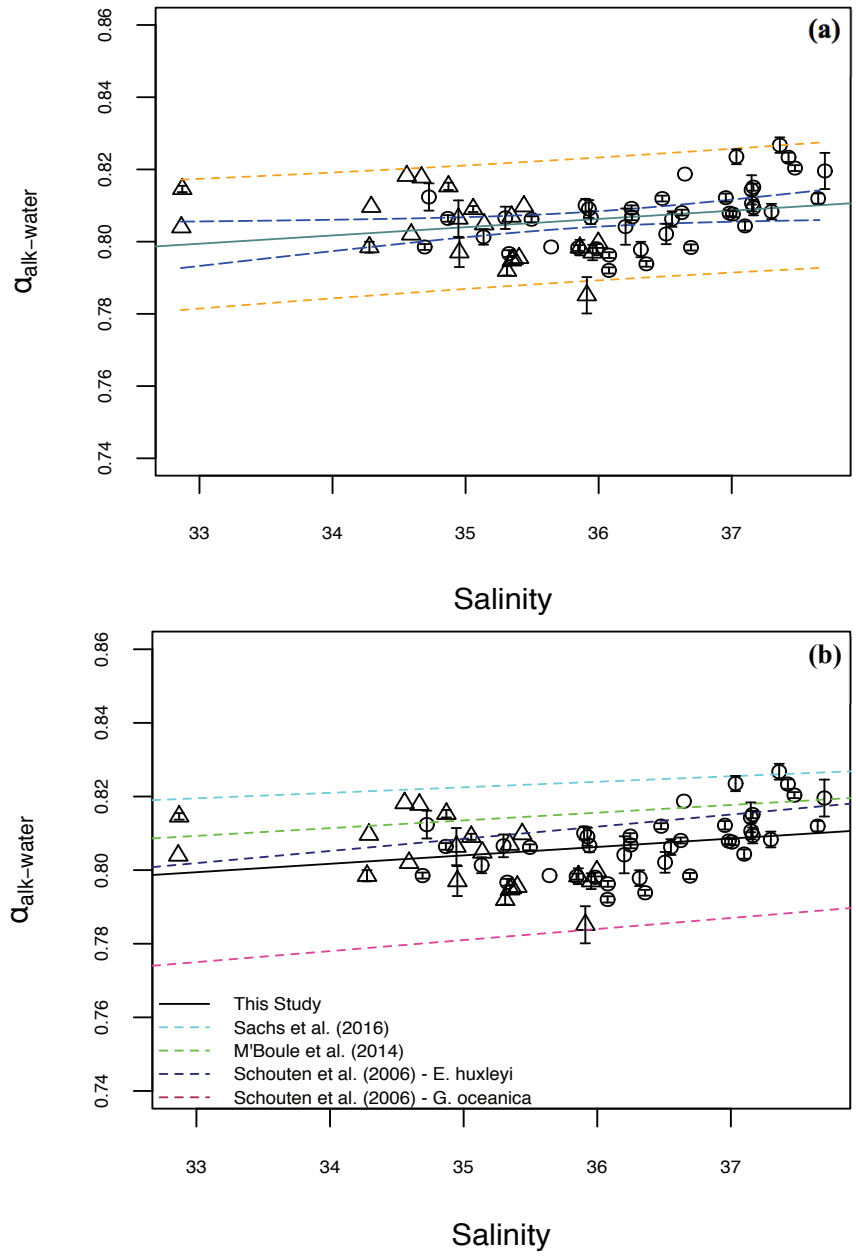

Figure 4.7: (a) Linear regression (teal line) between $\alpha_{alk\text{-}water}$ and SSS for the reduced SPOM dataset (Atlantic Ocean samples: circles and Pacific Ocean samples: triangles) $\alpha_{alk\text{-}water} = 0.002 * \text{Salinity} + 0.724$ ($R^2 = 0.08$, $p = 0.026$, $n = 63$). Also shown are the 95% confidence (blue-dashed lines) and prediction intervals (yellow-dashed lines). **(b)** Linear regression (black solid line) between $\alpha_{alk\text{-}water}$ and salinity for SPOM samples. Shown also are the culture study regressions from Schouten et al. 2006 (*E. huxleyi:* dark blue, *G. oceanica*: pink), and M'Boule et al. 2014 (green) and Sachs et al. 2016 (light blue). Error bars in both figures indicate calculated error in derived $\alpha_{alk\text{-}water}$. Samples without repeat injection are shown with no error bars.

Table 4.3 Linear regressions for $\alpha_{alk\text{-}water}$ vs. salinity from laboratory cultures and this study. Regression coefficient standard errors are reported for the relationships from this study only. Sachs et al. (2016) slope and intercepts are reported here as the average between the C37:2 and C37:3 alkenone $\alpha_{alk\text{-}water}$ vs. salinity coefficients reported.

Source	Species	Temperature range (°C)	Salinity range	δD_{water} range (‰)	α - salinity relationship	n	p-value
Schouten et al. 2006	*E. huxleyi*	10-21	25 - 35	-5 to 16	$\alpha = 0.0033(S) + 0.693$	11	
	G. oceanica	15-21	25 - 35	-4 to 11	$\alpha = 0.003(S) + 0.676$	6	
M'Boule et al. 2014	*E.huxleyi*	15 (constant)	27 - 37	-11 to 7	$\alpha = 0.0021(S) + 0.740$	20	
Sachs et al. 2016	*E.huxleyi*	19 (constant)	20 - 42	-76 to -67	$\alpha = 0.0015(S) + 0.77$	9	
This study-full dataset	SPOM	13-30	33 - 38	-1 to 12	$\alpha = 0.002 \pm 0.002(S) + 0.735 \pm 0.06$	69	0.232
This study-reduced dataset	SPOM	13-30	33 - 38	-1 to 12	$\alpha = 0.002 \pm 0.001(S) + 0.724 \pm 0.04$	63	0.026

4.3.3 $\delta D_{alkenone}$ vs. SSS

Linear regression analysis between $\delta D_{alkenone}$ and SSS for the reduced SPOM data collected in this study results in a strong significant positive relationship ($\delta D_{alkenone} = 4.32 \pm 1.0$(Salinity) - 343±37, p-value = 7.95×10^{-5}, n = 63; Figure 4.8; Appendix Table A21 and Figure A10). The slope of this relationship remains within one standard error of those reported in the culture study literature. While the $\delta D_{alkenone}$ values measured in this open-ocean SPOM dataset do reflect SSS values significantly and in a similar way to cultured algae regressions, there exists a fair amount of scatter in this relationship. As above, I infer from the published literature that this scatter is likely a result of the variability in physiological factors affecting the δD signature in alkenones synthesized in the open-ocean.

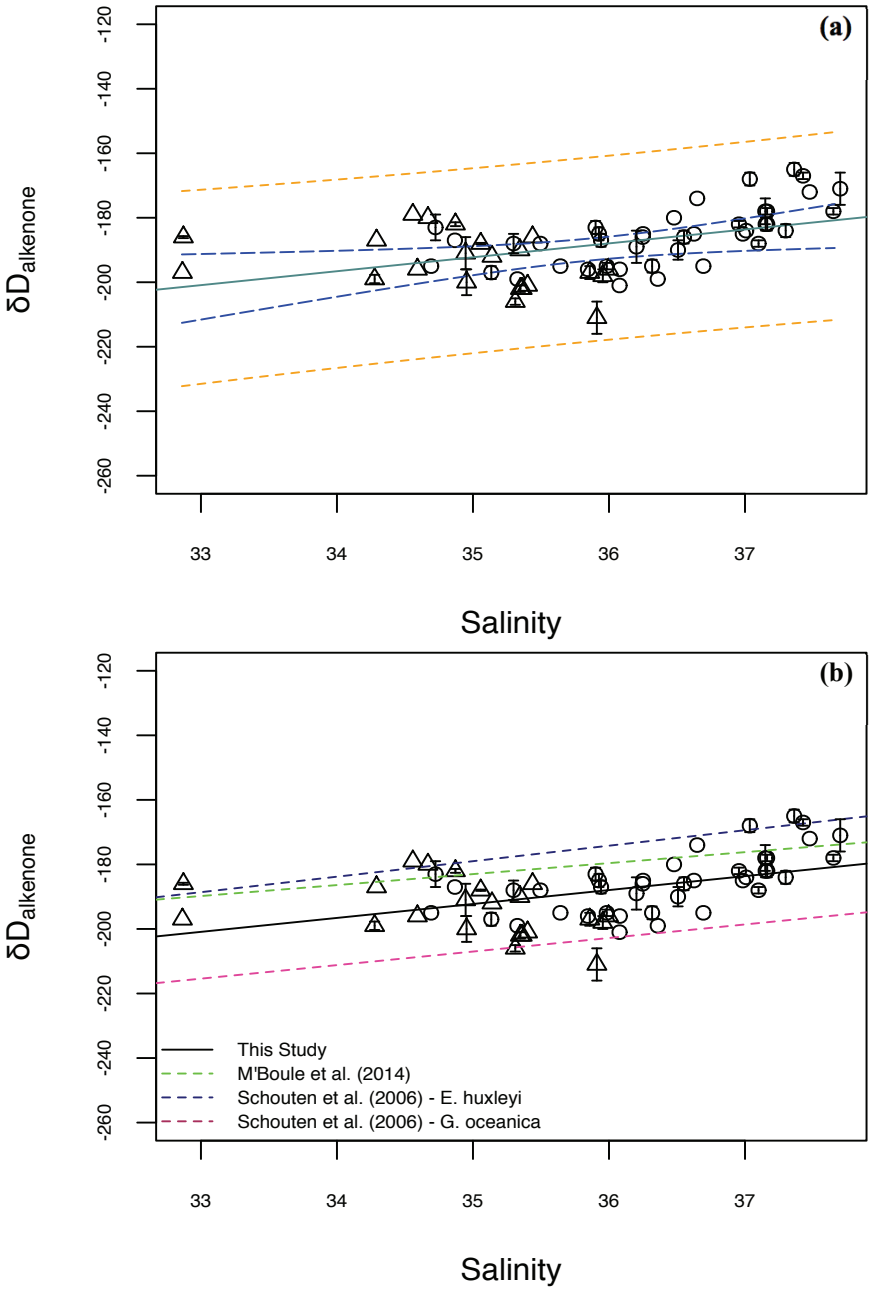

Figure 4.8: (a) Linear regression (teal line) between $\delta D_{alkenone}$ and SSS for the reduced SPOM dataset (Atlantic Ocean samples: circles and Pacific Ocean samples: triangles) $\delta D_{alkenone} = 4.32 * Salinity - 343$ ($R^2 = 0.23$, $p = 7.95x10^{-5}$, $n = 63$). Also shown are the 95% confidence (blue-dashed lines) and prediction intervals (yellow-dashed lines). **(b)** Linear regression (black solid line) between $\delta D_{alkenone}$ and salinity for 63 SPOM samples. Shown also are the culture study regressions from Schouten et al. 2006 (*E. huxleyi:* dark blue, *G. oceanica*: pink), and M'Boule et al. 2014 (green). Error bars in both figures indicate standard deviation of replicate isotope analysis. Samples without repeat injection are shown with no error bars.

Table 4.4 Linear regressions for $\delta D_{alkenone}$ vs. salinity from laboratory cultures and this study. Regression coefficient standard errors are reported for the relationships from this study only.

Source	Species	Temperature range (°C)	Salinity range	δD_{water} range (‰)	$\delta D_{alkenone}$ - salinity relationship	n	p-value
Schouten et al. 2006	*E. huxleyi*	10-21	25 - 35	-5 to 16	$\delta D_{alkenone} = 4.8(S) - 347$	11	
	G. oceanica	15-21	25 - 35	-4 to 11	$\delta D_{alkenone} = 4.2(S) - 354$	6	
M'Boule et al. 2014	*E. huxleyi*	15 (constant)	27 - 37	-11 to 7	$\delta D_{alkenone} = 3.4(S) - 302$	20	
This study-full dataset	SPOM	13-30	33 - 38	-1 to 12	$\delta D_{alkenone} = 4.04 \pm 1.7(S) - 334 \pm 60$	69	0.018
This study-reduced dataset	SPOM	13-30	33 - 38	-1 to 12	$\delta D_{alkenone} = 4.32 \pm 1.0(S) - 343 \pm 37$	63	7.95×10^{-5}

4.3.4 Summary

Although the exclusion of the 6 'anomalous' SPOM data from the analysis above certainly reduces the overall spread in residuals for the SPOM dataset, a substantial amount of scatter still remains in the $\delta D_{alkenone}$ values measured in the open-ocean environment. This scatter is likely a result of open-ocean variability in algal growth rates, resource availabilities, as well as in species compositions sampled in this study. While this preliminary analysis cannot definitively quantify these influences, the results of this study illuminate variability that should be addressed in the future (detailed in Chapter 5 below).

4.4 Quantification of Uncertainty in Salinity Reconstruction

Any proxy for paleo-sea surface salinity requires the development of a calibration accompanied with an associated metric of uncertainty. Ultimately, paleoceanographers are interested in measuring a 'response' variable ($\delta D_{alkenone}$) in the sediments in order to estimate an unknown value of an explanatory variable (SSS). Here, I use the R programming package *invest*r (inverse estimation in R, Greenwell & Schubert Kabban, 2014) to compute an inversion of the linear calibration of $\delta D_{alkenone}$ vs. SSS for the reduced dataset of SPOM alkenone presented in this study. I use the reduced SPOM dataset (Figure 4.8) only as an example

calibration, assuming this dataset is representative of the alkenone signatures that will eventually be recorded in the sediment record.

The package *investr* computes an estimate of SSS based on the inverted $\delta D_{alkenone}$ vs. SSS linear regression for point-wise values of the measured response variable (i.e. a new measured value of $\delta D_{alkenone}$) and also for mean values of the response variable (i.e. mean value of $\delta D_{alkenone}$) each with an associated inversion interval (Figure 4.9). Because replicate or repeat injections of alkenone hydrogen isotopic signatures are measured from a time-integrated 'mean' signal of alkenone flux to the sediments at any given depth in the sedimentary record, I first use a mean response variable (mean value of $\delta D_{alkenone}$) to construct an inverted 95% confidence interval (CI) around an estimated explanatory (SSS) variable.

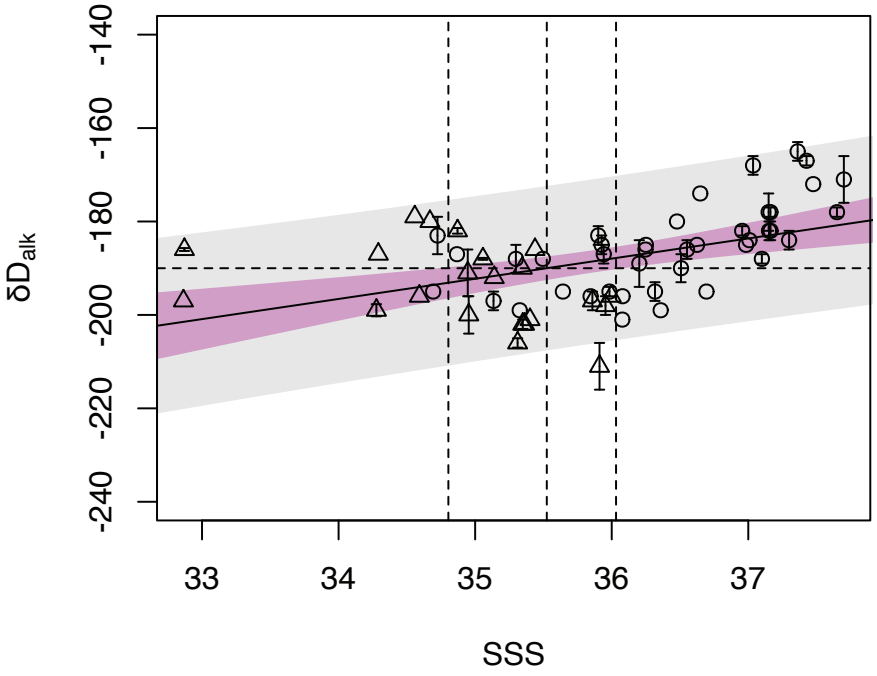

Figure 4.9: Linear regression (black line) for $\delta D_{alkenone}$ on SSS for the reduced SPOM dataset (Atlantic Ocean samples: circles and Pacific Ocean samples: triangles). Also shown are the 95% inversion confidence (purple shading) and prediction intervals (grey shading) built by *investr*. Error bars in both figures indicate standard deviation of replicate isotope analysis. As an example: the black dotted horizontal and vertical lines shown highlight the estimate SSS value (35.5) with 95% inversion confidence interval for the mean response variable $\delta D_{alkenone}$ = -190 (‰). Samples without repeat injection are shown with no error bars.

It is evident from the regression of $\delta D_{alkenone}$ on SSS for the reduced dataset that the data are sparse at both the high and low ends of the salinity range in the open-ocean, such that the associated confidence interval 'flares' out - is larger - at both ends of the $\delta D_{alkenone}$ vs. SSS relationship (Figure 4.9). Where most confidence in the regression line lies, the confidence interval is much narrower (i.e. between ~ -180 and -190‰). A table of estimated SSS values and upper and lower bounds of confidence for all mean response values of $\delta D_{alkenone}$ (between -170 and -210 at 1‰ intervals) is provided in Appendix Table A22.

As an example, for mean $\delta D_{alkenone}$ values of -185 and -190‰, estimates of SSS are 36.7 (upper CI: 37.7, lower CI: 36.2) and 35.5 (upper CI: 36.0, lower CI: 34.8), respectively. This exercise suggests that a difference on the order of 5‰ in $\delta D_{alkenone}$ would indeed be representative of two statistically different SSS values, and that SSS variations as low as ~ 1.2 in this case can be reconstructed. Alternatively, based on the SPOM dataset presented here, a mean $\delta D_{alkenone}$ measure of -205 vs. -210‰, would according to this inversion, yield estimates of SSS with much larger and indeed overlapping confidence intervals, such that these measurements could not be interpreted as statistically different SSS values. For instance, mean $\delta D_{alkenone}$ measures of -205 and -210‰ would have associated estimates of SSS of 32.0 (upper CI: 33.4, lower CI: 28.5) and 30.9 (upper CI: 32.6, lower CI: 26.4).

If, on the other hand measures of $\delta D_{alkenone}$ down-core are considered as point estimates (not of an average or the mean response as treated above), due to the scatter in the SPOM dataset analyzed here, the 95% inversion interval for the inverted estimates of SSS become very large (on the order of 10 salinity units), so much so that the applicability of the proxy would certainly not be feasible. In this case, a measurement of $\delta D_{alkenone}$ of -190‰ would result in the same estimated SSS value of 35.5, however the upper and lower inversion intervals would now be between 40.0 and 30.8. The 95% point-estimate inversion intervals are also reported in Appendix Table A22 for comparison. Clearly, depending on how the down-core measurements of $\delta D_{alkenone}$ are defined (i.e. mean response or single point measurements) will impact the reliability with which the proxy can be used.

Finally, for comparison I have computed a measure of uncertainty for reconstructions of SSS using the standard error of estimate from this open-ocean $\delta D_{alkenone}$ vs. SSS calibration. This technique is commonly applied in global ocean

core-top U^{K}_{37}' temperature calibrations, where the standard error of estimate is ±0.05 U^{K}_{37}' units or ± 1.5 °C (Müller et al. 1998). Reporting uncertainty associated with SSS reconstructions in this way results in an error of ± 2 salinity units for all $\delta D_{alkenone}$ values (± 8.62 $\delta D_{alkenone}$ (‰)). However, this measure does not take into consideration the increase in the confidence intervals as the open-ocean dataset becomes data-sparse at both low and high salinity values. This method, therefore, likely produces an overestimate, in some cases, of the confidence with which we can report salinity reconstructions based on this particular open-ocean calibration.

The collection of additional open-ocean samples in the future will help to develop a more complete calibration of the open-ocean $\delta D_{alkenone}$ vs. SSS relationship. In particular, filling in the dataset at both low (32) and high (38) salinities, for example with samples from regions like the Equatorial Pacific (low salinity) and the Mediterranean/ Red Sea (high salinity), would improve the confidence with which SSS can be estimated. I hypothesize that perhaps the most appropriate measure of uncertainty is to treat the down-core measurements of $\delta D_{alkenone}$ as average or mean response variables and to use a program like *investr* to construct inversion intervals on SSS reconstructions. I speculate that, especially for a sparse calibration dataset such as this, the computation of inversion intervals for SSS reconstructions would be more representative of the confidence with which to reliably interpret $\delta D_{alkenone}$ values measured down-core than would applying a standard error of estimate to all possible reconstructions of SSS.

CHAPTER 5: CONCLUSION

5.1 Conclusion

The lack of a well constrained proxy for paleo sea surface salinity is unfortunate as small changes in salinity can drive relatively large changes in ocean water density and thus affect ocean circulation. Furthermore, surface ocean salinity is an important indicator of the hydrological cycle. In recent years, the advancement of compound specific isotope measurements has made possible the development of a novel proxy for the reconstruction of past ocean surface salinities – the hydrogen isotopic composition of biomarkers. The proxy relies on the mechanistic link between isotopic fractionation of surface ocean water (δD_{water}) and surface ocean salinity as well as the systematic recording of the surface ocean δD_{water} signature in biomarker molecules (i.e. alkenone molecules) that can be measured in sediment records.

Thus far, the proxy has been examined extensively in laboratory culture studies, where the relationships between δD_{water} vs. $\delta D_{alkenone}$ and $\alpha_{alk\text{-}water}$ -SSS and $\delta D_{alkenone}$ – SSS have been constrained for a number of different algal alkenone producers. In addition, there have been three small-scale field studies (Schwab & Sachs, 2011; Häggi et al., 2015; Wolhowe et al., 2015) evaluating the $\delta D_{alkenone}$ salinity proxy in SPOM alkenone samples. However, a large-scale field evaluation of the proxy in the modern day open-ocean environment is still missing.

The results of this study shed light on the open-ocean variability in the δD_{water} vs. $\delta D_{alkenone}$ relationship (thesis objective (1)). The entire SPOM dataset analyzed here covers a wide array of natural open-ocean environments, which are not fully captured in laboratory studies, however, estimated slope parameters for all three regression equations examined ($\delta D_{alkenone} - \delta D_{water}$, $\alpha_{alk\text{-}water}$ -SSS and $\delta D_{alkenone}$ – SSS) align well with, and are within one or two standard errors in most cases of those reported in the literature (thesis objective (3)). This finding is especially significant due to the fact that the SPOM samples presented in this study represent only the 'tail-end' of the salinity values (33-38) analyzed in the relationships developed in the laboratory setting (~25-37).

Investigation of the scatter in the relationships between $\delta D_{alkenone} - \delta D_{water}$, $\alpha_{alk\text{-}water}$ -SSS and $\delta D_{alkenone}$ – SSS reveals a set of 6 samples in particular, determined

as anomalous mainly via coincident anomalous $\delta^{13}C_{alkenone}$ values (thesis objective (2)). Co-occurring anomalous $\delta D_{alkenone}$ and $\delta^{13}C_{alkenone}$ measurements in this SPOM dataset are inferred to be indicative of alkenones synthesized under 'extreme' physiological conditions. Indeed, this finding illustrates the potential power of combined $\delta D_{alkenone}$ and $\delta^{13}C_{alkenone}$ measurements for proxy validation in future SPOM and sedimentary studies.

Finally, the inversion of the $\delta D_{alkenone}$ vs. SSS SPOM regression, with associated inversion intervals, serves as an example of how the quantification of errors associated with reconstructions of SSS might be applied to previously published and future measurements of $\delta D_{alkenone}$ down-core (thesis objective (4)). However, because the regression between $\delta D_{alkenone}$ and SSS in this study is data poor at both ends of the salinity range, the uncertainty in SSS reconstructions for $\delta D_{alkenone}$ values approaching ~200 and ~170 ‰ are very large (between 6 and 10 salinity units). Future contributions of SPOM $\delta D_{alkenone}$ samples collected from high (38) and low (32) open-ocean salinities would help to improve the regression between $\delta D_{alkenone}$ and SSS, thus reducing the overall uncertainty associated with SSS reconstructions.

From the data presented here, I conclude that $\delta D_{alkenone}$ signals from open-ocean SPOM samples are reflective of both δD_{water} and SSS, and in general agree with observations reported in the literature from laboratory and small-scale field studies. However, the applicability of the proxy to reconstructions of (small-scale) variations in surface ocean salinities will depend on the ability to reliably constrain physiological and environmental effects on the fractionation of alkenone hydrogen isotopes (e.g. via concert measurements of $\delta^{13}C_{alkenone}$).

5.2 Recommendations for Future Analysis

Considering this is the first large-scale field study, to my knowledge, evaluating $\delta D_{alkenone}$ in SPOM from the open-ocean, many questions regarding the applicability of the proxy remain unresolved. Overall, the $\delta D_{alkenone}$ vs. δD_{water} relationship in the open-ocean agrees with many of the previously reported regressions developed from laboratory culture studies and some small-scale field studies. Significant scatter in this relationship, however, draws attention to factors

beyond salinity that may influence the hydrogen isotopic composition of alkenones in the natural surface ocean environment, which require further investigation. With specific regards to the observations made in this study, it would be informative to address whether the northern Atlantic group of samples with very low $\alpha_{alk\text{-}water}$ values are a consistent feature of this region. Ideally, to build an understanding of seasonal and Interannual variability in the open-ocean environment would be very informative, particularly in the high latitude regions known for quite substantial variability in haptophyte abundances (i.e. coccolithophore spring and fall blooms). The AMT program is one obvious place where the same or a similar transect of SPOM samples could be obtained from the Atlantic basin.

An important next step would be to build on the dataset presented in this study by incorporating additional open-ocean SPOM $\delta D_{alkenone}$ data. Particularly, to 'fill in' the calibration dataset with samples from high and low open-ocean salinity regions (e.g., the Equatorial Pacific and the Mediterranean Sea). Overall, a more complete SPOM dataset would enable a more accurate calibration of $\delta D_{alkenone}$ vs. salinity, and would allow for a more reliable quantification of uncertainty associated with SSS reconstructions.

Future investigations of $\delta D_{alkenone}$ signatures in the natural ocean environment should also aim to incorporate sampling of physiological and environmental parameters that have been shown in laboratory culture studies to significantly influence $\delta D_{alkenone}$. Where possible, species composition, growth rate estimations as well as resource availability (nutrients and irradiance) would be informative. A potentially powerful tool, as borne out by the inferences made in this study as well as by Wolhowe et al. (2015), would be the coincident measurements of $\delta D_{alkenone}$ and $\delta^{13}C_{alkenone}$. Indeed, as suggested by Wolhowe et al. (2009), $\delta D_{alkenone}$ may serve as a physiological proxy in addition to a salinity proxy. In particular, collection of $\delta^{13}C_{CO2}$ and $\delta^{13}C_{DIC}$ and $[CO_{2(aq)}]$ data in order to calculate the carbon isotopic fractionation factor (ε_p) would be instructive. It would also be useful to measure $\delta D_{alkenone}$ and $\delta^{13}C_{alkenone}$ isotope signatures in parallel in the laboratory setting.

As with all alkenone biomarker proxies, there is a broader need for a more thorough understanding of the depth at which alkenones are produced and ultimately exported to the sediments. In order to elucidate how alkenone hydrogen

isotopic signatures change throughout the water column, sampling at several depths – as done by Wolhowe et al. (2015)- would begin to address this variability. Further, SPOM $\delta D_{alkenone}$ measurements coupled with sediment trap and core-top sediment $\delta D_{alkenone}$ samples are necessary to shed light on how and when these alkenone molecules are reaching and recorded in the seafloor. While many culture studies have evaluated the alkenone $\delta D_{alkenone}$ proxy in the laboratory setting, there has been only one (to my knowledge) evaluation of a core-top 'calibration' in the open-ocean setting. Englebrecht & Sachs (2005) showed that $\delta D_{alkenone}$ signatures in SPOM and core-tops from the northwest Atlantic region align quite well, which illustrates the need for further studies of this kind.

REFERENCES

Airs, R., & Martinez-Vicenta, V. (2014). AMT20(JC053) HPLC pigment measurements from CTD bottle samples. British Oceanographic Data Centre-Natural Environment Research Council, UK. doi: 10/tk4

Andersen, N., Müller, P.J., Kirst, G., & Schneider, R. (1999). Alkenone d13C as a Proxy for Past PCO2 in Surface Waters: Results from the Late Quaternary Angola Current. In: G. Fischer & G. Wefer (Eds.), *Use of Proxies in Paleoceanography – Examples from the South Atlantic* (pp. 469-488). Springer: Berlin, Heidelberg.

Antonov, J. I., Locarnini, R. A., Boyer, T. P., Mishonov, A. V., & Garcia, H. E. (2006). *World Ocean Atlas 2005, Volume 2: Salinity*. *US Government Printing Office*, Washington, DC.

Baumgartner, A., & Reichel, E. (1975). World Water Balance: Mean Annual Global, Continental and Maritime Precipitation, Evaporation and Runoff. *Elsevier,* Amsterdam.

Bentaleb, I., Fontugne, M., Descolas-Gros, C., Girardin, C., Mariotti, A., Pierre, C., Brunet, C., & Poisson, A., (1996). Organic carbon isotopic composition of phytoplankton and sea surface pCO_2 reconstructions in the Southern Indian Ocean during the last 50,000 yr. *Organic Geochemistry, 24*(4), 399–410. doi: 10.1016/0146-6380(96)00043-5

Bentaleb, I., Grimalt, J.O., Vidussi, F., Marty, J.C., Martin, V., Denis, M., Hatté, C., & Fontugne, M. (1999). The C37 alkenone record of seawater temperature during seasonal thermocline stratification. *Marine Chemistry, 64*(4), 301-313. doi: 10.1016/S0304-4203(98)00079-6

Benthien, A., & Müller, P.J. (2000). Anomalously low alkenone temperatures caused by lateral particle and sediment transport in the Malvinas Current region, western Argentine Basin. *Deep-Sea Research I, 47*(12), 2369-2393. doi: 10.1016/S0967-0637(00)00030-3

Benthien, A., Andersen, N., Schulte, S., Müller, P.J., Schneider, R.R., & Wefer, G. (2002). Carbon isotopic composition of the $C_{37:2}$ alkenone in core top sediments of the South Atlantic Ocean: Effects of CO_2 and nutrient concentrations. *Global Biogeochemical Cycles, 16*(1), 12-1 – 12-12. doi: 10.1029/2001GB001433

Bidigare, R.R. et al. (1997). Consistent fractionation of 13C in nature and in the laboratory: growth-rate effects in some haptophyte algae. *Global Biogeochem. Cycles*, 11, 279-292.

Braconnot, P., Otto-Bliesner, B., Harrison, S., Joussaume, S., Peterchmitt, J.Y., Abe-Ouchi, A., Crucifix, M., Driesschaert, E., Fichefet, Th., Hewitt, C.D., Kageyama, M., Kitoh, A., Laîné, A., Loutre, M.F., Marti, O., Merkel, U., Ramstein, G., Valdes, P., Weber, S.L., Yu, Y., & Zhao, Y. (2007). Results of PMIP2 coupled simulations of the Mid-Holocene and Last Glacial Maximum – Part 2: feedbacks with emphasis on the location of the ITCZ and mid- and high latitudes heat budget. *Climate of the Past,* 3, 279-296. doi: 10.5194/cp-3-279-2007

Brassell, S. C., Eglinton, G., Marlowe, I. T., Pflaumann, U., & Sarnthein, M. (1986a). Molecular stratigraphy: a new tool for climatic assessment. *Nature,* 320, 129–133. doi:10.1038/320129a0

Brassell S. C., Brereton R. G., Eglinton G., Grimalt J., Liebezeit G., Marlowe I. T., Pflaumann U., & Sarnthein, M. (1986b). Palaeoclimatic signals recognized by chemometric treatment of molecular stratigraphic data. *Organic Geochemistry,10*(4-6), 649–660. doi: 10.1016/S0146-6380(86)80001-8

Broecker, W. S., & Peng, T.-H. (1982). Tracers in the sea. *Columbia University, Palisades, NY: Eldigio Press.*

Burgoyne, T.W., & Hayes, J.M. (1998). Quantitative production of H2 by pyrolysis of gas chromatographic effluents. *Analytical Chemistry, 70*(24), 5136-5141. doi: 10.1021/ac980248v

Chikaraishi, Y., Suzuki, Y., & Naraoka, H. (2004). Hydrogen isotopic fractionations during desaturation and elongation associated with polyunsaturated fatty acid biosynthesis in marine macroalgae. *Phytochemistry, 65*(15)*,* 2293–2300. Retrieved from https://www.ncbi.nlm.nih.gov/pubmed/15587713

Chivall, D., M'Boule, D., Sinke-Schoen, D., Sinninghe Damsté, J.S., Schouten, S., & van der Meer, M.T.J. (2014). The effects of growth phase and salinity on the hydrogen isotopic composition of alkenones produced by coastal haptophyte algae. *Geochimica et Cosmochimica Acta*, 140, 381-390. doi: 10.1016/j.gca.2014.05.043.

Coolen, M. J. L., Orsi, W. D., Balkema, C., Quince, C., Harris, K., Sylva, S. P., Filipova-Marinova, M., & Giosan, L. (2013). Evolution of the plankton paleome in the Black Sea from the Deglacial to Anthropocene. *Proc. Natl. Acad. Sci. U.S.A. 110*(21), 8609–8614. doi: 10.1073/pnas.1219283110

Conte, M., Volkman, J. K., & Eglinton, G. (1994a). Lipid biomarkers of the Haptophyta. In J.C. Green and B.S.C. Leadbeater (Eds.), *The Haptophyte Algae* (pp. 351–377). Clarendon Press, Oxford.

Conte, M.H., Thompson, A., & Eglinton, G. (1994b). Primary production of lipid biomarker compounds by *Emiliania huxleyi*: Results from an experimental mesocosm study in fjords of southern Norway. *Sarsia, 79*(4), 319–332. doi: 10.1080/00364827.1994.10413564

Conte, M.H., Sicre, M.A., Rühlemann, C., Weber, J.C., Schulte, S., Schulz-Bull, D., & Blanz, T. (2006) Global temperature calibration of the alkenone unsaturation index (UK'37) in surface waters and comparison with surface sediments. *Geochemistry, Geophysics, Geosystems, 7*(2). doi: 10.1029/2005GC001054.

Craig, H. (1961). Isotopic variations in meteoric waters. *Science, 133*(3465), 1702-1703. doi:10.1126/science.133.3465.1702

Craig, H., & Gordon, L.I. (1965). Deuterium and oxygen 18 variations in the ocean and marine atmosphere. *Proceedings of a Conference on Stable Isotopes in Oceanographic Studies and Paleotemperatures. Pisa: V. Lischi & Figli., Spoleto, Italy,* pp. 9–130. Retrieved from http://climate.colorado.edu/research/CG/CraigGordon1965_Noone_small3.pdf

D'Andrea, W. J., Liu, Z., Da Rosa Alexandre, M., Wattley, S., Herbert, T. D., & Huang, Y. (2007). An efficient method for isolating individual long-chain alkenones for compound-specific hydrogen isotope analysis. *Analytical Chemistry, 79*(9), 3430–3435. doi:10.1021/ac062067w

de Leeuw, J. W., van der Meer, F. W., Rijpstra, W. I. C., & Schenck, P. A. (1980). On the occurrence and structural identification of long chain unsaturated ketones and hydrocarbons in sediments. *Physics and Chemistry of the Earth,* 12, 211–217. doi: 10.1016/0079-1946(79)90105-8

de Vernal, A., Guiot, J., & Turon, J.L. (1993). Late and Postglacial Paleoenvironments of the Gulf of St. Lawrence: Marine and Terrestrial Palynological Evidence. *Géographie Physique et Quaternaire, 47*(2), 167–180. doi: 10.7202/032946ar

de Vernal, A., Turon, J.-L., & Guiot, J. (1994). Dinoflagellate cyst distribution in high latitude environments and quantitative reconstruction of sea-surface temperature, salinity and seasonality. *Canadian Journal of Earth Sciences,* 31, 48–62. Retrieved from http://www.nrcresearchpress.com/doi/pdf/10.1139/e94-006

de Vernal, A., Hillaire-Marcel, C., & Bilodeau, G. (1996). Reduced meltwater outflow from the Laurentide ice margin during the Younger Dryas. *Nature (London),* 381, 774–777. doi: 10.1038/381774a0

de Vernal, A., Rochon, A., Turon, J.-L., & Matthiessen, J. (1997). Organic-walled dinoflagellate cysts: palynological tracers of sea-surface conditions in middle to high latitude marine environments. *GEOBIOS, 30*(7), 905–920. doi: 10.1016/S0016-6995(97)80215-X

de Vernal, A., Hillaire-Marcel, C., Turon, J.L., & Matthiessen, J. (2000). Reconstruction of sea-surface temperature, salinity, and sea-ice cover in the northern North Atlantic during the last glacial maximum based on dinocyst assemblages. *Canadian Journal of Earth Sciences, 37*(5), 725-750. doi: 10.1139/e99-091

Ehrlich, A. (1978). The diatoms of the hyperhaline Solar Lake (NE Sinai). *Israel Journal of Botany, 27,* 1–13.

Eilers, P.H.C. & Peeters, J.C.H. (1988). A model for the relationship between light intensity and the rate of photosynthesis in phytoplankton. *Ecological Modelling,* 42, 199-215.

Eltgroth, M.L., Watwood, R.L., & Wolfe, G.V. (2005). Production and cellular localization of neutral long-chain lipids in the haptophyte algae *Isochrysis galbana* and *Emiliania huxleyi. J. Phycol.,* 41, 1000-1009. doi: 10.1111/j.1529-8817.2005.00128.x

Englebrecht, A.C., & Sachs, J.P. (2005). Determination of sediment provenance at drift sites using hydrogen isotopes and unsaturation ratios in alkenones. *Geochimica et Cosmochimica Acta*, *69*(17), 4253-4265. doi: 10.1016/j.gca.2005.04.011.

Epstein, B. L., D'Hondt, S., & Hargraves P. E. (2001). The possible metabolic role of C_{37} alkenones in *Emiliania huxleyi*. *Organic Geochemistry, 32*(6), 867–875. doi: 10.1016/S0146-6380(01)00026-2

Estep, M.F., & Hoering, T.C. (1980). Biogeochemistry of the stable hydrogen isotopes. *Geochim Cosmochim Acta,* 44, 1197-1206.

Fleitmann, D., Burns, S.J., Mangini, A., Mudelsee, M., Kramers, J., Villa, I., Neff, U., Al-Subbary, A.A., Buettner, A., Hippler, D., & Matter, A. (2007). Holocene ITCZ and Indian monsoon dynamics recorded in stalagmites from Oman and Yemen (Socotra). *Quaternary Science Reviews, 26*(1-2), 170-188. doi: 10.1016/j.quascirev.2006.04.012

Fontugne, M.R., & Calvert, S.E. (1992). Late Pleistocene variability of the carbon isotopic composition of organic matter in the Eastern Mediterranean: Monitor of changes in carbon sources and atmospheric CO_2 concentrations. *Paleoceanography, 7*(1), 1-20. doi: 10.1029/91PA02674

Friedman, I., Redfield, A.C., Schoen, B., & Harris, J. (1964). The variation of the deuterium content of natural waters in the hydrologic cycle. *Reviews of Geophysics, 2*(1), 177-224. doi: 10.1029/RG002i001p00177

Fritz, S.C. (2013). Salinity and Climate Reconstructions from Continental Lakes. In (Scott A. Elias and Cary J. Mock (Eds.) *Encyclopedia of Quaternary Science*, 2nd ed., pp. 507–515. Retrieved from http://digitalcommons.unl.edu/geosciencefacpub/448/

Ganachaud, A., & Wunsch, C. (2000). Improved estimates of global ocean circulation, heat transport and mixing from hydrographic data. *Letters to Nature, Nature,* 408, 453- 457. doi: 10.1038/35044048

Gasse, F. (1987). Diatoms for reconstructing palaeoenvironments and palaeohydrology in tropical semi-arid zones. *Hydrobiologia, 154*(1), 127-163. Retrieved from https://link.springer.com/article/10.1007/BF00026837

Gat, J.R. (1996) Oxygen and Hydrogen Isotopes in the Hydrological Cycle. *Annu. Rev. Earth Planet Sci.,* 24, 225-262.

Geider, R.J., MacIntyre, H.L., & Kana, T.M. (1997). Dynamic model of phytoplankton growth acclimation: responses of the balanced growth rate and the chlorophyll a:carbon ratio to light, nutrient-limitation and temperature. *Marine Ecology Progress Series,* 148, 187-200.

GEOTOP- UQAM Stable Isotope Geochemistry Laboratory. 201 President-Kennedy Avenue, Montreal, QC, Canada. URL: http://www.geotop.ca/fr/laboratoires/liste/10-labo/999-laboratoire-de-geochimie-des-isotopes-stables-uqam.html

Goñi, M.A., Hartz, D.M., Thunell, R.C., & Tappa, E. (2001). Oceanographic consideration for the application of the alkenone-based paleotemperature U^{K}_{37}' index in the Gulf of California. *Geochemica et Cosmochimica Act, 65*(4), 545-557. Retrieved from http://www.academia.edu/22921030/Oceanographic_considerations_for_the_application_of_the_852_M

Gould, J., Kienast, M., & Dowd, M. (2017). Investigation of the U^{K}_{37}' vs. SST relationship for Atlantic Ocean suspended particulate alkenones: An alternative regression model and discussion of possible sampling bias. *Deep Sea Research Part I: Oceanographic Research Papers,* 123, 13-21. doi: 10.1016/j.dsr.2017.02.007

Greenwell, B.M., & Schubert Kabban, C.M. (2014). Investr: An R Package for Inverse Estimation. *The R Journal, 6*(1), 90-100. URL: http://journal.r-project.org/archive/2014-1/greenwell-kabban.pdf.

Häggi, C., Chiessi, C.M., & Schefuß, E. (2015). Testing the D/H ratio of alkenones and palmitic acid as salinity proxies in the Amazon Plume. *Biogeosciences*, *12*(23), 7239-7249. doi: 10.5194/bg-12-7239-2015

Harada, N., Sato, M., Shiraishi, A., & Honda, M.C. (2006). Characteristic of alkenone distributions in suspended and sinking particles in the northwestern North Pacific. *Geochimica et Cosmochimica Acta, 70*(8), 2045-2062. doi: 10.1016/j.gca.2006.01.024

Harris, C., & Woodward, E.M.S. (2014). AMT20 (JC053) micro-molar nutrient measurements from CTD bottle samples. British Oceanographic Data Centre-Natural Environment Research Council, UK. doi: 10/r5x.

Harris, G. N., Scanlan, D. J., & Geider, R. J. (2005). Acclimation of *Emiliania huxleyi* (Prymnesiophyceae) to photon flux density. *Journal of Phycology, 41*(4), 851–862. doi: 10.1111/j.1529-8817.2005.00109.x

Herbert, T. D. (2013). Alkenone Paleotemperature Determinations. In *Treatise on Geochemistry: Second Edition, 8,* 399–433. doi:10.1016/B978-0-08-095975-7.00615-X

Hilkert, A.W., Douthitt, C.B., Schlüter, H.J., & Brand, W.A. (1999). Isotope ratio monitoring gas chromatography/mass spectrometry of D/H by high temperature conversion isotope ratio mass spectrometry. *Rapid Communications in Mass Spectrometry, 13*(13),1226–1230. doi: 10.1002/(SICI)1097-0231(19990715)13:13<1226::AID-RCM575>3.0.CO;2-9

Houghton, J. T. et al. (eds). (1995). IPCC Climate Change 1995. *Cambridge Univ. Press.*

Hustedt, F. (1953). Die Systematik der Diatomeen in ihren Beziehungen zur Geologie und Ökologie nebst einer Revision des Halobien-systems. *Botanisk Tidskkrift, 47*, 509–519.

Jasper, J.P., & Hayes, J.M. (1990). A carbon isotope record of CO_2 levels during the late Quaternary. *Letters to Nature, Nature, 347*, 462-464. doi: 10.1038/347462a0

Jasper, J.P., Hayes, J.M., Mix, A.C., & Prahl, F.G. (1994). Photosynthetic fractionations of ^{13}C and concentrations of dissolved CO_2 in the central equatorial Pacific during the last 255,000 years. *Paleoceanography, 9*(6), 781-798. doi: 10.1029/94PA02116

JPOTS (Joint Panel) (1980). The practical salinity scale 1978 and the international equation of state of seawater. *Paris, UNESCO* 25pp.

Kasper, S., van der Meer, M.T.J., Castañeda, I.S., Tjallingii, R., Brummer, G.A., Sinninghe Damsté, J.S., & Schouten, S. (2014). Testing the alkenone D/H ratio as a paleo indicator of sea surface salinity in a coastal ocean margin (Mozambique Channel). *Organic Geochemistry*, 78, 62-68. doi: 10.1016/j.orggeochem.2014.10.011

Kinkel, H., Baumann, K.H., & Čepek, M. (2000). Coccolithophores in the equatorial Atlantic Ocean: response to seasonal and Late Quaternary surface water variability. *Marine Micropaleontology, 39*(1-4), 87-112. doi: 10.1016/S0377-8398(00)00016-5

Kolbe, RW. (1927). Zur Okologie, Morphologie und Systematik der Brackwasser-Diatomeen. *Pflanzenforschung, 7*, 1–146.

Kreuzer-Martin, H. W., Ehleringer, J.R., & Hegg, E. L. (2005). Oxygen isotopes indicate most intracellular water in log-phase *Escherichia coli* is derived from metabolism. *Proc. Natl. Acad. Sci. U.S.A., 102*(48), 337–341. doi: 10.1073/pnas.0506531102

Ladd, S.M., Dubois, N., & Schubert, C.J. (2017). Interplay of community dynamics, temperature, and productivity on the hydrogen isotope signatures of lipid biomarkers. *Biogeosciences,* 14, 3979-3994. doi: 10.5194/bg-14-3979-2017

Landry, M.R., & Hasset, R.P. (1982). Estimating grazing impact of marine micro-zooplankton. *Marine Biology,* 67, 283-288.

Laws, E. A., Popp, B.N., Cassar, N., & Tanimoto, J. (2002). ^{13}C discrimination patterns in oceanic phytoplankton: likely influence of CO_2 concentrating mechanisms, and implications for paleoreconstructions. *Functional Plant Biology,* 29**,** 323-333.

Longhurst, A. (1995). Seasonal cycles of pelagic production and consumption. *Progress in Oceanography, 36*(2), 77-167. doi: 10.1016/0079-6611(95)00015-1

Longhurst, A. (2007). Ecological Geography of the Sea. *Academic Press, Boston.*

Luo, Y.-H., Steinberg, L., Suda, S., Kumazawa, S., & Mitsui, A. (1991). Extremely low D/H ratios of photoproduced hydrogen by cyanobacteria. *Plant Cell Physiology, 32*(6), 897–900. doi: 10.1093/oxfordjournals.pcp.a078158

Macdonald, A. M., & Wunsch, C. (1996). An estimate of global ocean circulation and heat fluxes. *Letters to Nature, Nature, 382*, 436–439. doi: 10.1038/382436a0

Marlowe, I. T., Green, J. C., Neal, a. C., Brassell, S. C., Eglinton, G., & Course, P. A. (1984). Long chain (n-C_{37}–C_{39}) alkenones in the Prymnesiophyceae: Distribution of alkenones and other lipids and their taxonomic significance. *British Phycological Journal, 19*(3), 203–216. doi:10.1080/00071618400650221

Martin, G. J., Zhang, B. L., Naulet, N., & Martin, M. L. (1986). Deuterium transfer in the bioconversion of glucose to ethanol studied by specific isotope labeling at the natural abundance level. *Journal of the American Chemical Society, 108*(17), 5116–5122. doi: 10.1021/ja00277a013

M'boule, D., Chivall, D., Sinke-Schoen, D., Sinninghe Damsté, J. S., Schouten, S., & van der Meer et al., M. T. J. (2014). Salinity dependent hydrogen isotope fractionation in alkenones produced by coastal and open ocean haptophyte algae. *Geochimica et Cosmochimica Acta, 130,* 126–135. doi: 10.1016/j.gca.2014.01.029

Millero, F. J. (1996). Chemical Oceanography (2nd ed). *New York, CRC Press.*

Müller, P.J., Kirst, G., Ruhland, G., von Storch, I., & Rosell-Melé, A. (1998). Calibration of the alkenone paleotemperature index $U_{37}^{K'}$ based on core-tops from the eastern South Atlantic and the global ocean (60°N-60°S). *Geochimica et Cosmochimica Acta, 62(*10), 1757-1772. doi: 10.1016/S0016-7037(98)00097-0

Müller, P.J., Schneider, R., & Ruhland, G. (1994). Late Quaternary PCO_2 variations in the Angola Current: Evidence from organic carbon $\delta^{13}C$ and alkenone temperatures. In R. Zahn et al. (Eds.) *Carbon Cycling in the Glacial Ocean: Constraints on the Ocean's Role in Global Change*, *NATO Asi Series,* 17, 25-30.

Nanninga, H. J., & Tyrell, T. (1996). The importance of light for the formation of algal blooms by *Emiliania huxleyi*. *Marine Ecology Progress Series, 136*(1/3), 195–203. Retrieved from http://www.jstor.org/stable/24856733?seq=1#page_scan_tab_contents

Ohkouchi, N., Kawamura, K., Kawahata, H., & Okada, H. (1999). Depth ranges of alkenone production in the central Pacific Ocean. *Global Biogeochemical Cycles, 13*(2), 695-704. doi: 10.1029/1998GB900024

Okada, H., & Honjo, S. (1973). The distribution of oceanic coccolithophorids in the Pacific. *Deep Sea Research: Abstracts, 20*(4), 335-374. doi: 10.1016/0011-7471(73)90059-4

Okada, H., & McIntyre, A. (1979). Seasonal distribution of modern coccolithophores in the western North Atlantic Ocean. *Marine Biology*, 54, 319–328.

Oppo, D.W., & Curry, W.B. (2012). Deep Atlantic Circulation During the Last Glacial Maximum and Deglaciation. *Nature Education Knowledge*, *3*(10): 1. Retrieved from https://www.nature.com/scitable/knowledge/library/deep-atlantic-circulation-during-the-last-glacial-25858002

Pagani, M., Arthur, M.A., & Freeman, K.H. (1999). Miocene evolution of atmospheric carbon dioxide. *Paleoceanography, 14*(3), 273-292. Retrieved from http://people.earth.yale.edu/sites/default/files/files/Pagani/13_2005_1999%20Pagani_Paleocean.pdf

Pahnke, K., Sachs, J.P., Keigwin, L.D., Timmermann, A., & Xie, S.-P. (2007). Eastern tropical Pacific hydrologic changes during the past 27,000 years from D/H ratios in alkenones. *Paleoceanography, 22*(4), doi: 10.1029/2007PA001468.

Paul, H. A. (2002). *Application of Novel Stable Isotope Methods to Reconstruct Paleoenvironments: compound specific hydrogen isotopes and pore-water oxygen isotopes* (Doctoral Dissertation). *Swiss Federal Institute of Technology Zurich*. Retrieved from https://www.research-collection.ethz.ch/bitstream/handle/20.500.11850/146790/eth-25757-02.pdf?sequence=2&isAllowed=y

Popp, B.N., Kenig, F., Wakeham, S.G., Laws, E.A., & Bidigare, R.R. (1998). Does growth rate affect ketone unsaturation and intracellular carbon isotopic variability in *Emiliania huxleyi*? *Paleoceanography, 13*(1), 35–41. doi: 10.1029/97PA02594

Prahl, F.G., Collier, R.B., Dymond, J., Lyle, M., & Sparrow, M.A. (1993). A biomarker perspective on prymnesiophyte productivity in the northeast Pacific Ocean. *Deep-Sea Research I, 40*(10), 2061-2076. doi: 10.1016/0967-0637(93)90045-5

Prahl, F.G., Pilskaln, C.H., & Sparrow, M.A. (2001). Seasonal record for alkenones in sedimentary particles from the Gulf of Maine. *Deep-Sea Research I, 48*(2), 515-528. doi: 10.1016/S0967-0637(00)00057-1

Prahl, F.G., Popp, B.N., Karl, D.M., & Sparrow, M.A. (2005). Ecology and biogeochemistry of alkenone production at Station ALOHA. *Deep-Sea Research I, 52*(5), 699-719. doi: 10.1016/j.dsr.2004.12.001

Prahl, F. G., Dymond, J., & Sparrow, M. A. (2000). Annual biomarker record for export production in the central Arabian Sea. *Deep-Sea Res II, 47*(7-8), 1581–1604. doi: 10.1016/S0967-0645(99)00155-1

Prahl, F. G., Muelhausen, L. A., & Zahnle, D. L. (1988). Further evaluation of long-chain alkenones as indicators of paleoceanography conditions. *Geochimica Cosmochimica Acta, 52*(9)*,* 2303–2310. doi: 10.1016/0016-7037(88)90132-9

Riebesell, U., Burkhardt, S., Dauelsberg, A., & Kroon, B. (2000). Carbon isotope fractionation by a marine diatom: dependence on the growth-rate-limiting resource. *Marine Ecology Progress Series,* 193, 295-303.

Richey, J.N., & Tierney, J.E. (2016). GDGT and alkenone flux in the northern Gulf of Mexico: Implications for the TEX_{86} and U^{K}_{37}' paleothermometers. *Paleoceanography, 31*(12), 12, 1547-1561. doi: 10.1002/2016PA003032

Rau, G.H., Takahashi, T., Des Marais, D.J., & Sullivan, C.W. (1991). Particulate Organic Matter $\delta^{13}C$ Variations Across the Drake Passage. *Journal of Geophysical Research, 96*(C8), 15131-15135. doi: 10.1029/91JC01253

Rochon, A., de Vernal, A., Sejrup, H.-P., & Haflidason, H. (1998). Palynological Evidence of Climatic and Oceanographic Changes in the North Sea during the Last Deglaciation. *Quaternary Research, 49,* 197–207. Retrieved from http://folk.uib.no/nglbh/Publications_UiB/Gamleartikler/NB!Rochon%20et%20al., %201998.pdf

Rohling, E.J., & De Rijk, S. (1999). Holocene Climate Optimum and the Last Glacial Maximum in the Mediterranean: the marine oxygen isotope record. *Marine Geology, 153*(1-4), 57-75. doi: 10.1016/S0025-3227(98)00020-6

Rosell-Melé, A., & McClymont, E.L. (2007). Chapter Eleven: Biomarkers as Paleoceanographic Proxies, In: Claude Hillaire–Marcel and Anne De Vernal (Eds.) *Developments in Marine Geology, Elsevier, Volume 1,* 441-490, ISSN 1572-5480, ISBN 9780444527554. doi: 10.1016/S1572-5480(07)01016-0.

Sachs, J. P., & Kawka, O. E. (2015). The influence of growth rate on $^{2}H/^{1}H$ fractionation in continuous cultures of the coccolithophorid *Emiliania huxleyi* and the diatom *Thalassiosira pseudonana*. *PLoS One, 10*(11): e0141643. doi: 10.1371/journal.pone.0141643

Sachs, J.P., Maloney, A.E., Gregersen, J., & Paschall, C. (2016). Effect of salinity on 2H/1H fractionation in lipids from continuous cultures of the coccolithophorid *Emiliania huxleyi. Geochimica et Cosmochimica Acta,* 189, 96-109. doi: 10.1016/j.gca.2016.05.041

Sachse, D., Billault, I., Bowen, G.J., et al. (2012). Molecular Paleohydrology: Interpreting the hydrogen-isotopic composition of lipid biomarkers from photosynthesizing organisms. *Annu. Rev. Earth Planet. Sci., 40,* 221–249. doi: 10.1146/annurev-earth-042711-105535

Sachse, D., & Sachs, J.P. (2008). Inverse relationship between D/H fractionation in cyanobacterial lipids and salinity in Christmas Island saline ponds. *Geochimica et Cosmochimica Acta, 72*(3), 793- 806. doi: 10.1016/j.gca.2007.11.022

Sauer, P. E., Eglinton, T.I., Hayes, J.M., Schimmelmann, A., & Sessions, A.L. (2001). Compound-specific D/H ratios of lipid biomarkers from sediments as a proxy for environmental and climatic conditions. *Geochimica Cosmochimica Acta,65*(2), 213– 222. doi: 10.1016/S0016-7037(00)00520-2

Schouten, S., Ossebaar, J., Schreiber, K., Kienhuis, M.V.M., Langer, G., Benthien, A., & Bijma, J. (2006). The effect of temperature, salinity and growth rate on the stable hydrogen isotopic composition of long chain alkenones produced by *Emiliania huxleyi* and *Gephyrocapsa oceanica*. *Biogeosciences;* 3, 113–119. doi: 10.5194/bg-3-113-2006

Schlitzer, R. (2016). Ocean Data View, http://odv.awi.de.

Schmidt, G.A., Bigg, G. R., & Rohling, E. J. (1999). Global Seawater Oxygen-18 Database - v1.21. https://data.giss.nasa.gov/o18data/

Schwab, V. F., & Sachs, J. P. (2009). The measurement of D/H ratio in alkenones and their isotopic heterogeneity. *Organic Geochemistry, 40*(1), 111–118. doi: 10.1016/j.orggeochem.2008.09.013

Schwab, V.F., & Sachs, J.P. (2011). Hydrogen isotopes in individual alkenones from the Chesapeake Bay estuary. *Geochimica et Cosmochimica Acta, 75*(23), 7552-7565. doi: 10.1016/j.gca.2011.09.031

Scrimgeour, C.M., Begley, I.S., & Thomason, M.L. (1999). Measurement of deuterium incorporation into fatty acids by gas chromatography isotope ratio mass spectrometry. *Rapid Communications in Mass Spectrometry, 13*(4), 271–274. doi: 10.1002/(SICI)1097-0231(19990228)13:4<271::AID-RCM468>3.0.CO;2-6

Sessions, A.L., Burgoyne, T.M., Schimmelmann, A., & Hayes, J.M. (1999). Fractionation of hydrogen isotopes in lipid biosynthesis. *Organic Geochemistry, 30*(9), 1193-1200. doi: 10.1016/S0146-6380(99)00094-7

Smith, B., & Epstein, S. (1970). Biogeochemistry of the stable isotopes of hydrogen and carbon in salt marsh biota. *Plant Physiology, 46*(5), 738–742. Retrieved from https://www.ncbi.nlm.nih.gov/pmc/articles/PMC396670/

Ternois, Y., Sicre, M.A., Boireau, A., Conte, M.H., & Eglinton, G. (1997). Evaluation of long-chain alkenones as paleo-temperature indicators in the Mediterranean Sea. *Deep-Sea Research I, 44*(2), 271-286. doi: 10.1016/S0967-0637(97)89915-3

Tobias, H.J., & Brenna, J.T. (1997). On-line pyrolysis as a limitless reduction source for high-precision isotopic analysis of organic-derived hydrogen. *Analytical Chemistry, 69*(16), 3148–3152. doi: 10.1021/ac970332v

Urey, H.C., Brickwedde, F.G., & Murphy, G.M. (1932). A Hydrogen Isotope of mass 2 and its concentration. *Physical Review 40*(1), 1–15. doi: 10.1103/PhysRev.40.1

van der Meer, M.T.J., Baas, M., Rijpstra, W.I.C., Marino, G., Rohling, E.J., Sinninghe Damsté, J.S., & Schouten, S. (2007). Hydrogen isotopic compositions of long-chain alkenones record freshwater flooding of the Eastern Mediterranean at the onset of sapropel deposition. *Earth and Planetary Science Letters, 262*(3-4), 594–600. doi: 10.1016/j.epsl.2007.08.014

van der Meer, M.T.J., Sangiorgi, F., Baas, M., Brinkuis, H., Sinninghe Damsté, J.S., & Schouten, S. (2008). Molecular isotopic and dinoflagellate evidence for Late Holocene freshening of the Black Sea. *Earth and Planetary Science Letters, 267*(3-4), 426–434. doi: 10.1016/j.epsl.2007.12.001

van der Meer, M. T. J., Benthien, A., Bijma, J., Schouten, S., & Sinninghe Damsté, J. S. (2013). Alkenone distribution impacts the hydrogen isotopic composition of the $C_{37:2}$ and $C_{37:3}$ alkenones in *Emiliania huxleyi*. *Geochimica et Cosmochimica Acta, 111*, 162–166. doi: 10.1016/j.gca.2012.10.041

van der Meer, M.T.J., Benthien, A., French, KL., Epping, E., Zondervan, I., Reichart, G-J., Bijma, J., Sinninghe Damsté, JS., & Schouten, S. (2015). Large effect of irradiance on hydrogen isotopic fractionation of alkenones in *Emiliania huxleyi*. *Geochemica et Cosmochimica Acta, 160*, 16-24. doi: 10.1016/j.gca.2015.03.024

Versteegh, G. J. M., Riegman, R., de Leew, J. W., & Jansen, J. H. F. (2001). U^{K}_{37}' values for *Isochrysis galbana* as a function of culture temperature, light intensity and nutrient concentrations. *Organic Geochemistry, 32*(6), 785–794. doi: 10.1016/S0146-6380(01)00041-9

VLIZ (2009). Longhurst Biogeographical Provinces. Retrieved from http://www.marineregions.org/.

Volkman, J. K., Eglinton, G., Corner, E. D. S., & Sargent, J. R. (1980). Novel unsaturated straight-chain C_{37}-C_{39} methyl and ethyl ketones in marine sediments and a coccolithophore *Emiliania huxleyi*. *Physics and Chemistry of the Earth,* 12, 219-227. doi: 10.1016/0079-1946(79)90106-X

Volkman, J. K., Barrett, S. M., Blackburn, S. I., & Sikes, E. L. (1995). Alkenones in *Gephyrocapsa oceanica*: Implications for studies of paleoclimate. *Geochimica Cosmochimica Acta, 59*(3), 513–520. doi: 10.1016/0016-7037(95)00325-T

Waliser, D.E., & Gautier, C. (1993). A Satellite-derived Climatology of the ITCZ. *Journal of Climate,* 6, 2162- 2174. doi: 10.1175/1520-0442(1993)006<2162:ASDCOT>2.0.CO;2

Weiss, G.M., Pfannerstill, E.Y., Schouten, S., Sinninghe Damsté, J.S., & van der Meer, M.T.J. (2017). Effects of alkalinity and salinity at low and high light intensity on hydrogen isotope fractionation of long-chain alkenones produced by *Emiliania huxleyi*. *Biogeosciences Discuss.,* in review.

Winter, A., Jordan, R., & Roth, P. (1994). Biogeography of living coccolithophores in ocean waters. *Coccolithophores.* In Winter, A. and Siesser, W.G. (Eds.) *Cambridge University Press,* Cambridge, UK, 161-177.

Wolhowe, M. D., Prahl, F. G., Probert, I., & Maldonado, M. (2009). Growth phase dependent hydrogen isotopic fractionation in alkenone-producing haptophytes. *Biogeosciences, 6*(8), 1681–1694. doi: 10.5194/bg-6-1681-2009

Wolhowe, M. D., Prahl, F. G., Langer, G., Oviedo, A. M., & Ziveri, P. (2015). Alkenone δD as an ecological indicator: A culture and field study of physiologically-controlled chemical and hydrogen-isotopic variation in C_{37} alkenones. *Geochimica et Cosmochimica Acta, 162*, 166–182. doi: 10.1016/j.gca.2015.04.034

Yakir, D., & DeNiro, M. J. (1990). Oxygen and Hydrogen Isotope Fractionation During Cellulose Metabolism in Lemna-Gibba L. *Plant Physiology, 93*(1), 325–332. doi: 10.1104/pp.93.1.325

Zhang, Z., & Sachs, J.P. (2007). Hydrogen isotope fractionation in freshwater algae: I. Variations among lipid species. *Organic Geochemistry, 38*(4), 582-608. doi: 10.1016/j.orggeochem.2006.12.004

Zhang, X., Gillespie, A.L., & Sessions, A.L. (2009). Large D/H variations in bacterial lipids reflect central metabolic pathways. *Proceedings of the National Academy of Sciences 106*(31), 12580–12586. doi: 10.1073/pnas.0903030106

APPENDIX

Table A1: Raw data table (including all AMT20, Northern Pacific, Southern Pacific). * Indicates an outlier sample.

Sample	Latitude (degrees N)	Longitude (degrees E)	δDwater (‰)	δDalkenone (‰)	δDalkenone Stdev. (‰)	Alpha	Alpha Stdev.	SSS	Range in SSS	SST (°C)	Range in SST (°C)	δ13Calkenone (‰)	δ13Calkenone Stdev. (‰)	U^k'37	[Alkenone] (ng/l)	[NO2 + NO3] (μmol/l)	[PO4] (μmol/l)	[19' Hex] (ng/l)
AMT 1	49.643	-8.134	2.1	-197	2	0.8013	0.00215	35.13	0.23	15.82	0.46	-25.5	0.28	0.451	83.59		0.745	0.08	29.100
AMT 2 *	48.123	-17.327	3.7	-228	0	0.7696	0.00081	35.55	0.17	16.11	0.78	NA	NA	0.467	19.52		0.205	0.05	281.75
AMT 3 *	45.700	-19.498	5.5	-223	4	0.7727	0.00405	35.76	0.18	17.24	1.12	-24.1	0.19	0.518	9.30		0.15	0.026666667	19.100
AMT 4 *	43.158	-21.700	5.7	-239	2	0.7571	0.00171	35.88	0.20	17.59	1.14	NA	NA	0.545	13.94		0.14	0.026666667	17.000
AMT 5 *	42.270	-22.446	4.9	-224	3	0.7722	0.00308	35.89	0.28	18.08	1.55	-24.6	0.17	0.557	17.81		0.315	0.035	216.00
AMT 6	40.516	-23.869	5.4	-199	0	0.7967	0.00093	36.15	0.14	19.78	0.82	-25.8	0.22	0.701	12.83		0.03	0.02	57.75
AMT 8	34.824	-29.071	5.9	-186	0	0.8092	0.00080	36.25	0.18	21.77	0.64	-24.8	0.16	0.690	8.11		0.03	0.02	NA
AMT 9	33.948	-30.077	7.3	-182	1	0.8122	0.00114	36.96	0.06	23.53	0.18	NA	NA	0.925	9.27		0.03	0.02	26.50
AMT 10	31.984	-32.293	9.1	-182	2	0.8106	0.00223	37.15	0.18	24.32	0.41	-26.4	0.02	0.897	10.72		0.03	0.02	17.50
AMT 11	30.735	-33.690	9.5	-184	2	0.8083	0.00214	37.30	0.44	25.02	0.93	-25.5	0.02	0.895	13.47		0.03	0.02	24.00
AMT 12	28.844	-35.721	10	-165	2	0.8267	0.00214	37.36	0.26	25.55	0.61	-26.1	0.26	0.928	17.55		0.03	0.025	21.50
AMT 13	27.758	-36.893	12.4	-178	1	0.8119	0.00141	37.65	0.27	26.16	0.39	NA	NA	0.982	9.24		0.03	0.025	30.25
AMT 14	26.397	-38.350	11.5	-171	5	0.8196	0.00501	37.70	NA	26.34	NA	-24.5	0.17	0.930	16.04		0.03	0.02	33.00
AMT 15	24.494	-40.345	11.7	-167	1	0.8234	0.00128	37.43	0.62	26.70	0.53	-24.5	0.04	0.933	11.09		0.03	0.02	38.50
AMT 17	21.714	-39.642	9.3	-172	0	0.8204	0.00081	37.48	0.22	27.03	0.66	-24.5	0.15	0.934	16.97		0.03	0.02	30.00
AMT 18	19.559	-38.127	8.5	-178	1	0.8151	0.00099	37.16	0.31	27.35	0.47	NA	NA	0.955	8.43		0.03	0.02	22.00
AMT 19	18.304	-37.253	10	-184	0	0.8076	0.00082	37.01	0.26	27.36	0.55	-25.2	0.40	0.959	6.45		0.035	0.02	27.50
AMT 20	16.848	-36.259	8.8	-185	0	0.8079	0.00080	36.98	0.16	27.37	0.38	-25.6	0.46	0.927	2.95		0.03	0.023333333	31.00
AMT 21	15.498	-35.338	8.9	-174	Single Injection	0.8187	NA	36.65	0.54	27.83	0.85	-24.8	0.06	0.959	3.41		0.03	0.02	25.17
AMT 22 *	13.005	-33.641	9.6	-147	Single Injection	0.8449	NA	36.11	0.24	28.26	0.31	-33.3	0.37	0.959	0.64		0.03	0.02	28.08
AMT 23	11.289	-32.485	8.3	-183	2	0.8101	0.00177	35.90	0.19	28.42	0.19	NA	NA	0.987	4.07	0.031666667	0.02	0.02	14.00
AMT 25	8.520	-30.633	8.2	-195	0	0.7985	0.00080	34.69	0.56	29.07	0.51	NA	NA	0.981	4.61	0.035	0.02	0.02	15.33
AMT 27	5.502	-28.628	6.7	-188	3	0.8066	0.00309	35.30	0.72	29.12	0.81	26.8	0.28	NA	5.97	0.03	0.02	0.02	22.50
AMT 28	4.186	-27.757	7.7	-187	0	0.8064	0.00091	34.87	0.81	29.04	0.69	NA	NA	0.995	4.79	0.03	0.02	NA	NA
AMT 29	1.549	-26.024	7.8	-185	2	0.8091	0.00245	35.93	0.15	27.57	0.19	-27.5	0.38	NA	4.67	NA	NA	NA	NA
AMT 30	-0.197	-25.252	8.6	-201	0	0.7920	0.00084	36.08	0.08	27.62	0.08	NA	NA	0.996	9.47	NA	NA	NA	NA
AMT 31	-1.751	-25.004	9.7	-196	0	0.7963	0.00079	36.08	0.07	27.70	0.51	-26.0	0.24	NA	6.46	NA	NA	NA	NA
AMT 32	-3.094	-25.013	8.5	-189	5	0.8042	0.00502	36.20	0.22	27.43	0.50	-28.0	0.38	0.977	1.46	0.03	0.106666667	NA	NA
AMT 34	-6.179	-23.137	9	-195	2	0.7978	0.00213	36.32	0.10	26.08	0.28	-25.6	0.38	0.925	7.24	0.03	0.125	10.00	NA
AMT 35	-7.017	-18.903	9	-199	0	0.7939	0.00079	36.36	0.08	25.97	0.38	-24.8	0.06	0.883	2.53	NA	NA	NA	NA
AMT 36	-10.450	-16.951	9.7	-190	3	0.8021	0.00282	36.51	0.22	24.26	0.52	-26.3	0.05	0.880	5.53	NA	NA	NA	NA
AMT 37	-11.851	-18.346	8.6	-185	0	0.8081	0.00080	36.62	0.13	24.28	0.35	-25.5	0.00	0.907	18.97	0.02	0.105	NA	NA
AMT 38	-13.030	-19.522	8.8	-195	0	0.7984	0.00084	36.69	0.18	24.30	0.44	NA	NA	0.923	12.36	0.025	0.1125	17.00	NA
AMT 40	-15.705	-22.218	9.5	-188	1	0.8044	0.00127	37.10	0.05	23.84	0.22	-26.5	0.30	0.910	11.12	0.03	0.14	18.00	NA
AMT 41	-17.500	-24.053	10.3	-182	2	0.8094	0.00214	37.16	0.10	24.24	0.47	-26.3	0.10	0.915	21.72	0.03	0.18	17.00	NA
AMT 42	-18.611	-25.102	9.4	-178	4	0.8143	0.00404	37.15	0.05	24.39	0.25	-26.8	0.11	0.934	11.82	0.03	0.195	NA	NA
AMT 43	-21.028	-25.097	10	-168	2	0.8235	0.00207	37.04	0.17	24.33	0.16	-27.6	0.08	0.961	18.70	0.04	0.17	16.00	NA
AMT 45	-24.390	-27.009	9.6	-186	2	0.8063	0.00214	36.55	0.35	23.63	1.36	-28.5	0.25	0.953	3.97	0.04	0.0825	19.50	NA
AMT 46	-25.897	-28.261	9.6	-180	0	0.8119	0.00080	36.48	0.32	22.66	1.50	-27.8	Single Injection	0.923	3.84	0.03	0.06	NA	NA
AMT 47	-27.404	-29.542	9.8	-185	0	0.8068	0.00089	36.25	0.51	21.90	0.60	NA	NA	0.898	2.39	0.0325	0.06	20.00	NA
AMT 48	-29.267	-31.194	8.7	-195	1	0.7981	0.00127	35.98	0.44	20.18	0.98	-27.9	0.13	0.740	3.11	0.03	0.09	26.00	NA
AMT 49	-30.848	-32.686	8.2	-187	2	0.8066	0.00176	35.94	0.44	19.66	1.95	NA	NA	0.733	7.49	0.046666667	0.086666667	29.50	NA
AMT 50	-32.368	-34.168	7.2	-196	0	0.7983	0.00080	35.85	0.29	18.81	1.05	-27.2	0.40	0.625	3.65	0.03	0.103333333	40.00	NA
AMT 52	-35.194	-37.116	8.1	-195	Single Injection	0.7985	NA	35.64	0.16	16.83	1.43	-27.0	Single Injection	0.489	1.80	0.035	0.1475	69.50	NA
AMT 54	-38.066	-40.415	7.2	-188	0	0.8062	0.00080	35.50	0.71	15.81	1.88	NA	NA	0.409	5.02	0.171666667	0.151666667	148.50	NA
AMT 60	-46.180	-52.386	6.3	-183	4	0.8124	0.00377	34.72	1.48	12.72	4.65	NA	NA	0.343	10.86	2.26	0.454	380.40	NA
WEP1	20.952	120.747	1.8	-199	1.3	0.7985	0.00152	34.28	NA	27.65	NA	-26.0	0.15	0.969	3.27	NA	NA	NA	NA
WEP30	0.083	144.499	-1.3	-186	0.311127	0.8146	NA	32.87	NA	30.40	NA	-27.1	NA	NA	4.67	NA	NA	NA	NA
WEP31 *	-0.566	143.275	2.6	-163	Single Injection	0.8373	NA	34.65	NA	29.65	NA	-33.7	NA	NA	0.93	NA	NA	NA	NA
WEP33	-1.625	147.248	1.9	-186.54	Single Injection	0.8096	NA	34.29	NA	29.85	NA	-27.0	NA	NA	1.95	NA	NA	NA	NA
WEP37	-6.803	147.923	0.0	-197	Single Injection	0.8040	NA	32.86	NA	28.55	NA	-26.7	NA	NA	5.56	NA	NA	NA	NA
WEP39	-8.425	151.143	2.9	-180	Single Injection	0.8178	NA	34.67	NA	28.45	NA	-30.0	NA	NA	2.92	NA	NA	NA	NA
WEP40	-9.794	151.624	2.8	-179	Single Injection	0.8182	NA	34.56	NA	28.65	NA	-28.0	0.30	NA	1.92	NA	NA	NA	NA
WEP41	-11.449	151.263	3.7	-188	0.2	0.8090	0.00083	35.06	NA	27.20	NA	-27.7	0.52	0.984	2.89	NA	NA	NA	NA
WEP42	-11.207	149.549	3.3	-191	5	0.8064	0.00505	34.95	NA	27.30	NA	NA	NA	NA	NA	NA	NA	NA	NA
WEP43	-10.791	146.807	3.3	-182	0.6	0.8153	0.00101	34.87	NA	27.25	NA	-29.1	NA	NA	4.73	NA	NA	NA	NA
SO256_1	-32.148	168.668	5.3	-211	5	0.7852	0.00503	35.91	0.15	22.52	1.50	NA	NA	NA	0.773	NA	NA	NA	NA
SO256_2	-31.382	166.733	5.8	-198	2	0.7970	0.00214	35.95	0.05	22.79	0.60	NA	NA	NA	8.48	NA	NA	NA	NA
SO256_3	-30.658	164.958	5.8	-196	Single Injection	0.7997	NA	36.00	0.07	23.97	0.80	NA	NA	NA	4.40	NA	NA	NA	NA
SO256_4	-29.894	163.183	5.7	-197	2	0.7983	0.00214	35.86	0.09	22.88	0.60	NA	NA	NA	8.75	NA	NA	NA	NA
SO256_10	-23.332	152.339	4.4	-201	Single Injection	0.7955	NA	35.40	0.08	26.02	0.10	NA	NA	NA	3.92	NA	NA	NA	NA
SO256_12	-22.836	152.289	4.7	-186	Single Injection	0.8098	NA	35.44	0.19	26.03	0.50	NA	NA	0.959	3.01	NA	NA	NA	NA
SO256_17	-15.954	146.572	3.9	-190	Single Injection	0.8069	NA	35.35	0.07	27.47	0.30	NA	NA	0.986	5.28	NA	NA	NA	NA
SO256_19	-15.691	145.910	4.1	-202	1	0.7948	0.00127	35.35	0.05	27.42	0.20	NA	NA	0.986	8.33	NA	NA	NA	NA
SO256_20	-14.515	145.847	4.1	-202	Single Injection	0.7952	NA	35.36	0.04	27.30	0.20	NA	NA	0.977	6.74	NA	NA	NA	NA
SO256_21	-12.686	144.019	4.2	-192	Single Injection	0.8048	NA	35.14	0.34	27.72	0.40	NA	NA	NA	3.07	NA	NA	NA	NA
SO256_23	-12.978	144.398	3.2	-206	1	0.7919	0.00127	35.31	0.30	27.45	0.30	NA	NA	NA	4.78	NA	NA	NA	NA
SO256_24	-9.461	144.426	4.0	-200	4	0.7970	0.00406	34.95	0.30	28.06	0.60	NA	NA	NA	7.69	NA	NA	NA	NA
SO256_25	-10.535	142.262	3.1	-196	Single Injection	0.8020	NA	34.59	0.08	27.84	0.10	NA	NA	NA	23.75	NA	NA	NA	NA

Table A2: δDalkenone vs. δDwater Regression Results

	Dependent variable:
	δDalk
δDwater	1.853^{***} (0.552)
Constant	-202.195^{***} (4.061)
Observations	69
R^2	0.144
Adjusted R^2	0.131
Residual Std. Error	13.700 (df = 67)
F Statistic	11.254^{***} (df = 1; 67)
P Value	0.001^{***}
Note:	*p<0.1; **p<0.05; ***p<0.01

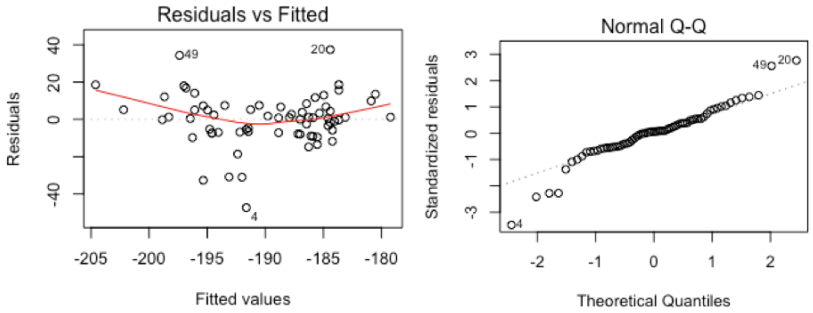

Figure A1: Residual values versus fitted values and normal Q-Q plot for residual values from the linear regression of δD_{alk} on δD_{water} (n=69).

Table A3: Pacific Ocean δDalkenone vs. δDwater Regression Results

	Dependent variable:
	δDalk
δDwater	-2.009 (1.260)
Constant	-185.617^{***} (4.835)
Observations	23
R^2	0.108
Adjusted R^2	0.066
Residual Std. Error	10.178 (df = 21)
F Statistic	2.543 (df = 1; 21)
P Value	0.13
Note:	*p<0.1; **p<0.05; ***p<0.01

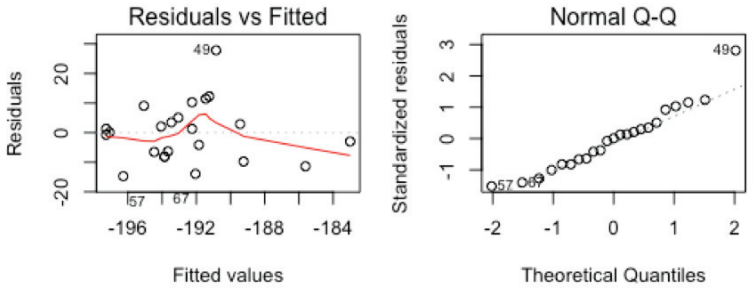

Figure A2: Residual values versus fitted values and normal Q-Q plot for residual values from the linear regression of Pacific Ocean δD_{alk} on δD_{water} (n=23).

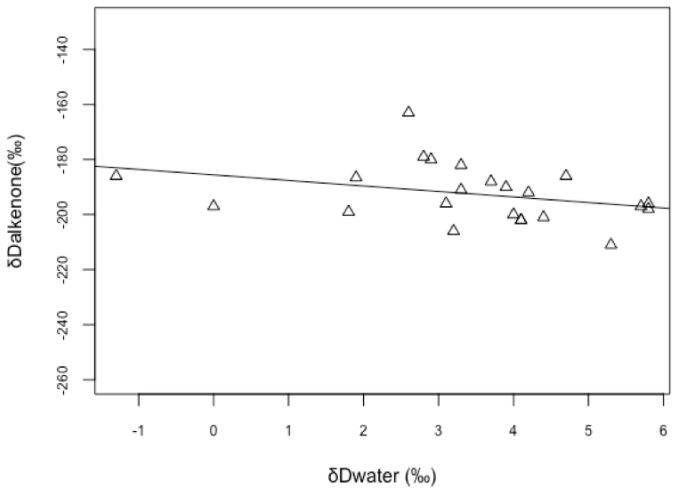

Figure A3: Linear regression of δD_{alk} on δD_{water} for Pacific Ocean samples only (n=23).

Equation A1: Error propagation equation used to compute $\alpha_{alk\text{-}water}$ error. In this case $^{\delta}Q$ is the error in $\alpha_{alk\text{-}water}$, $^{\delta}a$ and $^{\delta}b$ are the error associated with measurements of δD_{alk} and δD_{water} (Physical Sciences 2 – Harvard University, Fall 2007)

$$\frac{^{\delta}Q}{Q} = \sqrt{\left(\frac{^{\delta}a}{a}\right)^2 + \left(\frac{^{\delta}b}{b}\right)^2}$$

Table A4: Alpha vs. SSS Regression Results

	Dependent variable:
	Alpha
SSS	0.002 (0.002)
Constant	0.735*** (0.058)
Observations	69
R^2	0.021
Adjusted R^2	0.007
Residual Std. Error	0.014 (df = 67)
F Statistic	1.455 (df = 1; 67)
P Value	0.23
Note:	*p<0.1; **p<0.05; ***p<0.01

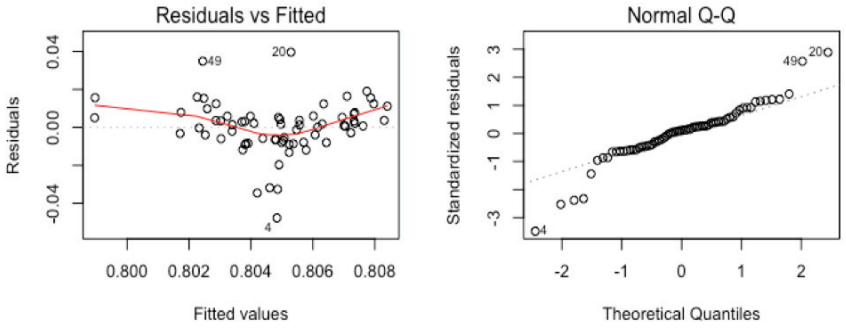

Figure A4: Residual values versus fitted values and normal Q-Q plot for residual values from the linear regression of $\alpha_{alk\text{-}water}$ on SSS (n=69).

Table A5: δDalkenone vs. SSS Regression Results

	Dependent variable:
	δDalk
SSS	4.043^{**} (1.663)
Constant	-334.846^{***} (59.717)
Observations	69
R^2	0.081
Adjusted R^2	0.067
Residual Std. Error	14.193 (df = 67)
F Statistic	5.909^{**} (df = 1; 67)
P Value	0.018^{**}
Note:	*p<0.1; **p<0.05; ***p<0.01

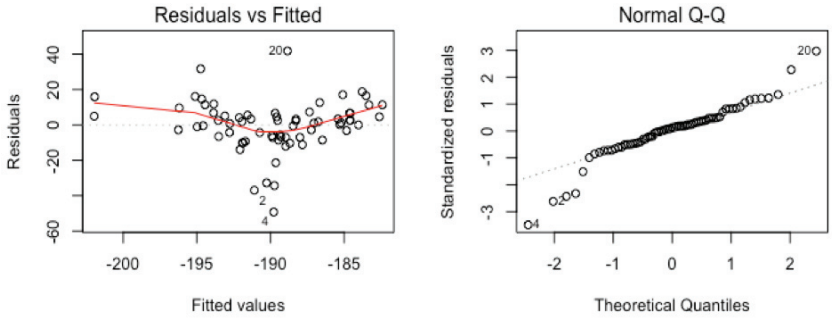

Figure A5: Residual values versus fitted values and normal Q-Q plot for residual values from the linear regression of δD_{alk} on SSS (n=69).

Table A6(a): Alpha vs. (Log) Alkenone Concentration (ng/l) Regression Results

	Dependent variable:
	Alpha
log_conc	-0.012^{***} (0.004)
Constant	0.814^{***} (0.004)
Observations	68
R^2	0.098
Adjusted R^2	0.084
Residual Std. Error	0.013 (df = 66)
F Statistic	7.155^{***} (df = 1; 66)
P Value	0.009^{***}
Note:	*p<0.1; **p<0.05; ***p<0.01

Table A6(b): Alpha Residuals vs. (Log) Alkenone Concentration (ng/l) Regression Results

	Dependent variable:
	Alpha residuals
log_conc	-0.014^{***} (0.004)
Constant	0.011^{***} (0.004)
Observations	68
R^2	0.132
Adjusted R^2	0.118
Residual Std. Error	0.013 (df = 66)
F Statistic	10.005^{***} (df = 1; 66)
P Value	0.002^{***}
Note:	*p<0.1; **p<0.05; ***p<0.01

Table A6(c): δDalk - δDwater Residuals vs. (Log) Alkenone Concentration (ng/l) Regression Results

	Dependent variable:
	δDalk residuals
log_conc	-13.043^{***} (4.332)
Constant	10.430^{***} (3.825)
Observations	68
R^2	0.121
Adjusted R^2	0.107
Residual Std. Error	12.930 (df = 66)
F Statistic	9.066^{***} (df = 1; 66)
P Value	0.004^{***}
Note:	*p<0.1; **p<0.05; ***p<0.01

Table A6(d): δDalk - SSS Residuals vs. (Log) Alkenone Concentration (ng/l) Regression Results

	Dependent variable:
	δDalk residuals
log_conc	-14.999^{***} (4.420)
Constant	12.043^{***} (3.903)
Observations	68
R^2	0.149
Adjusted R^2	0.136
Residual Std. Error	13.192 (df = 66)
F Statistic	11.517^{***} (df = 1; 66)
P Value	0.001^{***}
Note:	*p<0.1; **p<0.05; ***p<0.01

Table A7(a): Reduced Dataset: Alpha vs. (Log) Alkenone Concentration (ng/l) Regression Results

	Dependent variable:
	Alpha
log_conc	0.002 (0.003)
Constant	0.804*** (0.003)
Observations	62
R^2	0.005
Adjusted R^2	−0.011
Residual Std. Error	0.009 (df = 60)
F Statistic	0.332 (df = 1; 60)
P Value	0.57
Note:	*p<0.1; **p<0.05; ***p<0.01

Table A7(b): Reduced Dataset: Alpha Residuals vs. (Log) Alkenone Concentration (ng/l) Regression Results

	Dependent variable:
	Alpha Residuals
log_conc	−0.0005 (0.003)
Constant	0.0004 (0.003)
Observations	62
R^2	0.0004
Adjusted R^2	−0.016
Residual Std. Error	0.009 (df = 60)
F Statistic	0.022 (df = 1; 60)
P Value	0.88
Note:	*p<0.1; **p<0.05; ***p<0.01

Table A7(c): Reduced Dataset: δDalk - δDwater Residuals vs. (Log) Alkenone Concentration (ng/l) Regression Results

	Dependent variable:
	δDalk Residuals
log_conc	0.671 (3.399)
Constant	−0.588 (2.975)
Observations	62
R^2	0.001
Adjusted R^2	−0.016
Residual Std. Error	8.748 (df = 60)
F Statistic	0.039 (df = 1; 60)
P Value	0.84
Note:	*p<0.1; **p<0.05; ***p<0.01

Table A7(d): Reduced Dataset: δDalk - SSS Residuals vs. (Log) Alkenone Concentration (ng/l) Regression Results

	Dependent variable:
	δDalk Residuals
log_conc	−1.686 (3.368)
Constant	1.345 (2.948)
Observations	62
R^2	0.004
Adjusted R^2	−0.012
Residual Std. Error	8.669 (df = 60)
F Statistic	0.251 (df = 1; 60)
P Value	0.62
Note:	*p<0.1; **p<0.05; ***p<0.01

Table A8: Alpha vs. SST Regression Results

	Dependent variable:
	Alpha
SST	0.002^{***} (0.0004)
Constant	0.767^{***} (0.009)
Observations	69
R^2	0.203
Adjusted R^2	0.191
Residual Std. Error	0.012 (df = 67)
F Statistic	17.049^{***} (df = 1; 67)
P Value	0.0001^{***}
Note:	*p<0.1; **p<0.05; ***p<0.01

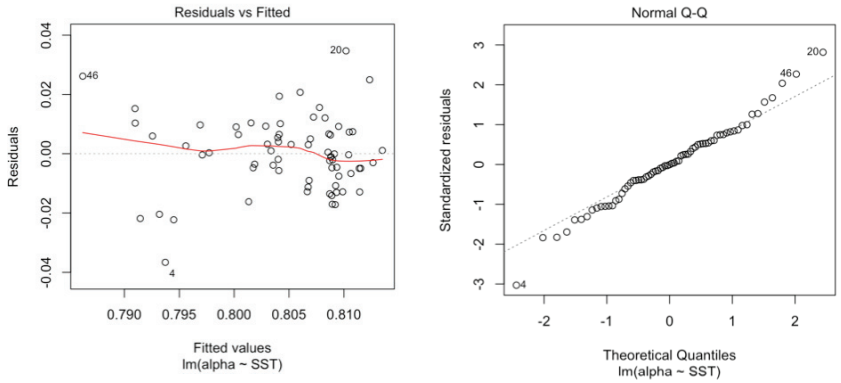

Figure A6: Residual values versus fitted values and normal Q-Q plot for residual values from the linear regression of on $\alpha_{\text{alk-water}}$ on SST (n=69).

Table A9(a): Alpha vs. SSS + SST Multiple Linear Regression Results

	Dependent variable:
	Alpha
SSS	0.003^{**} (0.001)
SST	0.002^{***} (0.0004)
Constant	0.657^{***} (0.054)
Observations	69
R^2	0.251
Adjusted R^2	0.228
Residual Std. Error	0.012 (df = 66)
F Statistic	11.064^{***} (df = 2; 66)
P Value	$7.18\text{x}10^{-5***}$
Note:	*p<0.1; **p<0.05; ***p<0.01

Table A9(b): Partial F- Test: Alpha vs. SSS + SST ANOVA Results

Model 1: Alpha vs. SSS
Model 2: Alpha vs. SSS + SST

Model	Res.Df	RSS	Df	Sum of Sq	F	Pr(>F)
1	67	0.0128				
2	66	0.0098	1	0.003	20.255	$2.82\text{x}10^{-5}$

Table A10(a): Alpha Residual vs. SST Regression Results

	Dependent variable:
	Alpha Residuals
SST	0.002^{***} (0.0004)
Constant	-0.040^{***} (0.009)
Observations	69
R^2	0.229
Adjusted R^2	0.217
Residual Std. Error	0.012 (df = 67)
F Statistic	19.897^{***} (df = 1; 67)
P Value	$3.199\text{x}10^{-5***}$
Note:	*p<0.1; **p<0.05; ***p<0.01

Table A10(b): δDalk - δDwater Residuals vs. SST Regression Results

	Dependent variable:
	δDalk Residuals
SST	1.638^{***} (0.358)
Constant	-40.637^{***} (9.002)
Observations	69
R^2	0.238
Adjusted R^2	0.227
Residual Std. Error	11.960 (df = 67)
F Statistic	20.915^{***} (df = 1; 67)
P Value	$2.129\text{x}10^{-5***}$
Note:	*p<0.1; **p<0.05; ***p<0.01

Table A10(c): δDalk - SSS Residuals vs. SST Regression Results

	Dependent variable:
	δDalk residuals
SST	1.667^{***} (0.373)
Constant	-41.356^{***} (9.377)
Observations	69
R^2	0.230
Adjusted R^2	0.218
Residual Std. Error	12.458 (df = 67)
F Statistic	19.964^{***} (df = 1; 67)
P Value	$3.114\text{x}10^{-5***}$
Note:	*p<0.1; **p<0.05; ***p<0.01

Table A11(a): Reduced Dataset: Alpha vs. SST Regression Results

	Dependent variable:
	Alpha
SST	0.0003 (0.0003)
Constant	0.798*** (0.008)
Observations	63
R^2	0.020
Adjusted R^2	0.004
Residual Std. Error	0.009 (df = 61)
F Statistic	1.272 (df = 1; 61)
P Value	0.26
Note:	*p<0.1; **p<0.05; ***p<0.01

Table A11(b): Reduced Dataset: Partial F- Test: Alpha vs. SSS + SST ANOVA Results

Model 1: Alpha vs. SSS
Model 2: Alpha vs. SSS + SST

Model	Res.Df	RSS	Df	Sum of Sq	F	Pr(>F)
1	61	0.0043				
2	60	0.0042	1	0.0002	2.48	0.12

Table A12(a): Reduced Dataset: Alpha Residuals vs. SST Regression Results

	Dependent variable:
	Alpha Residuals
SST	0.0004 (0.0003)
Constant	−0.011 (0.007)
Observations	63
R^2	0.039
Adjusted R^2	0.023
Residual Std. Error	0.008 (df = 61)
F Statistic	2.450 (df = 1; 61)
P Value	0.12
Note:	*p<0.1; **p<0.05; ***p<0.01

Table A12(b): Reduced Dataset: δDalk - δDwater Residuals vs. SST Regression Results

	Dependent variable:
	δDalk residuals
SST	0.461 (0.294)
Constant	−11.597 (7.460)
Observations	63
R^2	0.039
Adjusted R^2	0.023
Residual Std. Error	8.515 (df = 61)
F Statistic	2.468 (df = 1; 61)
P Value	0.12
Note:	*p<0.1; **p<0.05; ***p<0.01

Table A12(c): Reduced Dataset: δDalk - SSS Residuals vs. SST Regression Results

	Dependent variable:
	δDalk residuals
SST	0.439 (0.292)
Constant	−11.040 (7.413)
Observations	63
R^2	0.036
Adjusted R^2	0.020
Residual Std. Error	8.462 (df = 61)
F Statistic	2.264 (df = 1; 61)
P Value	0.14
Note:	*p<0.1; **p<0.05; ***p<0.01

Table A13: Alpha vs. δ13Calk Regression Results

	Dependent variable:
	Alpha
δ13Calk	-0.004^{***} (0.001)
Constant	0.710^{***} (0.023)
Observations	41
R^2	0.314
Adjusted R^2	0.297
Residual Std. Error	0.011 (df = 39)
F Statistic	17.886^{***} (df = 1; 39)
P Value	0.0001^{***}
Note:	*p<0.1; **p<0.05; ***p<0.01

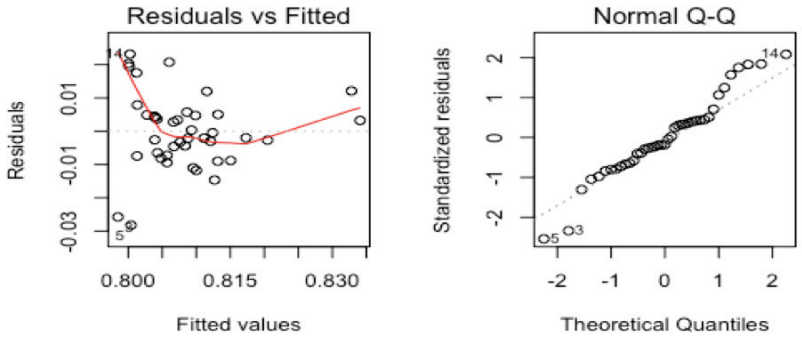

Figure A7: Residual values versus fitted values and normal Q-Q plot for residual values from the linear regression of on $\alpha_{alk\text{-}water}$ on $\delta^{13}C_{alk}$ (n=41).

Table A14(a): Alpha vs. SSS + δ13Calk Multiple Linear Regression Results

	Dependent variable:
	Alpha
SSS	0.004^{**} (0.002)
δ13C	-0.005^{***} (0.001)
Constant	0.547^{***} (0.067)
Observations	41
R^2	0.415
Adjusted R^2	0.384
Residual Std. Error	0.011 (df = 38)
F Statistic	13.454^{***} (df = 2; 38)
P Value	$3.822\text{x}10^{-5***}$
Note:	*p<0.1; **p<0.05; ***p<0.01

Table A14(b): Partial F- Test: Alpha vs. SSS + δ13Calk ANOVA Results

Model 1: Alpha vs. SSS
Model 2: Alpha vs. SSS + δ13Calk

Model	Res.Df	RSS	Df	Sum of Sq	F	Pr(>F)
1	39	0.0073				
2	38	0.0043	1	0.003	26.34	$8.77\text{x}10^{-6}$

Table A15(a): Alpha Residuals vs. δ13Calk Regression Results

	Dependent variable:
	Alpha Residuals
δ13C	-0.004^{***} (0.001)
Constant	-0.106^{***} (0.022)
Observations	41
R^2	0.388
Adjusted R^2	0.372
Residual Std. Error	0.011 (df = 39)
F Statistic	24.695^{***} (df = 1; 39)
P Value	$1.379\text{x}10^{-5***}$
Note:	*p<0.1; **p<0.05; ***p<0.01

Table A15(b): δDalk - δDwater Residuals vs. δ13Calk Regression Results

	Dependent variable:
	δDalk Residuals
δ13C	-4.020^{***} (0.839)
Constant	-104.282^{***} (22.516)
Observations	41
R^2	0.371
Adjusted R^2	0.354
Residual Std. Error	10.955 (df = 39)
F Statistic	22.956^{***} (df = 1; 39)
P Value	$2.415\text{x}10^{-5***}$
Note:	*p<0.1; **p<0.05; ***p<0.01

Table A15(c): δDalk - SSS Residuals vs. δ13Calk Regression Results

	Dependent variable:
	δDalk Residuals
δ13C	-4.126^{***} (0.830)
Constant	-106.932^{***} (22.270)
Observations	41
R^2	0.388
Adjusted R^2	0.372
Residual Std. Error	10.835 (df = 39)
F Statistic	24.718^{***} (df = 1; 39)
P Value	$1.369\text{x}10^{-5***}$
Note:	*p<0.1; **p<0.05; ***p<0.01

Table A16: Reduced Dataset: Alpha vs. δ13Calk Regression Results

	Dependent variable:
	Alpha
δ13C	-0.0003 (0.001)
Constant	0.802^{***} (0.029)
Observations	37
R^2	0.002
Adjusted R^2	-0.027
Residual Std. Error	0.009 (df = 35)
F Statistic	0.054 (df = 1; 35)
P Value	0.82
Note:	*p<0.1; **p<0.05; ***p<0.01

Table A17: Reduced Dataset: Partial F- Test: Alpha vs. SSS + δ13Calk ANOVA Results

Model 1: Alpha vs. SSS
Model 2: Alpha vs. SSS + δ13Calk

Model	Res.Df	RSS	Df	Sum of Sq	F	Pr(>F)
1	35	0.0025				
2	34	0.0024	1	$7.00\text{x}10^{-5}$	0.98	0.33

Table A18(a): Reduced Dataset: Alpha Residuals vs. δ13Calk Regression Results

	Dependent variable:
	Alpha Residuals
δ13C	−0.001 (0.001)
Constant	−0.029 (0.027)
Observations	37
R^2	0.035
Adjusted R^2	0.008
Residual Std. Error	0.008 (df = 35)
F Statistic	1.285 (df = 1; 35)
P Value	0.26
Note:	*p<0.1; **p<0.05; ***p<0.01

Table A18(b): Reduced Dataset: δDalk - δDwater Residuals vs. δ13Calk Regression Results

	Dependent variable:
	δDalk Residuals
δ13C	−0.865 (1.093)
Constant	−20.532 (29.012)
Observations	37
R^2	0.018
Adjusted R^2	−0.010
Residual Std. Error	8.807 (df = 35)
F Statistic	0.627 (df = 1; 35)
P Value	0.43
Note:	*p<0.1; **p<0.05; ***p<0.01

Table A18(c): Reduced Dataset: δDalk - SSS Residuals vs. δ13Calk Regression Results

	Dependent variable:
	δDalk Residuals
δ13C	−1.242 (1.005)
Constant	−30.547 (26.687)
Observations	37
R^2	0.042
Adjusted R^2	0.014
Residual Std. Error	8.101 (df = 35)
F Statistic	1.528 (df = 1; 35)
P Value	0.22
Note:	*p<0.1; **p<0.05; ***p<0.01

Table A19: Reduced Dataset: δDalk vs. δDwater Regression Results

	Dependent variable:
	δDalk
δDwater	1.480^{***} (0.363)
Constant	-198.536^{***} (2.714)
Observations	63
R^2	0.215
Adjusted R^2	0.202
Residual Std. Error	8.685 (df = 61)
F Statistic	16.668^{***} (df = 1; 61)
P Value	0.0001^{***}
Note:	*p<0.1; **p<0.05; ***p<0.01

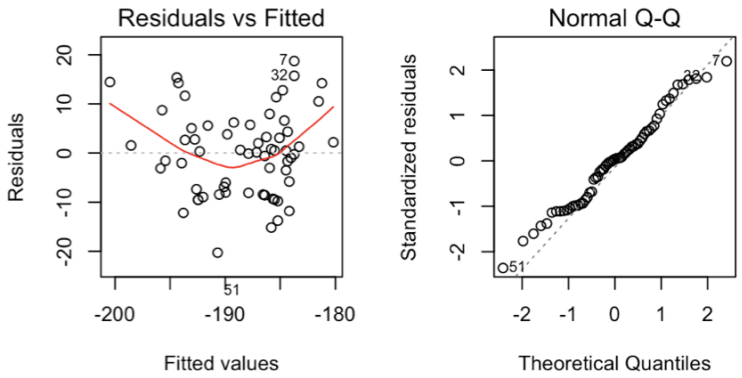

Figure A8: Residual values versus fitted values and normal Q-Q plot for residual values from the reduced dataset linear regression of on δD_{alk} on δD_{water} (n=63).

Table A20: Reduced Dataset: Alpha vs. SSS Regression Results

	Dependent variable:
	Alpha
SSS	0.002** (0.001)
Constant	0.724*** (0.036)
Observations	63
R^2	0.079
Adjusted R^2	0.064
Residual Std. Error	0.008 (df = 61)
F Statistic	5.237** (df = 1; 61)
P Value	0.026**
Note:	*p<0.1; **p<0.05; ***p<0.01

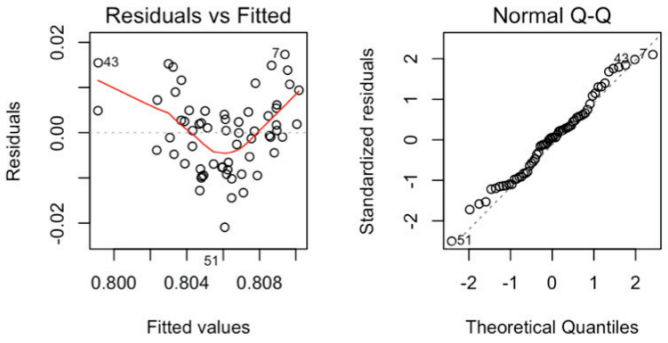

Figure A9: Residual values versus fitted values and normal Q-Q plot for residual values from the reduced dataset linear regression of on $\alpha_{\text{alk-water}}$ on SSS (n=63).

Table A21: Reduced Dataset: δDalk vs. SSS Regression Results

	Dependent variable:
	δDalk
SSS	4.316^{***} (1.020)
Constant	-343.337^{***} (36.639)
Observations	63
R^2	0.227
Adjusted R^2	0.214
Residual Std. Error	8.617 (df = 61)
F Statistic	17.898^{***} (df = 1; 61)
P Value	$7.95\text{x}10^{-5***}$
Note:	*p<0.1; **p<0.05; ***p<0.01

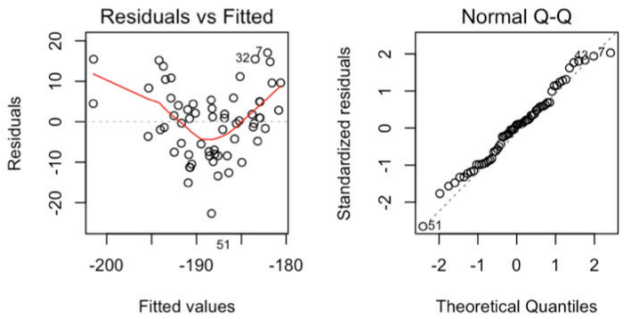

Figure A10: Residual values versus fitted values and normal Q-Q plot for residual values from the reduced dataset linear regression of on δD_{alk} on SSS (n=63).

Table A22: *Investr* lookup-table. SSS estimates from the inverse $\delta D_{alkenone}$ vs. SSS regression for the reduced SPOM dataset (for $\delta D_{alkenone}$ values between -170‰ and -210‰) and associated inversion intervals. The mean response 95% CIs and the point estimate 95% CIs are both shown for comparison. Ranges are computed as the difference between the upper and lower CI.

	Mean Response				Point Estimate Response		
δDalkenone	SSS estimate	lower CI	upper CI	RANGE	lower CI	upper CI	RANGE
-170	40.2	38.7	44.0	5.3	36.1	46.6	10.5
-171	39.9	38.6	43.6	5.0	35.9	46.3	10.4
-172	39.7	38.4	43.2	4.8	35.7	45.9	10.2
-173	39.5	38.2	42.7	4.5	35.4	45.5	10.1
-174	39.2	38.1	42.3	4.2	35.2	45.2	10.0
-175	39.0	37.9	41.9	3.9	35.0	44.8	9.8
-176	38.8	37.8	41.4	3.7	34.7	44.5	9.8
-177	38.5	37.6	41.0	3.4	34.5	44.1	9.6
-178	38.3	37.4	40.6	3.1	34.2	43.8	9.6
-179	38.1	37.3	40.1	2.9	33.9	43.5	9.6
-180	37.8	37.1	39.7	2.6	33.7	43.1	9.4
-181	37.6	36.9	39.3	2.4	33.4	42.8	9.4
-182	37.4	36.7	38.9	2.1	33.2	42.5	9.3
-183	37.1	36.6	38.5	1.9	32.9	42.1	9.2
-184	36.9	36.4	38.1	1.7	32.6	41.8	9.2
-185	36.7	36.2	37.7	1.5	32.3	41.5	9.2
-186	36.5	35.9	37.3	1.3	32.0	41.2	9.2
-187	36.2	35.7	36.9	1.2	31.7	40.9	9.2
-188	36.0	35.4	36.6	1.1	31.4	40.6	9.2
-189	35.8	35.1	36.3	1.2	31.1	40.3	9.2
-190	35.5	34.8	36.0	1.2	30.8	40.0	9.2
-191	35.3	34.4	35.8	1.4	30.5	39.7	9.2
-192	35.1	34.1	35.6	1.5	30.2	39.4	9.2
-193	34.8	33.7	35.4	1.7	29.9	39.1	9.2
-194	34.6	33.2	35.2	1.9	29.6	38.9	9.3
-195	34.4	32.8	35.0	2.2	29.3	38.6	9.3
-196	34.1	32.4	34.8	2.4	28.9	38.3	9.4
-197	33.9	32.0	34.7	2.7	28.6	38.1	9.5
-198	33.7	31.6	34.5	2.9	28.3	37.8	9.5
-199	33.4	31.1	34.3	3.2	27.9	37.5	9.6
-200	33.2	30.7	34.2	3.5	27.6	37.3	9.7
-201	33.0	30.3	34.0	3.7	27.2	37.0	9.8
-202	32.7	29.8	33.8	4.0	26.9	36.8	9.9
-203	32.5	29.4	33.7	4.3	26.5	36.5	10.0
-204	32.3	29.0	33.5	4.5	26.2	36.3	10.1
-205	32.0	28.5	33.4	4.8	25.8	36.1	10.3
-206	31.8	28.1	33.2	5.1	25.4	35.8	10.4
-207	31.6	27.7	33.0	5.4	25.1	35.6	10.5
-208	31.4	27.2	32.9	5.6	24.7	35.4	10.7
-209	31.1	26.8	32.7	5.9	24.3	35.2	10.9
-210	30.9	26.4	32.6	6.2	24.0	34.9	10.9